

LOCKHEED MARTIN ENERGY RESEARCH LIBRARIES



3 4456 0515416 9

CENTRAL RESEARCH LIBRARY

ORNL-4793

cy.1

THERMONUCLEAR DIVISION ANNUAL PROGRESS REPORT

Period Ending December 31, 1971

OAK RIDGE NATIONAL LABORATORY
CENTRAL RESEARCH LIBRARY
DOCUMENT COLLECTION

LIBRARY LOAN COPY

DO NOT TRANSFER TO ANOTHER PERSON

If you wish someone else to see this
document, send in name with document
and the library will arrange a loan.

UCR-7564
13 3-67



OAK RIDGE NATIONAL LABORATORY

OPERATED BY UNION CARBIDE CORPORATION • FOR THE U.S. ATOMIC ENERGY COMMISSION

Printed in the United States of America. Available from
National Technical Information Service
U.S. Department of Commerce
5285 Port Royal Road, Springfield, Virginia 22151
Price: Printed Copy \$3.00; Microfiche \$0.95

This report was prepared as an account of work sponsored by the United States Government. Neither the United States nor the United States Atomic Energy Commission, nor any of their employees, nor any of their contractors, subcontractors, or their employees, makes any warranty, express or implied, or assumes any legal liability or responsibility for the accuracy, completeness or usefulness of any information, apparatus, product or process disclosed, or represents that its use would not infringe privately owned rights.

ORNL-4793
UC-20 – Controlled Thermonuclear Processes

Contract No. W-7405-eng-26

THERMONUCLEAR DIVISION
ANNUAL PROGRESS REPORT
For Period Ending December 31, 1971

AUGUST 1972

OAK RIDGE NATIONAL LABORATORY
Oak Ridge, Tennessee 37830
operated by
UNION CARBIDE CORPORATION
for the
U.S. ATOMIC ENERGY COMMISSION

LOCKHEED MARTIN ENERGY RESEARCH LIBRARIES



3 4456 0515416 9

Reports previously issued in this series are as follow:

ORNL-2693	Period Ending January 30, 1959
ORNL-2802	Period Ending July 31, 1959
ORNL-2926	Period Ending January 31, 1960
ORNL-3011	Period Ending July 31, 1960
ORNL-3104	Period Ending January 31, 1961
ORNL-3239	Period Ending October 31, 1961
ORNL-3315	Period Ending April 30, 1962
ORNL-3392	Period Ending October 31, 1962
ORNL-3472	Period Ending April 30, 1963
ORNL-3564	Period Ending October 31, 1963
ORNL-3652	Period Ending April 30, 1964
ORNL-3760	Period Ending October 31, 1964
ORNL-3836	Period Ending April 30, 1965
ORNL-3908	Period Ending October 31, 1965
ORNL-3989	Period Ending April 30, 1966
ORNL-4063	Period Ending October 31, 1966
ORNL-4150	Period Ending April 30, 1967
ORNL-4238	Period Ending October 31, 1967
ORNL-4401	Period Ending December 31, 1968
ORNL-4545	Period Ending December 31, 1969
ORNL-4688	Period Ending December 31, 1970

Contents

ABSTRACTS	vii
1. PLASMA THEORY AND COMPUTATION	1
1.1 Confinement in Magnetic Mirrors	1
1.1.1 Instabilities in a Low-Beta, Short, Mirror-Contained Plasma	1
1.1.2 Coupling of Transverse Waves to Electrostatic Modes in a Magnetized Plasma	1
1.1.3 Microinstabilities in Inhomogeneous Plasmas: Finite Beta Effects	1
1.1.4 Nonlinear Stabilization of Single, Resonant, Loss-Cone Flute Instabilities	3
1.1.5 Nonlinear Loss-Cone Flute Modes	4
1.2 Toroidal Plasma Studies	4
1.2.1 Simulation of Energy Transport in Tokamak	4
1.2.2 An Implicit Numerical Method for Simulating Tokamak Plasma Discharges	4
1.2.3 Neutral Beam Injection	4
1.2.4 Bootstrap Currents in Tokamak	5
1.2.5 Neutral Atom Distribution in Tokamak	6
1.3 Computational Services	7
1.3.1 Equilibria in the Canted Mirror and ELMO Bumpy Torus	7
1.3.2 Interchange Stability in Anisotropic Plasmas	7
1.3.3 Double Adiabatic Theory of the Interchange Instability in a Closed-Line, High-Beta System	8
1.4 Data Acquisition Computers and Remote Terminal System	9
1.5 General Theory; Abstracts of Published Articles	9
1.5.1 Flute Stabilization Via Electrostatically Confined Cold Electrons	9
1.5.2 Energy Transfer to Ions from an Unneutralized Electron Beam	9
1.5.3 On the Derivation of the Quasilinear Equations	9
2. MIRROR CONFINEMENT	10
2.1 Introduction	10
2.2 Target Plasma Experiments in IMP	11
2.3 Target Plasma Studies in INTEREM	14
3. THE ORMAK PROGRAM	18
3.1 Introduction	18
3.2 The ORMAK Device	18

3.3	Experimental Results	20
3.4	Related Theory	22
3.5	Diagnostics	24
3.5.1	Thomson Scatter Experiment	24
3.5.2	Other Diagnostics and Plasma Production	24
3.5.3	Computer-Diagnostics Interfacing	25
3.6	Engineering	25
3.6.1	Toroidal Field Coil Power Supply	25
3.6.2	Control of Transistor-Battery Power Supplies	26
3.6.3	Electrical Insulation	26
3.6.4	Cooling	26
3.6.5	Injection-Related Changes	27
3.6.6	Back Bias	27
3.7	Future Plans	27
4.	HIGH-BETA PLASMAS	28
4.1	High-Beta Relativistic Electron Plasmas in Axisymmetric and Nonaxisymmetric Mirrors	28
4.2	The ELMO Bumpy-Torus Experiment	28
4.2.1	Introduction	28
4.2.2	High-Beta Experiments in Open Traps	29
4.2.3	Particle Confinement and Equilibrium	29
4.2.4	Stability	30
4.2.5	Plasma Heating and Confinement	30
4.2.6	Extension to High Magnetic Field	31
4.2.7	ELMO Bumpy-Torus (EBT) Technology	31
4.3	Macroscopic Instability Stimulation	31
4.4	Pulsed Microwave Heating Experiments in ELMO	31
4.5	Numerical Calculations of Off-Resonance Heating	32
4.6	Polarization of Free-Free Bremsstrahlung from Magnetically Confined Plasmas	32
4.7	Off-Resonance Effects on Electrons in Mirror-Contained Plasmas	32
4.8	Computer Calculations of Electron-Cyclotron Heating in a Nonuniform Magnetic Field	32
5.	TURBULENT HEATING	33
5.1	Introduction	33
5.2	Revisions to Turbulent Heating Theory	33
5.2.1	Introduction	33
5.2.2	Advanced Theory	33
5.3	Diagnostics on Burnout VI	34
5.3.1	Correlator Studies on Burnout VI	34
5.3.2	Off-Axis Plasma Source on Burnout VI	34
5.3.3	Power Pulsing of the Plasma Source Bias	36
5.3.4	Stabilization by Inherent Positive Plasma Potential	37
5.3.5	Mirror Stoppering by Plasma Rotation	37

5.4	Extrapolation to a Next-Generation Experiment	37
5.4.1	Ion Temperature Exceeds Centrifugal Splitting	37
5.4.2	Next-Generation Turbulent Heating Experiment	38
5.4.2.1	Introduction	38
5.4.2.2	Magnetic Field Strength	38
5.4.2.3	Power Pulse	38
5.4.2.4	Predicted Ion Energy	39
5.4.2.5	Plasma Volume	39
5.4.2.6	Stability Against Flutes	39
5.4.2.7	Power Requirement	40
5.5	Basic Plasma Physics	40
5.5.1	Simulation of Pseudowaves and Ion Acoustic Waves	40
5.5.2	Pseudowaves – Cerenkov Radiation Form	41
5.5.3	Isotope Separator Studies	41
5.5.4	High-Z Ion Source	42
6.	ENERGETIC-PARTICLE INJECTION	43
7.	ATOMIC PHYSICS AND PLASMA DIAGNOSTICS	46
7.1	High Excited States of Hydrogen Molecules	46
7.2	Energy Loss in Carbon and Aluminum Foils	46
7.3	Hydrogen Particle Interaction with Surfaces	47
7.4	Diagnostics	48
7.5	Controlled Fusion Atomic Data Center	48
8.	MAGNETICS AND SUPERCONDUCTIVITY	49
8.1	Superconducting Coils for IMP	49
8.2	ORMAK Cryogenics	49
8.3	Coils with Azimuthally Variable Current Density for EBT	52
8.4	Coils for the Target Plasma Group Long-Field Experiment	53
8.5	Thin Film Targets	53
8.6	Superconductor Stabilization Studies	54
8.7	Investigation of Fluctuations of Liquid-Helium Surfaces	54
8.8	A 7.6-cm-Diameter, 100-kG Coil	54
8.9	Ribbon Coil Endurance Testing	55
8.10	Fusion Feasibility	55
8.11	Cryogenic Test Facility	56
8.12	Power-Transmission Technology	56

9. FUSION REACTOR TECHNOLOGY	57
9.1 Published Work	57
9.1.1 Magnet Design	57
9.1.2 The Blascon – An Exploding-Pellet Fusion Reactor	57
9.1.3 Environmental Considerations	58
9.2 Work in Progress	58
9.2.1 Radiation Damage Experiment	58
9.2.2 Tritium Handling and Recovery	58
9.2.3 Neutron Cross-Section Requirements for Fusion Reactor Design	59
9.2.4 Fusion Reactor Blanket Benchmark Calculations	59
9.2.5 Fusion Reactors as Radioactive-Waste Burners (RWB's)	59
9.2.6 Blanket-System Studies	59
9.2.7 Engineering Requirements for Scatter-Dominated Mirror-Confined Plasmas	60
9.2.8 Beam Technology	60
9.2.9 Use of Synchrotron Radiation to Provide Ionization of Wall-Originated Impurities in a Thermonuclear Reactor	60
9.3 International Working Sessions on Fusion Reactor Technology	60
PUBLICATIONS, PAPERS, AND ORNL REPORTS	61

Abstracts

1. PLASMA THEORY AND COMPUTATION

Theoretical work continues to be directed mainly toward support of the experimental programs in: (1) magnetic-mirror confinement, (2) confinement and heating in the ORMAK device, and (3) the new high-beta ELMO Bumpy Torus proposal.

The linear theory of stability of finite-size mirror-confined plasmas has been continuously improved, especially with regard to realism of the plasma model. Estimates of maximum stable plasma length, however, remain rather short in the presence of appreciable density gradients perpendicular to the magnetic field. These critical lengths have been studied for varying electron temperature and plasma pressures to examine the effects of varying Landau damping and the coupling between electrostatic and electromagnetic waves.

The nonlinear evolution of "double-hump" instabilities characteristic of the buildup phase of target plasma experiments has been studied by numerical techniques of plasma simulation. The growth of the instabilities has been observed to saturate at very low levels, in agreement with an analytic theory developed in close conjunction with the simulation effort.

We have used numerical solution of one-dimensional transport models to study the time evolution of Tokamak discharges with Ohmic heating and heating from energetic neutral atom injection. Various sets of transport coefficients have been compared with available experimental data, the most satisfactory agreement being obtained with a somewhat modified form of the pseudoclassical model.

In support of the ELMO Bumpy Torus (EBT) program, we have sought ways of optimizing single-particle confinement in the vacuum magnetic fields, using compound coils rather than single concentric current loops. Numerical techniques have been developed to permit combined theoretical and experimental studies of the high-beta equilibria in the EBT as well as the present-day canted-mirror device; and stability criteria are being derived for incorporation into these equilibrium studies.

2. MIRROR CONFINEMENT

Experiments have begun in the superconducting mirror-quadrupole facility, IMP. Target plasmas are produced by electron-cyclotron heating, using up to 600 W at 36 GHz (resonant at $B = 12.5$ kG) with supplemental nonresonant power (up to 1 kW at 55 GHz). Measurements of the maximum target density indicate $n_e \approx 3 \times 10^{12} \text{ cm}^{-3}$ (with an uncertainty of a factor of 2), an order of magnitude higher than those found in INTEREM, therefore implying a scaling like B^2 .

Measurements of the axial density profile of the hot-electron plasma were made in INTEREM based on bremsstrahlung intensity, using an array of collimated NaI(Tl) detectors. The components of perpendicular and parallel pressure produced by the plasma can also be obtained from these measurements. The observed peaking of high-energy particles close to the midplane can be caused by two processes: (1) nonresonant heating of high-energy particles and (2) influence of the plasma pressure to distort the vacuum magnetic field which results in the observed equilibrium. At high beta, we cannot yet distinguish between these possibilities.

The stabilizing influence of nonresonant heating on the observed microinstabilities in INTEREM is interpreted as due to the increased population of relativistic electrons in the distribution function. The postulate that such heating reduces the anisotropy and therefore improves stability is refuted by axial density measurements.

3. THE ORMAK PROGRAM

ORMAK has had a period of operation at reduced fields and currents. The plasma which was produced was not diagnosed completely before the experiments were stopped to permit the completion of the systems necessary for full field operation. Construction and installation of these systems are now complete, and testing is proceeding for the second experimental phase in which the machine can operate at maximum design

parameters. We expect soon to be able to answer many questions concerning the effects of low collision frequency and small aspect ratio. In the initial plasma experiments, high x-ray fluxes were observed, implying the existence of fast electrons. The question of whether or not most of the current was carried by these electrons in our first experiments is not resolved. Higher magnetic fields, implying higher density, and the provision for preionization in the second experimental phase reduce the tendency for operation in a regime of intense x-ray production. Sometime during the coming year we will add energetic neutral-particle injection to make a large increase in the power input to the plasma.

4. HIGH-BETA PLASMAS

The largest fraction of the experimental effort during 1971 was concentrated on the canted-mirror facility. Experimental evidence was obtained for the location and size of the high-beta annulus, the magnitude of the stored energy, and the location of the particle drift surfaces. Much of this work was included in a paper given at the I.A.E.A. meeting in Madison, Wisconsin, and is presented in abstract form.

An expanded abstract is given of a document prepared on the proposed ELMO Bumpy Torus (EBT). This report contains experimental evidence from the canted-mirror facility, as well as theoretical work on the equilibrium and stability of the Bumpy Torus plasma, the power balance in the Bumpy Torus, technological aspects of the Bumpy Torus, and extrapolation of the Bumpy Torus to reactor conditions.

Experimental and theoretical work on the polarization of free-free bremsstrahlung from magnetically confined plasmas is also mentioned. Numerical studies on off-resonance heating, heating studies with pulsed microwave power, and experiments on triggering of an instability by a pulsed coil in ELMO are presented. Abstracts of other papers published in 1971 are included.

At present, work is continuing on the canted mirror in determining the position of the high-beta annulus, using diamagnetic and end-loss measurements.

The mechanical and technological design of the EBT is continuing. Future diagnostics for the EBT are under development.

5. TURBULENT HEATING

This is a final report of the ORNL study of, and experiment with, the turbulent heating of plasmas. It contains the latest revisions to the turbulent heating theory and corroborating experimental data. There is

now ample evidence that the maximum average velocity to which plasma ions may be heated is controlled by the energy density of the turbulence, and not the lower drift velocity difference between ions and electrons. Final experiments on Burnout VI, scaling laws, the extrapolation to a "next-generation" experiment, and some basic plasma physics are included.

6. ENERGETIC-PARTICLE INJECTION

Multiampere (equivalent) neutral-particle beams have been developed for either filling or heating plasma experiments. The duoPIGatron ion source is used with multiaperture accel-decel electrodes up to 5 cm in diameter for 4-A beams at 20 to 40 keV. This source is used with a closely coupled hydrogen gas cell for a neutral-particle-injector heating system for toroidal plasma devices. Source plasma and beam studies are in progress with a goal of 10-A beam modules.

7. ATOMIC PHYSICS AND PLASMA DIAGNOSTICS

Studies are being made to determine the feasibility of replacing the gas stripping cell in the neutral-particle spectrometer with 100- to 300-Å carbon and aluminum foils. Transmission through the foils of 250-eV protons has been achieved with an energy loss of 170 eV. All thin foils tested have microscopic cracks which prevent accurate calibration of the transmission coefficient.

Experimental work concerning the physics of excited states of hydrogen molecules has been suspended and awaits the further theoretical development that the effect of level crossing between the $1-\sigma_g$ ground electronic state and the $1-\sigma_u$ excited state has on the electron capture process and the high Rydberg-state populations. Plasma diagnostics development during the past year includes: (1) detection of total energy escaping a plasma, using pyroelectric crystals, (2) neutron spectrometers, (3) feasibility studies of heavy-ion beam and CO₂ laser-beam probing of plasmas.

8. MAGNETICS AND SUPERCONDUCTIVITY

During this year the group concentrated its efforts on support to plasma physics programs. The IMP superconducting mirror quadrupole was installed and tested. It has been energized routinely up to 71% of the design current density of the quadrupoles and has required little attention from the group. A cryogenic system for cooldown and operation of ORMAK at liquid-nitrogen temperatures was designed. The system was fabricated and tested under group supervision and, although not

completely debugged, is now operated by the ORMAK Group. Assistance in solving other cryogenic problems was provided. Magnetic design studies for the Target Plasma Group and the ELMO Bumpy Torus were initiated and carried to partial completion. Thin films of carbon and aluminum were produced for IMP and for general plasma diagnostic studies.

Other group activities included continuation of the study of stabilization of superconductors, investigation of fluctuations in boiling liquid helium, design of a 100-kG superconducting coil, tests of a 100-kG copper ribbon coil insert magnet, feasibility studies of magnets for fusion reactors, participation in a fusion feasibility workshop, survey of advanced technology in power transmission, and the layout of a cryogenic test facility.

9. FUSION REACTOR TECHNOLOGY

During the past year, published work has appeared in the areas of (1) magnet design; (2) the Blascon, an exploding-pellet fusion reactor; and (3) environmental considerations. Work in progress includes: (1) a radiation damage experiment; (2) an investigation of alternate methods for recovering tritium from the breeding blanket of a fusion reactor; (3) neutron cross-section evaluations; (4) fusion reactor blanket benchmark calculations; (5) an evaluation of fusion reactors as radioactive-waste burners; (6) blanket system studies; (7) an evaluation of the engineering requirements for scatter-dominated, mirror-confined plasmas; and (8) beam technology assessments.

1. Plasma Theory and Computation

1.1 CONFINEMENT IN MAGNETIC MIRRORS

1.1.1 Instabilities in a Low-Beta, Short, Mirror-Contained Plasma¹

C. O. Beasley J. E. McCune³
W. M. Farr² Abhijit Sen⁴

Results from calculations employing a numerical Vlasov model of a mirror-contained, low-beta plasma show that for a realistic aspect ratio, a drift-cone-type microinstability will exist when the plasma density exceeds some critical value for any plasma length, no matter how short. To obtain these results, we have examined the threshold of this instability for various plasma lengths and radii. Tests for the existence of this instability are well within the range of feasible experiments.

1.1.2 Coupling of Transverse Waves to Electrostatic Modes in a Magnetized Plasma

J. D. Callen⁵ G. E. Guest

The following is an abstract submitted for publication in *Physics of Fluids*.

The complete dispersion relation governing longitudinal and transverse waves in an infinite, homogeneous, magnetized plasma is discussed for arbitrary directions of wave propagation. Various forms suitable for computing modifications of the electrostatic dispersion relation arising from the coupling to transverse waves when $\omega_{pe} \gtrsim ck$ are compared. The modifications which arise for electrostatic ion gyroharmonic instabilities are determined in an ordering scheme appropriate for the important unstable modes of a mirror-confined thermo-

nuclear plasma. The resultant effects on a number of electrostatic modes are discussed.

1.1.3 Microinstabilities in Inhomogeneous Plasmas: Finite Beta Effects

C. O. Beasley J. D. Callen⁵
Abhijit Sen

Previous investigations of ion gyroharmonic microinstabilities in a model mirror-confined plasma, using the model of Beasley, Farr, and Grawe,⁶⁻⁸ have been restricted to an electrostatic analysis. For an infinite, homogeneous plasma it has been shown^{9,10} that the electrostatic analysis of such modes must be modified to include the coupling to transverse (electromagnetic) waves when the coupling parameter, ω_{pe}^2/c^2k^2 , approaches or exceeds unity. Here, ω_{pe} is the electron plasma frequency, c the velocity of light, and k the wave number. We have incorporated the appropriate modifications into the mirror-confined plasma instability model^{6,7} and have investigated the influence of these finite β_i (or $KT_i/m_e c^2$) effects in an inhomogeneous plasma.

In infinite-medium theory, the transverse wave modification of the electrostatic modes can be computed^{9,10} from perturbed currents \mathbf{J} induced by the oscillating potential of the electrostatic modes. The

5. Consultant, Department of Aeronautics and Astronautics, Massachusetts Institute of Technology.

6. C. O. Beasley, Jr., W. M. Farr, and H. Grawe, *Phys. Fluids* **13**, 2563 (1970).

7. D. E. Baldwin, C. O. Beasley, Jr., H. L. Berk, W. M. Farr, R. C. Harding, J. E. McCune, L. D. Pearlstein, and A. Sen, "Loss-Cone Modes in Inhomogeneous Mirror Machines," published in *Proceedings of Fourth IAEA Conference*, Madison, Wis., June 1971.

8. C. O. Beasley, W. M. Farr, J. E. McCune, and A. Sen, to be published in *Physical Review Letters*.

9. J. D. Callen and G. E. Guest, *Phys. Fluids* **14**, 1588 (1971).

10. J. D. Callen and G. E. Guest, ORNL-TM-3671 (January 1972).

1. Abstract of paper submitted for publication in *Physical Review Letters*.

2. Permanent address: University of Arizona.

3. Consultant, Massachusetts Institute of Technology.

4. Present address: Physical Research Laboratory, Navrangpura, Ahmedabad-9, India.

transverse-wave components of the electric field, \mathbf{E}^T , are computed from the electromagnetic wave equation

$$\vec{\nabla} \times (\vec{\nabla} \times \mathbf{E}) = -\nabla^2 \mathbf{E}^T = \frac{4\pi i\omega}{c} \mathbf{J} + \frac{\omega^2}{c^2} \mathbf{E}. \quad (1)$$

We assume this same phenomenological procedure is valid¹⁰ for an inhomogeneous model mirror-confined plasma as well. Following techniques similar to those used to determine the perturbed charge density,⁶ we may calculate this perturbed current, which is a result principally of electron motion. To do so, we Fourier analyze the electric field

$$E_z^L = \sum_{\mu} E_{z\mu}^L \exp(i\mu z/r_L L_p), \quad (2)$$

where L_p is the scale length of the plasma density, and $\pi r_L L_p$ is the distance over which the Fourier decomposition takes place. We finally arrive at the equation

$$E_{z_i}^T = \sum_{\mu} T_{l\mu} E_{z\mu} = \sum_{\mu} T_{l\mu} (E_{z\mu}^L + E_{z\mu}^T), \quad (3)$$

where

$$T_{l\mu} = -\frac{\omega_{pe}^2 r_L C_0 \exp\{-[(\mu - l)/2r_L]^2\}}{c^2 \pi^{1/2} (k_{\perp}^2 + l^2/r_L^2 L_p^2)} \times \sum_{\nu} \frac{\nu^2}{\mu l} I_{\nu} \left(\frac{\mu l}{2r_L^2} \right) \exp\left(-\frac{\mu l}{2r_L^2}\right) \frac{\omega}{\omega - \nu\omega_b} \quad (4)$$

are the matrix elements. ($C_0 \cong 1$ is the $n = 0$ combination of modified Bessel functions.)¹¹ We may solve Eq. (3) for $E_{z_i}^T$ and form

$$E_{z_i} = E_{z_i}^L + E_{z_i}^T = \sum_{\mu} [I_{l\mu} + \sum_p (I - T)_{lp}^{-1} T_{p\mu}] E_{z\mu}^L. \quad (5)$$

Next we consider the components of the electric field perpendicular to the magnetic field. It has been shown^{9,10} that E_{\perp} (here E_y) is not significantly affected by the transverse-wave couplings as long as $\omega_{pe}^2/c^2 k^2 < M_i/m_e$. However, since the ion $\mathbf{E}^L \times \mathbf{B}$

drift is inhibited by finite Larmor radius effects for $ka_i \gtrsim 1$, the lack of cancellation of ion and electron $\mathbf{E}^L \times \mathbf{B}$ drift produces a current which in turn induces a (transverse) electric field in the $\mathbf{E}^L \times \mathbf{B}$ (x) direction. This electric field is given approximately by

$$E_x^T \cong -i \frac{\omega}{\Omega_e} \frac{\omega_{pe}^2}{c^2 k^2} E_y^L. \quad (6)$$

This new component of the electric field induces an $E_x^T \times \mathbf{B}$ drift in the y (or k_{\perp}) direction and hence leads to a contribution to the perturbed charge density of the form

$$4\pi\rho_e(E_x^T) = -\frac{\omega_{pe}^2}{\Omega_e^2} \frac{\omega_{pe}^2}{c^2 k^2} k_{\perp}^2 E_x^L. \quad (7)$$

Thus the basic electrostatic Fourier eigenvalue equation⁶ may be modified to obtain a nonlinear eigenvalue equation of the form

$$\frac{\Omega_i^2}{\omega_{pi}^2} \varphi_l = -\frac{m_e}{M_i} \left(1 + \frac{\omega_{pe}^2}{c^2 k^2} \right) \frac{k_{\perp}^2}{(k_{\perp}^2 + l^2/r_L^2 L_p^2)} \varphi_l + \frac{\Omega_i^2}{\pi^{1/2} \omega_b^2 (l^2 + k_{\perp}^2/r_L^2 L_p^2)} \sum_{\mu} \left\{ R_{l\mu}^{\perp} \varphi_l + R_{l\mu}^z \right. \\ \left. \times \sum_q [I_{\mu q} + \sum_k (I - T)_{\mu k}^{-1} T_{kq}] \frac{q}{\mu} \varphi_q \right\}. \quad (8)$$

We solve Eq. (8) by numerically searching for an ω_{pi}^2/Ω_i^2 (density) which is real and for which Eq. (8) is satisfied.

At low densities and for ion temperatures of interest in thermonuclear plasma, our results show little evidence of stabilization of the loss-cone mode. These results are shown in Fig. 1.1. They apply to the one residual mode which remains unstable to very short plasma lengths in the absence of a radial density gradient, and to all plasma lengths when the (drift cone) term is included.

At high densities where the instability is dominated by the drift-cone mechanism, there is a stabilizing effect even for reasonably low ion temperatures. This is illustrated by the contours of constant growth rate shown in Fig. 1.2. As the density is increased beyond a certain point, or as the plasma pressure is increased, the mode's growth rate decreases. The overall flutelike

11. G. E. Guest and R. A. Dory, *Phys. Fluids* 8, 1853 (1965).

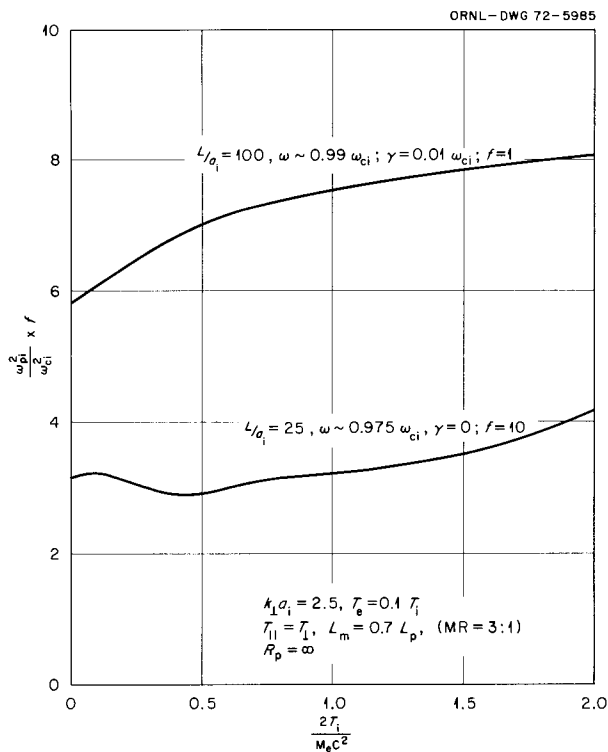


Fig. 1.1. Density as a function of plasma β (ion temperature).

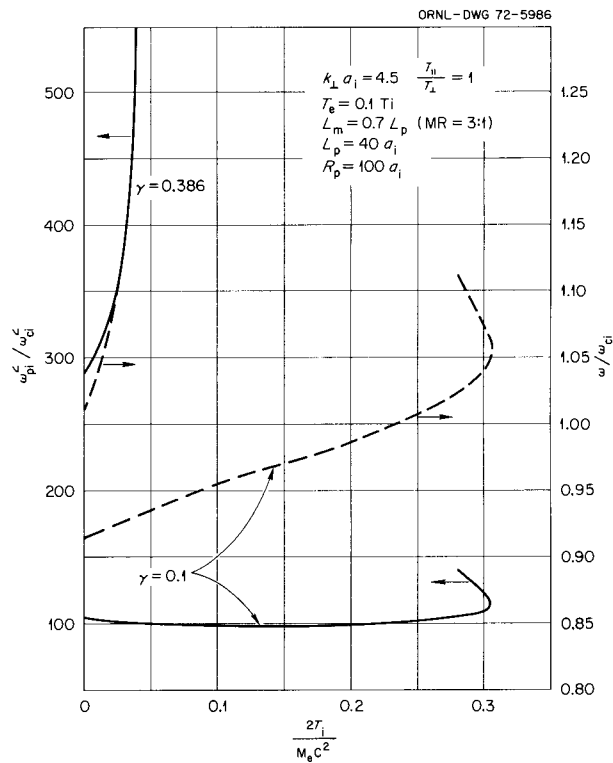


Fig. 1.2. Contours of constant growth rate – density vs β .

character of the mode does not change, as shown in Fig. 1.3. This stabilizing influence has also been found by Tang et al.¹²

The upshot of these calculations is that there is some stabilization of the high-growth-rate drift-cone mode from finite beta effects. However, the mode which dominates at short plasma lengths is not stabilized to any appreciable extent for ion temperatures of physical interest.

1.1.4 Nonlinear Stabilization of Single, Resonant, Loss-Cone Flute Instabilities¹³

E. C. Crume¹⁴ Owen Eldridge¹⁵
H. K. Meier

The evolution of linearly unstable, high-frequency ($\omega \approx n\Omega$), flutelike ($k_{||} = 0$), electrostatic modes which can occur in a multicomponent, magnetic-mirror-confined collisionless plasma has been studied by computer

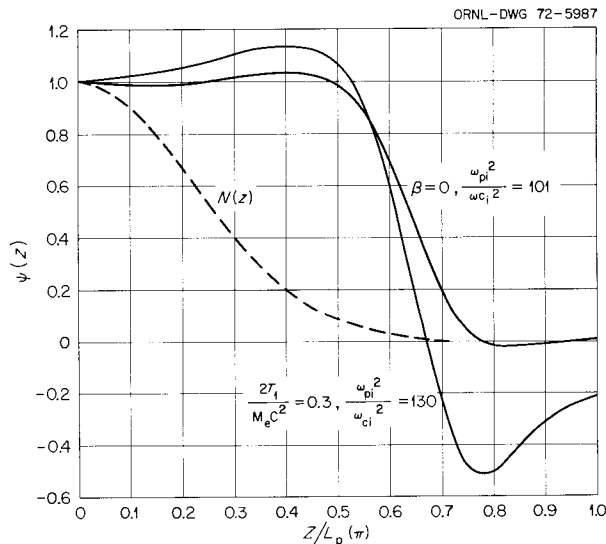


Fig. 1.3. Perturbed potential along B at two different β_s – drift cone mode.

12. W. M. Tang, L. D. Pearlstein, and H. L. Berk, UCRL preprint 73498, September 1971.

13. Abstract of ORNL-TM-3675.

14. On loan from Y-12.

15. Consultant, University of Tennessee.

simulation. An infinite, periodic, sheet charge model was used in which particle motion is followed in one spatial coordinate and two velocity coordinates normal to a constant magnetic field. Approximately one

quarter of the particles in the initial velocity distributions formed a warm, Maxwellian background component; the remainder belonged to a hot, linearly stable, loss-cone component. These velocity distributions were constructed in such a way as to provide initial states relatively free of randomly fluctuating electric fields. The early evolution of single-wave (either traveling or standing) resonant instabilities agrees well with linear theory. A rapid, coherent heating of the warm component occurs, and spatial harmonics of the unstable wave appear. The electrostatic field of the wave then saturates at an energy level as much as two orders of magnitude lower than those reported in previous simulation studies of the same and related instabilities or predicted from earlier nonlinear analysis. The field amplitude decreases rapidly to zero after saturation and then grows again nonlinearly. The temperature of the warm component reaches a maximum when the field amplitude vanishes. During and subsequent to this nonlinear growth period, details of the evolution of the field amplitude vary from case to case. The saturation levels and early postsaturation behavior are in agreement with a recently reported nonlinear analysis which was motivated by the results reported here.

1.1.5 Nonlinear Loss-Cone Flute Modes¹⁶

E. C. Crume¹⁴ Owen Eldridge¹⁵
H. K. Meier

A class of linearly unstable loss-cone flute modes is investigated by computer simulation and nonlinear theory. The instability occurs through the coupling of a negative-energy ion cyclotron wave with the lower hybrid mode of a cold ion component. Stabilization occurs through a rapid and efficient heating of the cold ions, with very little energy appearing in electric fields. The analytic theory is in qualitative and quantitative agreement with the results of the simulation.

1.2 TOROIDAL PLASMA STUDIES

1.2.1 Simulation of Energy Transport in Tokamak

R. A. Dory J. T. Hogan
M. M. Widner¹⁷

Results of this investigation have been described in refs. 18 and 19. The abstract of ref. 18 is reproduced in

16. Abstract of paper submitted for publication in *Physics of Fluids*, "Research Notes."

17. Present address: Sandia Laboratories, Albuquerque, N.M.

18. Presently available as ORNL-TM-3637, to be published in *Proceedings of the Academy of Sciences (Ukraine) Conference on Plasma Theory*, Kiev, U.S.S.R. (1971).

19. *Bull. Amer. Phys. Soc.* 16, 1262 (1971).

part here:

A time and space dependent computer calculation was used to evaluate the single anomaly coefficient C of the Artsimovich/Yoshikawa pseudoclassical model²⁰ for a standard Tokamak. Good agreement was found with the available T-3 data if $C = (1.1 \times 10^{14}/n)^{3/2}$. This scaling was used to study the dependence of β_I and T_e on plasma current I and density n . Additional plasma heating by beams of energetic neutral atoms has also been studied with the computer model. Although significant temperature increases can be obtained in small machines, the observation by Yoshikawa that a plasma ignition demonstration will require a very large machine appears valid unless the $C \sim n^{-3/2}$ scaling holds into the high-density regime $n \gtrsim 5 \times 10^{13} \text{ cm}^{-3}$ and unless this regime can be entered stably.

The computer code is now being improved to include effects of plasma diffusion, impurities, neutral fluxes, and radiation, and the transport model has been revised to use the latest coefficients calculated by Hinton and Rosenbluth (to be published).

1.2.2 An Implicit Numerical Method for Simulating Tokamak Plasma Discharges²¹

M. M. Widner R. A. Dory

A numerical model, appropriate for field penetration and thermal diffusion, is used for time evolution studies of Tokamak discharge plasmas. The model, which includes anomalous resistivity and anomalous electron heat conductivity, is applied to a plasma cylinder, although transport coefficients are given for a torus. An implicit set of difference equations is derived which includes the time changes in the nonlinear transport coefficients. The calculations are compared with experiment and found in agreement, using the appropriate model for anomalous electron heat flow.

1.2.3 Neutral Beam Injection

J. D. Callen²² J. F. Clarke
J. A. Rome

Neutral beam injection has been proposed as a means of creating, heating, offsetting the radial diffusion losses, and maintaining the Ohmic heating current of plasmas in a toroidal configuration. The successful development of 2-A, 30-keV neutral beam injectors at

20. See, for example, S. Yoshikawa and N. C. Christofilos, paper CN-28/F-1, Fourth International Conference on Plasma Physics and Controlled Nuclear Fusion Research, Madison, Wis., June 17-23, 1971, IAEA/CN-28.

21. Abstract of ORNL-TM-3498, submitted for publication in the *Journal of Computational Physics* (1970).

22. Consultant, Department of Aeronautics and Astronautics, Massachusetts Institute of Technology.

ORNL will enable these injectors to be installed on ORMAK in 1972. Theoretical work on neutral beam injection has concentrated on optimization of the use of these injectors in ORMAK and a study of the effects of injection.

To maximize the path length for beam absorption, injection will be in the equatorial plane such that at their innermost penetration toward the axis of symmetry ($R = R_B$), the injected particles are moving either parallel or antiparallel to the Ohmic heating current. The optimum value of R_B is determined by the plasma density profile (which governs the ionization and charge exchange rate of the neutrals) and by the deviation of the ion orbits from their birth flux surface (which determines whether ions are lost to the limiter). For a parabolic density profile, the optimum R_B is about halfway between the inner plasma edge and the magnetic axis. A flatter density profile moves this point inward, while a more centrally peaked profile moves it toward the magnetic axis.

The orbits of injected particles have been studied in some detail. When a neutral is ionized (usually via charge exchange), the electron is confined to its birth flux surface due to its low mass and small gyro orbit. The ion will deviate from this surface by about $2qa_i$, where a_i is the gyroradius in the toroidal magnetic field and $q = 2\pi/\iota$. This is about 5 cm in ORMAK for 30-keV H^+ ions. The deviation is *inward* for coinjected ions and *outward* for counter-injected ions (coinjected and counter injected refer to direction of Ohmic heating current). Thus the counter-injected ions which are born in the outer ~ 5 cm of plasma are lost to the limiter or liner. If R_B is within about 5 cm of the inner plasma edge, coinjected ions are also lost. For this reason the beam should not be injected close to the inner plasma edge. It is also clear that there is no way to avoid the loss of counter-injected ions; hence counter injection will lead to a net charge buildup in the plasma.

Even if there is no *net* charge buildup in the plasma due to ion loss, injection will cause local charge imbalances in the plasma due to the separation of the ion and electron orbits. Since the injection current is constant, this charge (unless relaxed by the plasma) will increase linearly with time and will generate large (and increasing) electric fields. The buildup of these fields and the anisotropic velocity space distribution of the hot ions might lead to microscopic and/or magnetohydrodynamic instabilities. Since the effects of these instabilities are presently unclear, they have been ignored in our work so far.

Specific results for the charge distribution calculation are complicated, so that only an outline of the methods

used will be given here. A birth distribution in the equatorial plane was found by using the injection geometry, the plasma profile, and the mean free path for ionization. By also knowing the injected particle's energy and magnetic moment, the complete distribution function for the injected charge density, $f(x,v,t)$, was found. For times longer than the characteristic time of the toroidal drifts of the particles, this distribution is axisymmetric.

The background plasma reacts to the presence of this charge distribution. Since the background electrons are free to move along the magnetic field lines, they tend to make the charge distribution uniform on a flux surface and hence in the poloidal direction. This has been shown by means of a detailed kinetic analysis.

Thus the net result of neutral beam injection is to set up a radial electric field. This field will increase with time, since the only relaxation mechanism is perpendicular ion viscosity, which is a very slow effect.

The radial electric field is intimately related to the momentum transfer from the neutral beam to the plasma. Part of this momentum comes from the direct slowing down of the ions. After slowing down to the ion thermal velocity, the injected ion resides on a flux surface which is about halfway between the innermost and outermost flux surfaces which were reached by the ion just after injection. This accounts for the remainder of the momentum.

The radial electric field, due to local charge buildup, causes a nonuniform poloidal $\mathbf{E} \times \mathbf{B}/B^2$ rotation. The parallel ion viscosity of the plasma induces flow along the magnetic field which cancels the poloidal $\mathbf{E} \times \mathbf{B}/B^2$ flow and leaves only a toroidal flow. This renders the total plasma flow divergence free and incompressible. The toroidal velocity is the final repository for the injected beam momentum.

To avoid shock conditions and an undoing of the beneficial rotational transform effects by the radial electric field, we must require that the toroidal flow velocity be less than the sound speed, and it is this condition which ultimately limits the product of the injection current and the injection time. For times less than the perpendicular ion viscosity relaxation time-scale of about 25 sec, a preliminary estimate gives about 6.4 A-sec in ORMAK, which is no problem.

1.2.4 Bootstrap Currents in Tokamak

J. T. Hogan

Although Tokamaks can compete favorably as reactor candidates in their present pulsed mode of operation, there is a feeling that matters would be helped if a way

were found to run them in a steady state. The discovery that the neoclassical theory allowed a steady "bootstrap" equilibrium came as welcome news.^{23,24} This equilibrium excludes poloidal flux to the boundary and requires a mass source and an injected "seed" current which is then amplified by the plasma. It needs no externally supplied electric field. We describe here some remaining questions of approach to a steady state and criteria for experimental observation.

Some clarification is required first for the eventual equilibrium which, as reported in refs. 23 and 24, is the result of a "banana theory" of particle transport. This theory takes its name from the banana orbits traced out in a minor cross section of the torus by particles trapped in the "toroidal mirrors": $B_{\max}/B_{\min} \cong (R + r)/(R - r)$. The calculated diffusion coefficients diverge at the magnetic axis as $r^{-3/2}$ (r is the torus minor radius coordinate), an obviously unphysical result. Since the toroidal mirror ratio is unity on the magnetic axis, particles in the so-called "plateau" regime contribute to the diffusion. (The "plateau" is the transition from a collision-free to a collision-dominated regime.) Several methods yield finite results at the magnetic axis and modify the bootstrap equilibrium: (1) introduction of an arbitrary cutoff to limit the divergence, (2) a smooth analytical fit of existing banana and plateau coefficients, and (3) a re-derivation of the transport rates using an ordering which allows the whole transition regime to be treated.²⁵ The density profile given in ref. 23 was singular at the origin, for no obvious reason. The new result is finite, as it should be. The seed current is no longer required; a simple mass source suffices to give the needed diffusion current.

The question of time dependence arises next and has been treated both analytically and numerically, since the particle diffusion equations are coupled and non-linear. An implicit time and space-centered difference scheme was chosen, and results are compared with exact similarity solutions of the equations. A linear analysis showed that the relaxation rates of the similarity solutions were representative, since an arbitrary initial distribution approached them as $1/t^\lambda$, where $\lambda \gg 1$.

The particle diffusion equilibrium is reached as the last in a series of equilibration processes in the plasma, and so the calculations were performed at constant electron and ion temperature and with fixed total

plasma current. The result is that evolution occurs on a time scale, $\tau = \tau^* \sqrt{A/\beta_p}$, where τ^* is the resistive skin diffusion time which varies as the square of the plasma size and inversely as the resistivity, A is the aspect ratio (the major radius of the torus divided by its minor radius), and β_p is the ratio of plasma pressure to the magnetic pressure of the field of the heating current. The resistivity is computed at elevated temperature, because of the time ordering of heating and diffusion processes, and hence the relaxation time is quite long. It is improbable that this equilibrium bootstrap current will be observed in ORMAK.

This long approach to the bootstrap state may be helpful. Since the poloidal field is excluded, the current density is peaked at the boundary. This profile is especially susceptible to local interchange and resistive tearing modes. Either a close-fitting conducting shell or feedback stabilization might prevent catastrophe, but there seems to be no place for a conducting shell in a reactor, and feedback stabilization seems to be impractical.²⁶

1.2.5 Neutral Atom Distribution in Tokamak

J. F. Clarke J. T. Hogan

We have computed the distribution function of neutral atoms in an Ohmically heated Tokamak discharge. The distribution function is used to calculate:

1. The magnitude and shape of the charge-exchange energy spectrum. Significant effects of plasma spatial variations are found on the shape and position of the breakpoint of this spectrum.
2. The Doppler broadening of spectral lines, to be compared with the deuterium pulse experiment.²⁷
3. The radial profiles of neutral atom density and energy, for use in the Tokamak simulation code (described in Sect. 1.2.1).

The numerical results agree well with analytical solutions, which can be obtained when plasma properties are assumed uniform in space and the ions are assumed to have a delta function distribution.

The results agree as well with experimental data,²⁸ although only relative fluxes are available for the energy spectrum, and the density values are obtained by an

23. R. J. Bickerton et al., *Nature, Phys. Sci.* **229**, 110 (1971).

24. B. B. Kadomtsev and V. S. Shafranov, Fourth International Conference on Plasma Physics and Controlled Nuclear Fusion Research, Madison, Wis., June 17-23, 1971, IAEA/CN-28.

25. F. Hinton, *Bull. Amer. Phys. Soc.* **16**, 1276 (1971).

26. J. F. Clarke and R. A. Dory, in *Feedback and Dynamic Control of Plasmas*, ed. by T. K. Chu and H. W. Hendel, American Institute of Physics, New York, 1970.

27. S. V. Mirnov and I. B. Semenov, *Sov. At. Energy* **28**, 129 (1970).

28. E. Hinnov and H. P. Eubank (private communication).

Abel inversion of an annular function and are thus somewhat inaccurate.

1.3 COMPUTATIONAL SERVICES

1.3.1 Equilibria in the Canted Mirror and ELMO Bumpy Torus

C. L. Hedrick

The purpose of this investigation was to calculate (numerically) self-consistent, finite beta equilibria for both the canted mirror and the ELMO Bumpy Torus. From these equilibria, single-particle drift trajectories can be calculated and various magnetohydrodynamic (MHD) stability criteria can be examined.

It appears that finite beta can eliminate a loss mechanism which exists for particles in the vacuum fields alone. Calculation of drift trajectories in the vacuum field shows that there is a small class of poorly confined particles whose drift surfaces are not topologically equivalent to concentric circles but have a banana-like structure. The underlying reason for this structure becomes apparent if one examines $|B|$ in a plane perpendicular to the magnetic axis, this plane being located approximately two-thirds the distance between a midplane and the plane of a coil. In this plane, contours of constant $|B|$ exhibit the same banana-like structure that the drift surfaces have. If the plasma pressure is sufficiently high near this region, the topology of these $|B|$ contours can be changed so that the banana-like structure no longer exists, and hence the loss mechanism ceases to exist. A major objective of this investigation was to put this qualitative argument on a quantitative footing.

One objective of the calculation of MHD stability is to determine the importance of line-tying from a theoretical standpoint. It is possible that finite beta equilibria exist which are stable against interchanges. If this is the case, one can have greater confidence in omitting limiters from the ELMO Bumpy Torus. Even if such a situation does not exist, one can determine how much of the annular plasma must be line-tied to provide stability and design limiters accordingly.

We now review the present and projected status of this project. We have developed a three-dimensional code which calculates the self-consistent equilibria and drift surfaces for the canted mirror. This code produces plausible results. In order to verify these results in the limit of zero cant angle, a two-dimensional code has been developed which calculates axisymmetric equilibria. When the three-dimensional code is fully operational, we will begin to explore the question of particle trajectories.

The two-dimensional code has proved to be useful in its own right. It is just now being modified to calculate various stability criteria for interchanges and to provide values of B which can be compared with experimentally determined values. This modification is nearly complete, and we can expect to undertake various parameter studies in a matter of days.

The present three-dimensional code for the canted mirror is readily modified to calculate equilibria for the ELMO Bumpy Torus. This will be done as soon as results for the canted mirror begin to flow in.

The algorithms for the present three-dimensional code were suggested to us by H. Grad. It is assumed that the pressure can be written as a function of B and a single-flux line coordinate. It appears that a more general formulation in which the pressure is a function of B and two-flux line coordinates is practical. This formulation will allow us to compute equilibria consistent with the microscopic distributions which can be unfolded from experimental data.²⁹

1.3.2 Interchange Stability in Anisotropic Plasmas

D. B. Nelson

Magnetic field structure and heating mechanisms in ELMO, Canted Mirror, and the Bumpy Torus lead to plasmas which are intrinsically anisotropic. Hence, questions concerning their MHD stability are poorly addressed within the scalar pressure framework, and we turn instead to the more general guiding center theory. In low-pressure plasmas the dominant low-frequency instabilities are the interchange modes. At higher pressure, modes which compress field lines without altering their shape (generalized interchanges) become energetically favorable as well. However, in this analysis we treat exclusively the simple interchange in which magnetic field strength is not varied.

Within the scalar pressure theory, the necessary and sufficient condition for variational stability to interchanges is that

$$p'(q) + \gamma p/q > 0, \quad q = \int dl/B.$$

Among the properties of this condition are the stabilizing effect of increasing beta and the requirement of an average magnetic well at the plasma edge [$p'(q) > 0$]. The added flexibility of the guiding center formulation does not allow such a simple stability condition. Different criteria result from each choice of distribution

29. G. E. Guest, C. L. Hedrick, and J. T. Hogan, *Hot-Electron Equilibrium in the Canted Mirror*, ORNL-TM-3473 (June 1971).

function. We here consider distribution functions of the form $f(\epsilon, \mu, \alpha, \beta) = \hat{f}(\epsilon, \mu) g(\alpha, \beta)$, where ϵ is the energy, μ the magnetic moment, and (α, β) are flux coordinates. This functional form produces reasonable agreement of the calculated equilibria with experimental data. For axisymmetry (α, β) can be replaced by the flux function ψ . The results reported here use this simpler formulation, but the generalization to nonaxisymmetry is immediate.

We also require local stability, which is equivalent to

$$\partial f / \partial \epsilon < 0,$$

$$\sigma > 0, \sigma = 1 + (p_{\perp} - p_{\parallel}) / B^2,$$

$$\tau > 0, \tau = 1 + \partial p_{\perp} / \partial B (B)^{-1}.$$

Since magnetic energy density is invariant under an interchange, we consider only the variational characteristics of the plasma energy, ϕ . The first variation leads to the equations of equilibrium; the second variation (for interchanges) is³⁰

$$\delta^2 \phi = - \int u^2 \left(\frac{\partial \epsilon}{\partial \psi} \right)^2 \frac{\partial f}{\partial \epsilon} dJ d\mu d\psi - \int u^2 \frac{\partial \epsilon}{\partial \psi} \frac{\partial f}{\partial \psi} dJ d\mu d\psi.$$

The condition for stability is $\delta^2 \phi > 0$.

The first term is manifestly positive if $\partial f / \partial \epsilon < 0$. A sufficient condition for stability is then positivity of the second term, which can be reduced to the requirement that on each flux surface

$$\frac{dg}{d\psi} \int [\hat{p}_{\perp} \nabla_{\perp} B + \hat{p}_{\parallel} \kappa] ds / B^2 < 0,$$

where \hat{p} is the moment of $\hat{f}(\epsilon, \mu)$, ∇_{\perp} is the component of the gradient perpendicular to the flux surface, and κ is the curvature vector. Since the magnetic field is depressed in the interior of the plasma, $\nabla_{\perp} B$ can be reversed and the interior rendered more stable by this criterion. Since it is difficult to reverse the sign of κ , stability favors $\hat{p}_{\perp} > \hat{p}_{\parallel}$. However, at the plasma edge this criterion cannot be satisfied unless the vacuum field is an average magnetic well.

Since the first term in our expression for $\delta^2 \phi$ is stabilizing, its contribution should give a more optimistic criterion. The derivative, $\partial \epsilon / \partial \psi$ at constant J , is difficult to evaluate, because it involves an integral over particle trajectories. An overestimate of the first term, leading to a necessary condition for interchange stability (and therefore a necessary condition for absolute stability), is obtained by approximating $\nabla_{\perp} B$ and κ by a constant over the particle trajectory. For ELMO this is not unreasonable, because most of the electrons mirror near the midplane. The necessary condition is then

$$\int \left[C_2 (\nabla_{\perp} B)^2 + \frac{2p_{\perp}}{B^2} \nabla_{\perp} B \cdot \kappa + \frac{3p_{\parallel}}{B} \kappa^2 \right] ds - \frac{dg}{d\psi} \int [\hat{p}_{\perp} \nabla_{\perp} B + \hat{p}_{\parallel} \kappa] ds / B^2 > 0,$$

where $C_2 = -m \int \mu^2 \partial f / \partial \epsilon dv d\mu$ is a positive quantity. It is related to pressure anisotropy because $C_2 > p_{\perp}^2 / 3p_{\parallel} B^3$.

Since the stabilizing term is pressure dependent, its contribution is greatest in the plasma interior. However, increasing C_2 up to the limit set by the mirror stability criterion should extend the stability boundary closer to the plasma surface.

Thus interchange stability of the guiding center plasma is similar to that of the scalar pressure plasma in being favored by high beta and an average magnetic well. A qualitatively new result is the advantage of large p_{\perp} compared with p_{\parallel} . It appears that interchange stability is enhanced in a plasma on the verge of the mirror instability. This observation is consistent with experimental data from ELMO, which in its stable state does exhibit $\tau \approx 0$, very nearly mirror unstable.

1.3.3 Double Adiabatic Theory of the Interchange Instability in a Closed-Line, High-Beta System

E. G. Harris³¹

The well-known $\oint dl/B$ criterion for hydromagnetic interchange instabilities in a closed-line system has been extended to anisotropic, high-beta plasmas. The double adiabatic (Chew-Gold-Berger-Low) theory is used. Since the formulas are rather cumbersome in their general form, we are investigating some special cases.

30. H. Grad, *Plasma Physics and Controlled Nuclear Fusion Research (Culham Conference)*, vol. II, p. 161, IAEA, 1966.

31. Consultant, Physics Department, University of Tennessee, Knoxville.

1.4 DATA ACQUISITION COMPUTERS AND REMOTE TERMINAL SYSTEM

Nancy A. Betz³² R. A. Dory
J. E. Francis O. C. Yonts

A computer system was designed and proposed³³ for ensuring rapid data sampling, storage, and analysis for the Thermonuclear Division experimental devices. Each large experiment (ORMAK, IMP, Bumpy_Torus) is to have a small autonomous computer attached to allow independent (noninterfering) operation of the experiments. However, to permit use of the more powerful computer facilities at the computer center, these will be connected through a central "pooling" computer and a phone line to the computer center. The pooling computer will serve to handle the encoding, transmission, and switching of data between the experiments and the large computer, and also very importantly, it will provide on-site (Building 9201-2, Y-12 Area) access to the computer center (Building 4500, X-10 Area) for computer users needing rapid job submission and data retrieval.

Detailed technical specifications have been prepared and submitted for competitive bids. The system is expected to be on hand by July 1972, and in routine operation by December 1972.

1.5 GENERAL THEORY; ABSTRACTS OF PUBLISHED ARTICLES

1.5.1 Flute Stabilization via Electrostatically Confined Cold Electrons³⁴

G. E. Guest E. G. Harris³¹

Flute instabilities driven by unfavorable magnetic field curvature can be stabilized by a positive ambipolar

32. Mathematics Division.

33. N. Betz, R. A. Dory, J. E. Francis, and O. C. Yonts, *Proposal for Computer Assisted Data Acquisition for ORNL Fusion Experiments*, ORNL-TM-3593 (October 1971).

34. Abstract of published paper: *Phys. Rev. Lett.* 27, 1500 (1971).

potential which confines cold electrons electrostatically. This mechanism does not depend on line-tying in the conventional sense. We derive stability criteria and discuss their relation to experimental observations.

1.5.2 Energy Transfer to Ions from an Unneutralized Electron Beam³⁵

M. M. Widner^{1 7} G. E. Guest
R. A. Dory

Simulation studies of the response of an inhomogeneous plasma to an unneutralized electron beam have led to an analytic theory of the energy transfer from the beam to ambient ions. Energy is transferred to the plasma by the ion-hybrid resonance and is retained because of phase mixing.

1.5.3 On the Derivation of the Quasilinear Equations³⁶

Junichiro Fukai^{3 7} E. G. Harris^{3 1}

A derivation of the quasilinear equations is given which is sufficiently general to include damped waves. The origin of some difficulties in previous derivations, the conservation of momentum and energy, and the origin of irreversibility are discussed.

35. Abstract of published paper: *Phys. Fluids* 14, 2547 (1971).

36. Abstract of paper accepted for publication in the *Journal of Plasma Physics*.

37. Present address: Department of Physics, University of Tennessee, Knoxville.

2. Mirror Confinement

W. B. Ard	N. H. Lazar
M. C. Becker ¹	J. F. Lyon
C. W. Blue	L. A. Massengill
R. J. Colchin	O. D. Matlock
J. L. Dunlap	R. G. Reinhardt
R. S. Edwards	W. J. Schill
G. R. Haste	O. C. Yonts

2.1 INTRODUCTION

The idea that a plasma, consisting of energetic electrons but cold ions, produced by electron-cyclotron heating can be used as a target for trapping of an injected, energetic atomic beam of hydrogen particles (primarily by charge exchange) has been discussed in previous annual reports and elsewhere. Our objective, in the past several months, has been the study of target plasmas, their stability and confinement, and particularly the attainable density and target quality (n_e/n_0) as a function of macroscopic parameters: magnetic field,

neutral pressure, applied rf power, and, to a limited extent, field shape.

Experiments have been carried out in two facilities: INTEREM, described earlier, and the new deep well facility, IMP. A comparison of the macroscopic parameters in the two facilities is given in Table 2.1. Earlier experiments have shown $n_e \sim 1-3 \times 10^{11} \text{ cm}^{-3}$ in INTEREM with

$$n_e/n_0|_{\text{max}} \cong 10.$$

The initial experiments at the higher fields in IMP indicate $n_e|_{\text{max}}$ scales as B_0^2 . Comparison of experiments in simple mirrors at much higher pressure, in the PTF and ELMO facilities, had previously shown a similar parametric behavior.

1. Instrumentation and Controls Division.

Table 2.1. Comparison of IMP and INTEREM Parameters

	INTEREM	IMP
Magnetic field		
B_0	~3 kG	~10 kG
R_z	2	2
R_\perp	1.2	1.75
B_{res}	3.78 kG	12 kG
Heating power		
Resonant	10.6 GHz (<15 kW)	36 GHz (<1 kW)
Nonresonant	36 GHz (<1 kW)	55 GHz (<10 kW)
Neutral density		
Base	5×10^{-8} Torr ($1.8 \times 10^9 \text{ cm}^{-3}$)	$<5 \times 10^{-9}$ Torr ($1.8 \times 10^8 \text{ cm}^{-3}$)
Operating	$n_0 > 1.5 \times 10^{10} \text{ cm}^{-3}$	
Electron density		
For $\omega_{pe}/\omega_{ce} = 1$	$1.3 \times 10^{12} \text{ cm}^{-3}$	$1.4 \times 10^{13} \text{ cm}^{-3}$

A density scaling as B^2 is necessary if an electron-cyclotron heated (ECH) plasma is to be used as a target plasma. This is because shielding and beam trapping considerations require densities of the order of 10^{13} , about 100 times the density of the early experiments. Microwave power sources were available at ten times higher frequencies, corresponding to a tenfold increase in B . Thus, from the first, the target plasma concept was based on the assumption $n \propto B^2$. The required densities imply $\omega_{pe}^2/\omega_{ce}^2 \gtrsim 1/3$ at 10–20 kG. The early experiments in IMP show $\omega_{pe}^2/\omega_{ce}^2 \approx 1/3$ at 10 kG.

In addition to the experiments in IMP, a series of studies has been carried on in the INTEREM facility to determine the plasma shape and volume when using ECH in a magnetic well. The motivation for these studies is: (1) to establish quantitative comparisons between total stored energy ($nT_{\perp}V$) and alternate measurements of density and mean energy, (2) to determine if the plasma pressure influences the equilibrium distribution, and (3) to determine if the heating process can be better understood with more complete spatial distribution information. The results of the experiments gave information on all three of these points. Most illuminating is the evidence that resonant heating, that is, heating of particles in the “resonant zone,” has greatest effect when the particles are below ~ 100 keV. When low resonant power is applied, the density profile, when unfolded, shows a strong peak in P_{\perp} corresponding to low-energy particles reflecting near the resonant zone. When the power is raised, higher-energy particles appear, in general closer to the mid-plane, that is, with larger μ/E . This increase in μ/E results only when particles are heated inside their mirror reflection points; that is, when $v_{\parallel} \neq 0$. It is not yet possible to determine if the spatial distributions are strongly influenced by finite plasma pressure; nor can we make quantitative comparisons between predictions from the theory of “mirror” instabilities, since a determination of the self-consistent equilibria, including the proper influence of plasma pressure, has not been completed. More detailed calculations of this type are being undertaken.

2.2 TARGET PLASMA EXPERIMENTS IN IMP

The superconducting mirror-quadrupole facility IMP became operational at midyear. Our principal experimental interest to date has been to secure data for comparison with the hot-electron plasma in the INTEREM facility, also a mirror quadrupole. We anticipate that the major differences will result from the

difference in magnetic field strengths, or correspondingly the microwave heating frequencies. INTEREM operates with $B_0 = 3$ kG, a factor of about $1/3$ that used thus far in IMP.

Figure 2.1 shows a magnetic field configuration typical of those we have employed in IMP. An 8-mm microwave supply provides resonant heating at the 12.5-kG contour for nonrelativistic electrons. In addition, many experiments have made use of 5.5-mm microwaves for off-resonance heating. The two microwave supplies are continuous wave, each nominally 1 kW.

The experiments are done either with steady-state plasmas or with those decaying from steady state. Base pressures in the microwave cavity were usually in the range $1-2 \times 10^{-8}$ torr. An automatically controlled leak of hydrogen gas established the operating pressure level.

Discussion of the four basic diagnostics follows:

1. A measure of hot-electron density n_e is provided by ionization current flow to a small positively biased probe mounted on the Z axis in the high field region of one mirror coil. Measurements are made during the decay of the microwave plasma, which has a time constant of about 1 sec. Density is related to the ionization rate by assuming that the hot electrons are uniformly distributed along the Z axis between the limits of the resonant contour.
2. A measure of the mean energy of the hot electrons and a second measure of their density are provided by bremsstrahlung resulting from ion-electron collisions in the plasma. We use a single scintillation spectrometer and reduce the data with an on-line computer. The collimator is arranged to view across the plasma through the B_0 point, at a very slight inclination to the median plane. For reduction to n_e , we assume that the hot-electron density is uniform across the resonant mod- B contour.
3. Diamagnetic pickup loops register total stored W_{\perp} upon plasma decay. Calibrations for this diagnostic were provided by a driving coil of dimensions comparable with the resonant volume, and the calibrations were performed with the facility at operating temperatures.
4. The background neutral density, the ratio n_e/n_0 , and hence n_e itself are determined by use of an injected fast H^0 beam. The technique involves measuring charge-exchange signals from the decay of an injected fast-proton component and comparing signals for trapping on the hot-electron plasma with

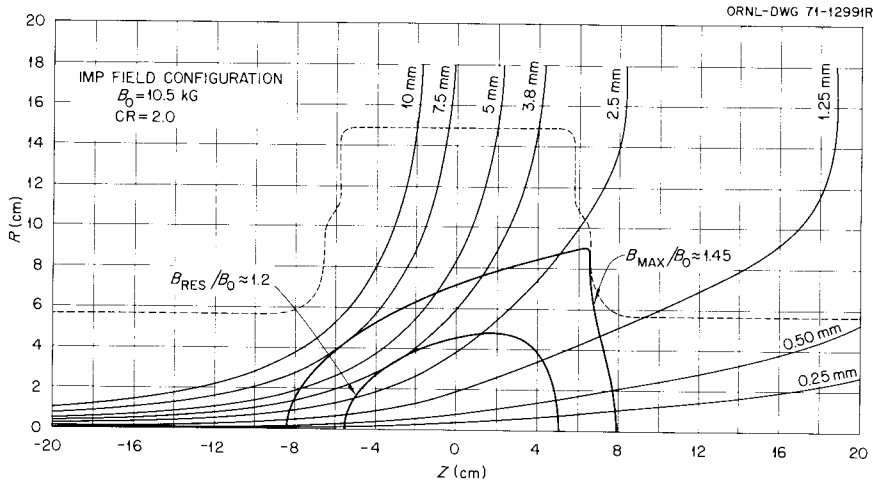


Fig. 2.1. Typical IMP field configuration. B_0 , the central field value, is 10.5 kG, and the compensation ratio is 2.0. The broken line indicates the outline of the microwave cavity. The field lines and modulus B contours are for a plane midway between the quadrupole "bars." The field lines are identified by their distance from the central field line at $Z = 20$ cm, at the converging end. The marginally closed contour, $B/B_0 \approx 1.45$, has an enclosed volume of about 2 liters; the resonant heating contour, $B/B_0 \approx 1.2$, has a volume of about 0.5 liter.

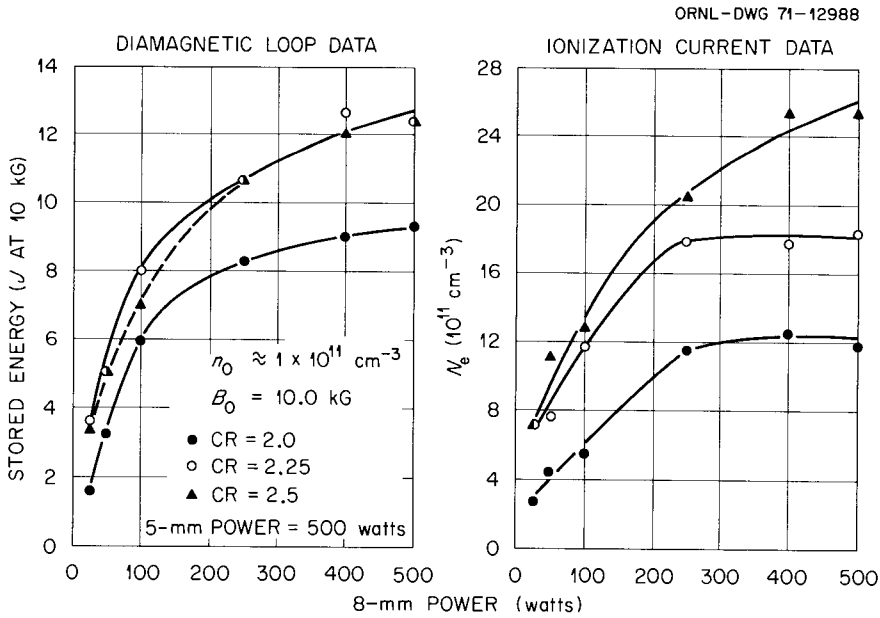


Fig. 2.2. Comparisons of electron densities obtained by diamagnetic loop and ionization current measurements.

those for gas ionization trapping at the same cavity pressure, that is, trapping with and without the target. In principle, two estimates of target density may be obtained: (1) from comparison of the trapping rates as deduced from the initial amplitudes of the decaying charge-exchange signals and (2) from comparison of the decay times, since the target acts as an ionizing shield to reduce the density of charge-exchange centers in its interior relative to its exterior. Low signal-to-noise is the basic problem with this technique, and this experiment is done

under computer control to average up to 10^4 decays for a single experimental point.

Figures 2.2--2.7 indicate the nature of results obtained with these diagnostics. Systematic variations of target density with power levels of the two microwave frequencies are reproduced by different methods of measurement (Figs. 2.2, 2.3, and 2.5). Figure 2.6 shows evidence for target shielding that also implies these same systematic variations. Figure 2.7 is a quantitative comparison of target densities obtained by different methods. (The shielding effect indicated by Fig. 2.6 implies densities comparable with those obtained from ionization current data, Fig. 2.7.) We have a spread in

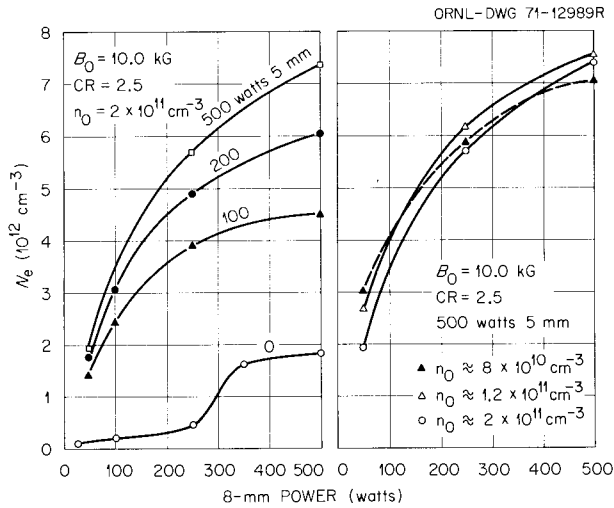


Fig 2.3. Target plasma density from bremsstrahlung measurements.

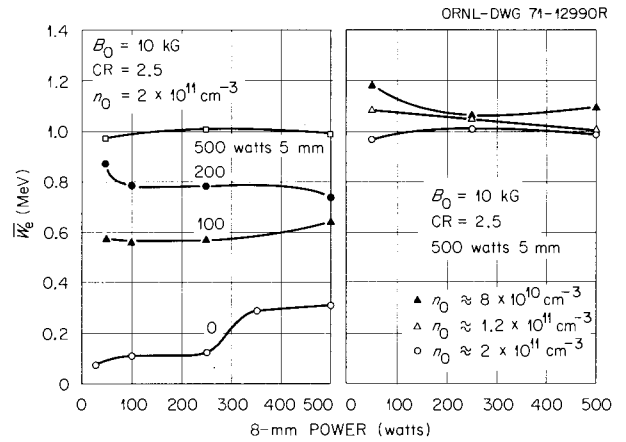


Fig. 2.4. Mean energies of hot electrons from bremsstrahlung measurements.

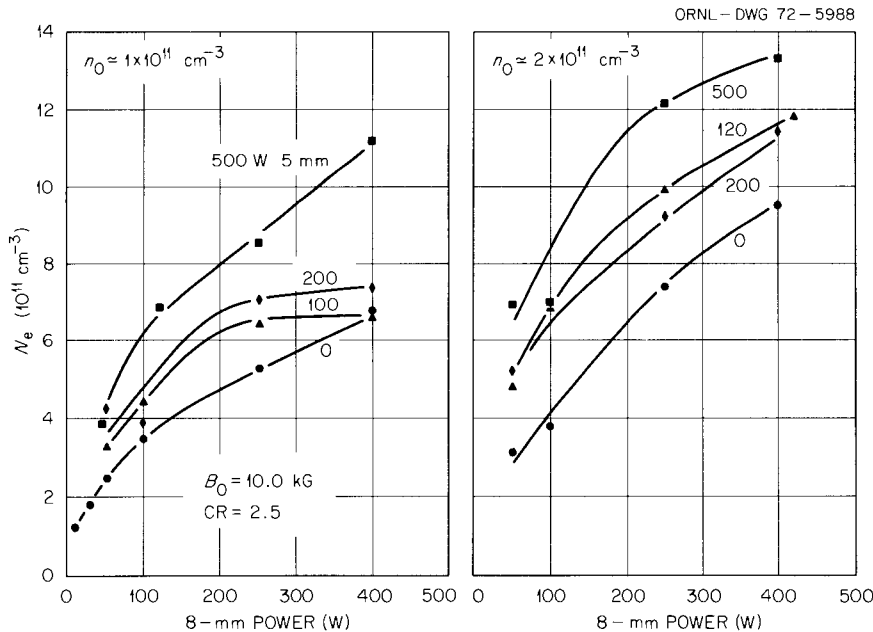


Fig. 2.5. Target plasma density from injected beam technique, comparing trapping rates with and without the target. Ion source optimized for H_2^+ production, 20-keV extraction.

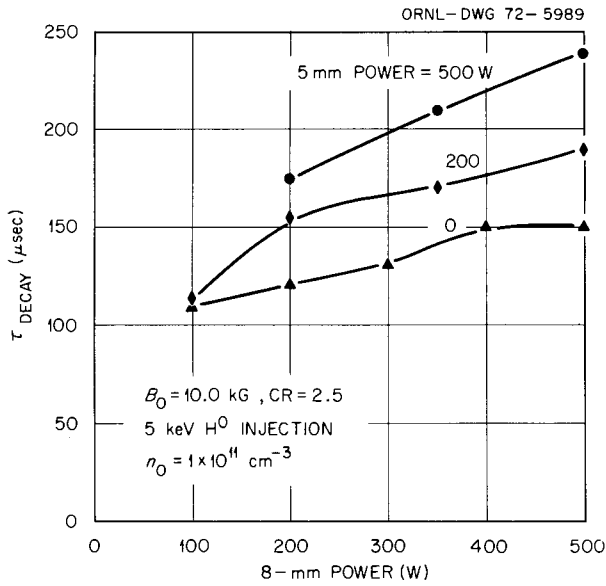


Fig. 2.6. Decay time of injected hot ion component as a function of microwave power. Ion source optimized for H^+ production, 5-keV extraction.

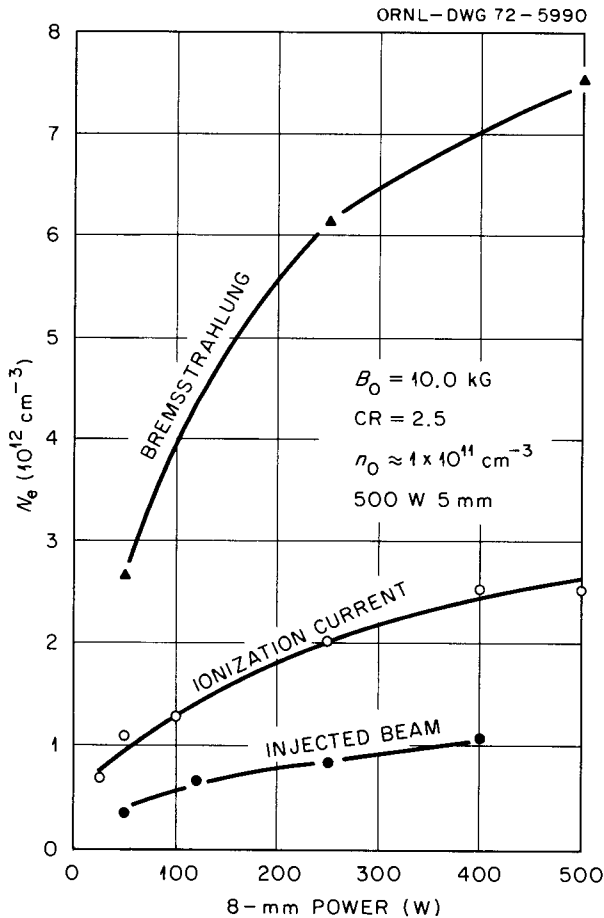


Fig. 2.7. Comparison of target density determinations by different techniques.

density determinations of a factor of 7. At this stage of our investigations, there are additional correction factors, easily of the order of a factor of 2, that are required for each of the diagnostics. These factors arise both from the basic mechanics of the measurements and from their sensitivities to the plasma's spatial distributions in density and mean energy, distributions which we have not defined in IMP.

Although we cannot definitively assign a density to the plasma, the convergence seems headed to the order of $3 \times 10^{12} \text{ cm}^{-3}$, an order of magnitude higher than in INTEREM and therefore implying a scaling like B^2 . Additional support for this conclusion is found in other comparisons with INTEREM, where similar diagnostics have been in use for a much longer time. The systematic variations with resonant and nonresonant power levels shown here are observed at both facilities. The spread in quantitative density determinations by the different diagnostics also appears at each facility, and a diagnostic-by-diagnostic comparison of the plasma densities shows values higher in IMP by about an order of magnitude.

The emphasis of work in progress is directed at convergence of the density determinations and at systematic studies of the plasma with wider ranges of field configuration and ambient hydrogen gas density. In this last connection, we are encouraged that brief studies at lower n_0 values, down to $\sim 3 \times 10^{10} \text{ cm}^{-3}$, have indicated plasmas not very different than at $n_0 \approx 1 \times 10^{11} \text{ cm}^{-3}$.

2.3 TARGET PLASMA STUDIES IN INTEREM

We have continued the bremsstrahlung measurements of the axial distribution of the hot-electron density in INTEREM. These measurements are made with an array of collimated detectors distributed along the axis arranged to view the plasma at various Z positions. The bremsstrahlung spectra obtained from each detector are analyzed by an on-line computer to give the electron distribution function at the corresponding Z location. Although changes in the shape of the distribution function may be noted, as a first step we use only the integral information, that is, density and mean energy.

We have measured the profiles of density and mean energy as a function of magnetic field, neutral gas pressure, and microwave power level.

The variation with magnetic field is shown in Fig. 2.8. The position of the resonant field was varied by increasing the strength of the mirror component of the magnetic field; the power level was varied to give approximately the same density for the three cases. It is

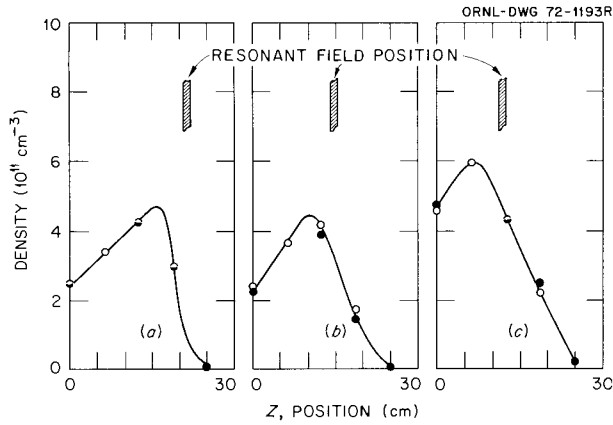


Fig. 2.8. Variation of density profile with magnetic field. The mirror and quadrupole field strengths were scaled by the same factors. Pressure $P = 4 \times 10^{-7}$ torr (gage) with hydrogen leak. (a) $B_0 = 3.0$ kG, microwave power $P = 800$ W; (b) $B_0 = 3.3$ kG, $P = 400$ W; (c) $B_0 = 3.6$ kG, $P = 200$ W. The solid and open circles correspond to successive measurements.

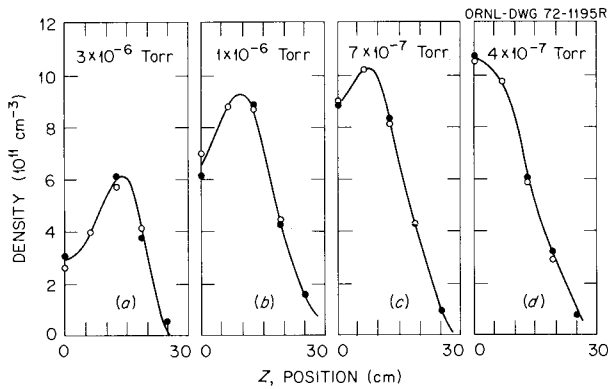


Fig. 2.9. Variation of density profile with hydrogen gas pressure. $B_0 = 3$ kG, microwave power = 800 W. (a) $P = 3 \times 10^{-6}$ torr (gage); (b) $P = 1 \times 10^{-6}$ torr; (c) $P = 7 \times 10^{-7}$ torr; (d) $P = 4 \times 10^{-7}$ torr.

seen that the peak of the density profile occurs near the resonant field position in each case.

The variation of the profiles with neutral gas pressure is shown in Fig. 2.9. At the highest pressure, Fig. 2.9a, the profile is peaked near the resonant field position. As the pressure is reduced, Fig. 2.9b and c, the peak moves toward $Z = 0$. At the lowest pressure, Fig. 2.9d, the peak of the profile occurs at $Z = 0$.

The variation of the density profile with microwave power level is shown in Fig. 2.10. This variation is similar to that seen with neutral gas pressure. At the lowest power level, Fig. 2.10a, the profile is peaked near the resonant position. At the highest power level,

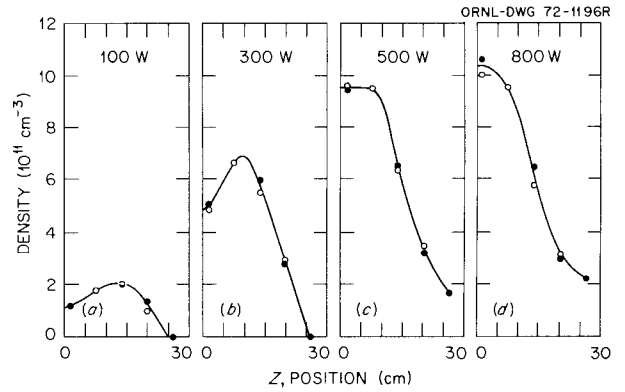


Fig. 2.10. Variation of density profile with microwave power. Pressure $P = 4 \times 10^{-7}$ torr (gage); microwave power (a) 100 W, (b) 300 W, (c) 500 W, (d) 800 W.

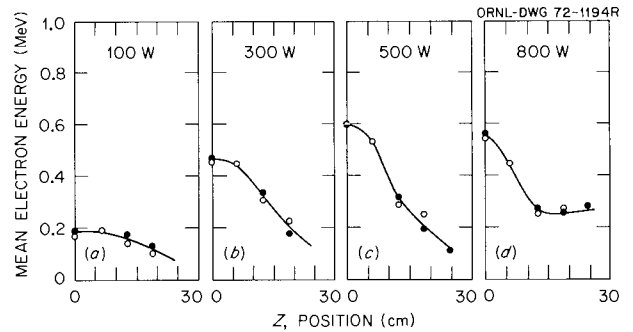


Fig. 2.11. Variation of mean energy profile with microwave power. Same conditions as Fig. 2.10.

Fig. 2.10d, the peak is at the midplane. The profiles of mean energy shown in Fig. 2.11 behave similarly. At the lowest power level, Fig. 2.11a, the mean energy is low and relatively uniform along the axis. As the power level is raised, the mean energy increases and the profile shows a peak on the midplane.

It is possible to obtain profiles of the plasma pressure components from the density profiles. The present technique involves assuming the plasma particles execute simple harmonic motion along the Z axis and then finding the mean v_{\perp}^2 and v_{\parallel}^2 for the distribution at each point. The profiles of the pressure components, P_{\perp} and P_{\parallel} , are shown in Fig. 2.12 for the data of Fig. 2.10. These profiles are normalized to a peak amplitude of 0.25. Also shown in the figure is the ratio P_{\parallel}/P_{\perp} which is a measure of the plasma anisotropy.

These results lead to several conclusions. It appears that reducing the neutral gas pressure is equivalent to raising the heating power, in that they have similar

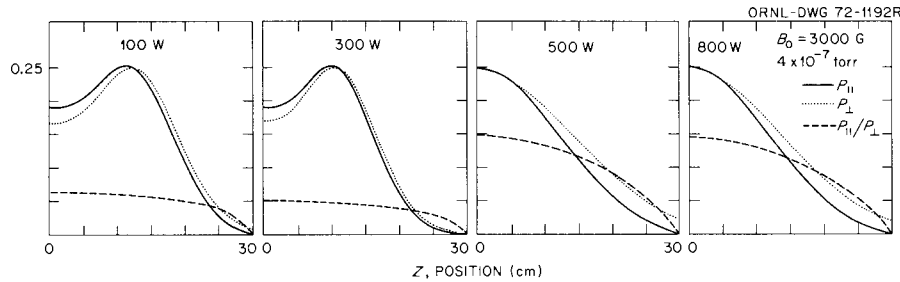


Fig. 2.12. Variation of profiles of plasma pressure and anisotropy with microwave power level. Same conditions as Fig. 2.10.

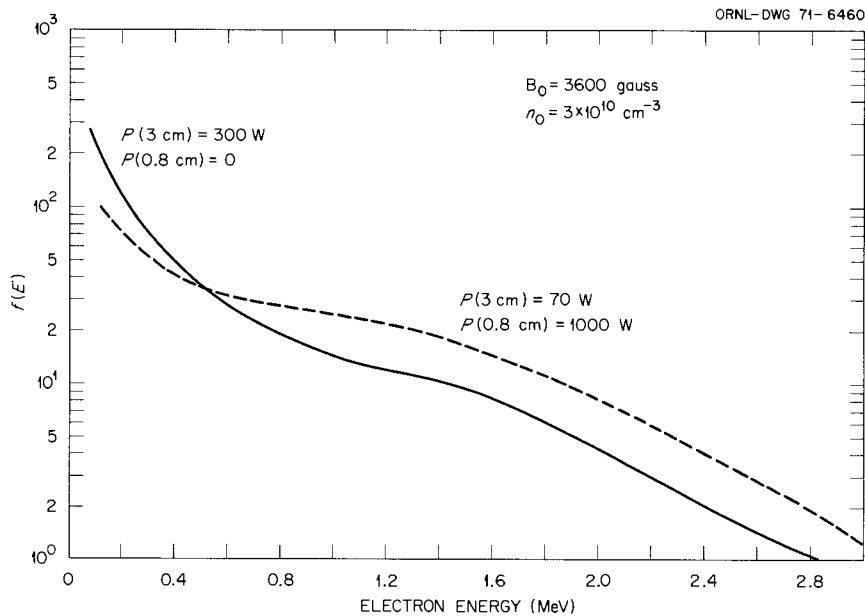


Fig. 2.13. Illustration of changes in the electron distribution function with upper off-resonance heating. The solid curve is with 300 W of 10.6-GHz power alone; the dotted curve is with 70 W of 10.6-GHz power plus 600 W of 36-GHz power. $B_0 = 3.6$ kG; pressure = 3×10^{-7} torr.

effects on the gross plasma properties (plasma density, energy, and volume). It seems plausible that the effective heating rate should increase either with increased power or with reduced pressure. The increased heating rate with power is a natural consequence of the increased electric field, but the reason for the increased heating rate resulting from lower pressure is less transparent. As the pressure is lowered, the ionization rate is reduced and thus less power escapes the plasma volume in the form of low-energy particles. For a given power input, the net power supplied to the plasma is increased, thus increasing the heating rate per particle. Another conclusion is that at the highest effective heating rate the plasma is confined near the midplane. Two explanations for this effect are possible. First,

there is appreciable plasma diamagnetism in some cases, so the plasma magnetic field may influence the equilibrium configuration. Second, if the particles gain perpendicular energy at positions where $v_{||} \neq 0$, then their pitch angle diminishes as their energy increases. Thus the highest-energy particles would be nearest the midplane, as observed.

We have examined the electron energy distribution function when using upper off-resonance heating. In the previous annual report,² we stated that adding power at 8 mm (36 GHz) resulted in stable plasmas. The electron distribution functions are shown in Fig. 2.13 for two cases. The solid curve corresponds to a high-density

2. *Thermonuclear Div. Annu. Progr. Rep. Dec. 31, 1970, ORNL-4688, p. 24.*

plasma obtained with single-frequency heating at 10.6 GHz. This plasma is highly unstable. The dotted curve is the distribution function obtained when using both heating frequencies. This plasma is stable; that is, no rf activity can be detected nor can low-frequency fluctuations in the ionization current be seen. The principal difference in the distributions is the increase in the population of relativistic electrons when nonresonant heating is applied. In the case of whistler instabilities,

Hedrick³ has shown that relativistic particles in the distribution tend to stabilize the mode, because the spread of cyclotron frequencies contributes to damping. One might reasonably expect similar effects for the other observed instabilities, the double distribution mode, and negative mass.

3. C. L. Hedrick, *ibid.*, p. 6.

3. The ORMAK Program

D. D. Bates ¹	S. M. DeCamp	William Halchin	V. J. Meece
L. G. Bean	P. H. Edmonds	R. E. Hill ²	Masanori Murakami
L. A. Berry	J. C. Ezell	G. G. Kelley	R. V. Neidigh
J. F. Clarke	J. E. Francis	J. R. McNally, Jr.	Michael Roberts

3.1 INTRODUCTION

The most exciting thing about Tokamak devices³ is that they produce relatively hot plasmas in which the ion thermal losses are not essentially greater than those predicted for classical processes. So far, the plasmas have not been hot enough to allow the ion orbits to be affected, between collisions, by the gross shape of the magnetic field. The qualitatively different regime in which the ions are sufficiently hot to be affected by the magnetic field is called the collisionless regime. This is the regime in which a fusion reactor will operate. Scaling considerations indicate that the ion temperature in an Ohmically heated ORMAK will be sufficiently high to put the plasma well into this regime. We are particularly anxious to get a high-temperature plasma, because there are some reasons (thermal conductivity is $\sim T^{-3/2}$ in the collisionless regime) to believe that the thermal insulation will be greater at higher temperatures, and on the other hand some reasons (the possibility of instabilities caused by trapped particles) to believe that things will get worse. We need the experiment to find out. ORMAK is unique among Tokamaks in its combination of low plasma aspect ratio ($A \equiv R/r = 3.4$), its relatively large minor diameter, its high plasma current, moderate toroidal magnetic field, and long pulse duration. The Russian Tokamak T-6 experiment,⁴ which is now operational, has a very

similar configuration but is presently limited to lower design magnetic fields and shorter experiment times. Other experiments in operation in this country, the model ST⁵ at the Princeton Plasma Physics Laboratory and Doublet II⁶ at Gulf General Atomic, have different configurations but operate in the same range of magnetic fields.

At present, Tokamak plasmas are heated by the toroidal current. This method of heating does not put as much power into the plasma as we would like. We expect in the future to increase ion temperatures further by energetic neutral particle injection — as will be described in Sects. 1.2.3, 3.4, and 6.

3.2 THE ORMAK DEVICE

Figure 3.1 is a cutaway view of the device. The plasma fills a toroidal region having a minor radius r of 23.5 cm and a major radius R of 79.5 cm, giving the plasma aspect ratio A of 3.4. The toroidal magnetic field is provided by 56 generator-driven coils held in aluminum frames. Currents up to about 450 kA can be induced in the plasma by conductors wound parallel to the major circumference of the torus on the outside of a surrounding 1-in.-thick aluminum shell. The combination of the imposed toroidal magnetic field and the poloidal field produced by the plasma current itself contributes to the equilibrium and stability properties of this kind of discharge. A small, nearly uniform vertical field, necessary for controlling the position of the plasma, is provided by conductors wound inside the aluminum shell. The plasma region is surrounded by a 0.25-mm-thick stainless steel liner which is continuous,

1. Instrumentation and Controls Division.

2. General Engineering Division.

3. L. A. Artsimovich et al., paper CN-28/C-8, IAEA Conference on Plasma Physics and Controlled Nuclear Fusion Research, Madison, Wis., June 1971.

4. V. S. Vlasenkov, E. P. Gorbunov, V. S. Mukhovatov, M. P. Petrov, and L. D. Sinitsyna, paper CN-28/F-8, IAEA Conference on Plasma Physics and Controlled Nuclear Fusion Research, Madison, Wis., June 1971.

5. H. P. Furth, *Bull. Amer. Phys. Soc.* **16**, 1231 (1971).

6. T. H. Jensen, A. A. Schupp, Jr., and T. Ohkawa, *Bull. Amer. Phys. Soc.* **16**, 1231 (1971).

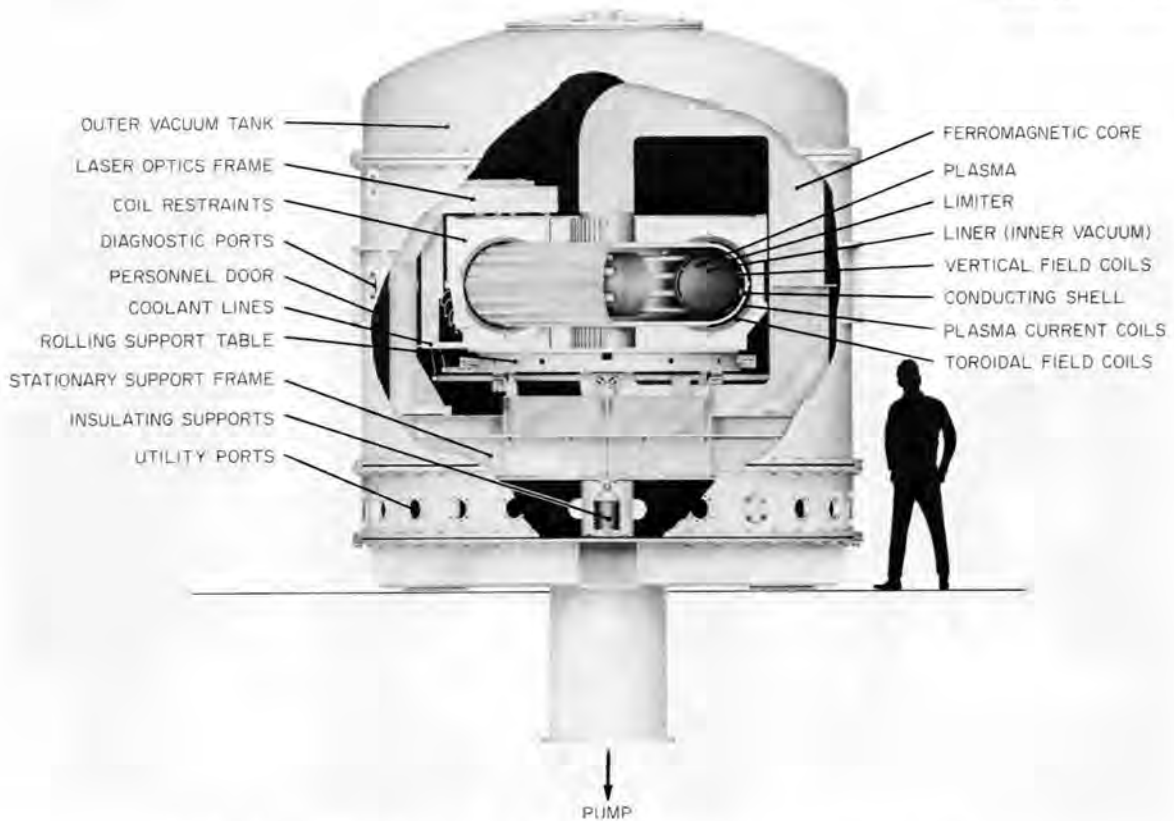


Fig. 3.1. Cutaway view of ORMAK device illustrating major components and access.

and separately pumped. A solid tungsten, azimuthally segmented aperture (limiter) determines the minor diameter of the plasma. The entire device is in an outer vacuum region, and all parts will be operated at liquid-nitrogen temperature. This low temperature reduces the resistivity of copper by about a factor of 8 and permits the use of coils with smaller cross sections. To increase the inductance of the plasma driving transformer, there is an iron core which with back bias has a flux change capability of 0.55 V-sec. The maximum design toroidal magnetic field is 25 kG and can be held flat for more than 0.2 sec.

The mechanical construction of ORMAK was finished in January 1971, and at that time shakedown of the components was begun. There were difficulties with the vacuum system, with the generator control circuitry, and with electrical breakdowns, which kept us from beginning operation until about mid-June. In addition, the minimal-cost liquid-nitrogen cooling system actually was unsatisfactory and had to be redesigned; so the first phase of operation was at room temperature and therefore at about a third of the design magnetic field.

We set as our objectives for this phase the checkout of all the electrical systems and the diagnostics, with a quick look at the properties of the plasma on the philosophy that more significant results would be obtained at full field. This limited phase was ended in late summer with most of the objectives attained. All the diagnostics were tested, but the Thomson scatter laser, the soft x-ray analyzer, the optical spectrometer, and the neutral-particle analyzer did not give useful data because of interference from hard x rays in their detectors. The complete generator regulator system was not needed for room-temperature operation and was not tested.

By the end of the year the new liquid-nitrogen cooling system was operational (Sect. 8.2 discusses the character of the system in some detail), the coils had been cooled, and the vacuum was about 2×10^{-7} torr in the outer vacuum region. Testing of the complete toroidal field supply has begun, and at year-end, regulated currents ($\sim 1/3$ design level) have been passed through the coils.

3.3 EXPERIMENTAL RESULTS

During the summer, approximately 100 plasma discharges were made for which we recorded loop voltage and plasma current (by Rogowski loop) and x-ray emission. On a few shots we have microwave interferometer data and a measurement of H_{α} and H_{β} light, both of which are obscured by x-ray interference. In addition, there is an indication of plasma position from magnetic probe measurements. We were able to record photographically hydrogen spectra and first ionization levels of impurities that are probably indicative of the initial breakdown phase of the discharge.

Fig. 3.2 shows one of our typical shots. In this case a potential difference of 44 V was applied around the loop at $t = 0$, using a 20-kJ capacitor bank. No preionization was used during these experiments, and in this particular shot, breakdown did not occur until 1.4

msec. (There is an initial step in current due to conduction of the liner.) The plasma current rose to a peak of 84 kA in 34 msec. The voltage at peak current was 0.31 V, implying a Spitzer conductivity temperature of 350 eV. At about 10 msec the voltage had fallen to less than 6 V. This is the voltage at which a transistor-controlled storage battery supply begins to share the plasma current load. This supply was providing all the current during the latter part of the discharge. When it was turned off at about 95 msec, the voltage swung negative where it was clamped by diodes. There are small, positive, irregular step fluctuations in the voltage trace and small, correlated negative steps in the current signal. Frequency response is limited in both channels, however, to about 10 kHz, since measurements are made outside the stainless steel liner. There is considerable x-ray emission early and late in the discharge but very little during most of the pulse.

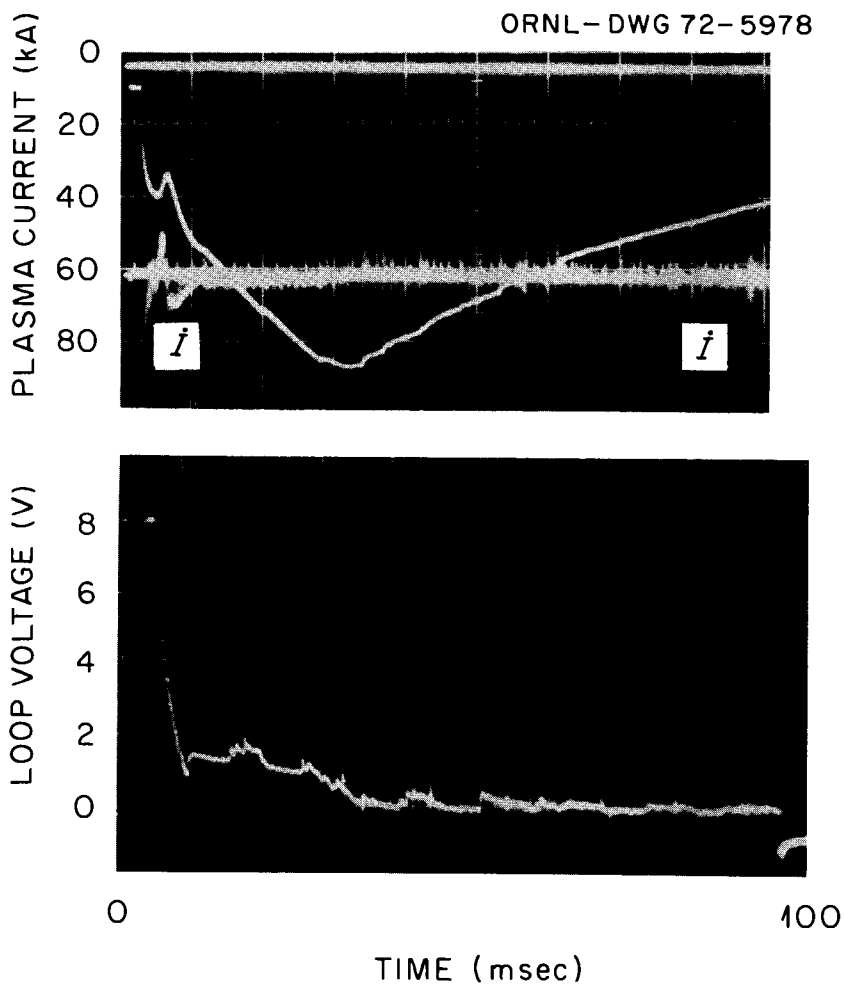


Fig. 3.2. Typical discharge conditions in early ORMAK experiments. Plasma current, voltage, and current derivative as a function of time. Shot No. 75.

Some shots such as in Fig. 3.3 show a more regular and marked pattern of fluctuations. The steps here occur with a repetition frequency of 1 to 1.5 kHz. We have microwave interferometer scans but only in this regime. These data show the line density rising abruptly during a burst and then falling more than a factor of 2 along an exponential-like curve. We infer from the interferometer data an average density of about $5 \times 10^{12} \text{ cm}^{-3}$. The voltage steps and sudden increase in density were accompanied by bursts of very hard x rays. The x-ray emission may be very great during a burst, but the average level was of the order of 100 mR/sec – through 0.25 mm of lead and at a distance of 1.5 m from the source. Five centimeters of lead gave a film dose reduction of a factor of between 4 and 5. A shadow experiment showed two sources of x rays – the tungsten limiter and a 0.25-mm stainless steel electrode, which is supposedly in the shadow of the limiter. The initially sharp limiter edges showed a rounding at the outer edge of the plasma of approximately 0.75 mm radius extending a few centimeters about the center line. Compared with this damage, the rest of the limiter showed negligible effects. About 20% of the hard x rays came from the stainless steel. This very thin electrode showed almost no damage, implying that very little average power is in relativistic electrons. In fact, only

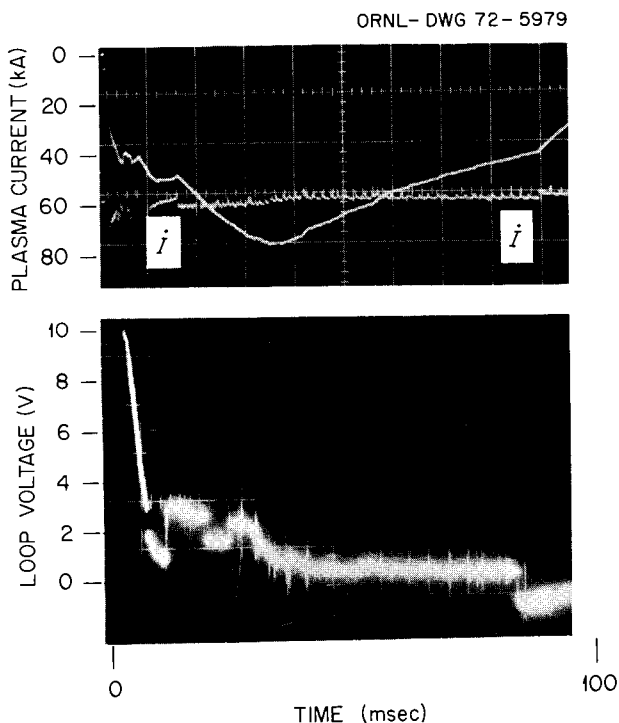


Fig. 3.3. Another early discharge condition in ORMAK, showing rapid current fluctuations. Shot No. 87.

Table 3.1. Comparison between ORMAK and T-6 devices

	ORMAK	T-6
Major radius	79.5 cm	70 cm
Shell inner radius	28.5 cm	25 cm
Shell thickness	2.5 cm Al	0.8 cm Cu
Limiter radius	23.5 cm	15 to 25 cm
Toroidal magnetic field	7 kG warm 25 kG cold	Data at 7 kG 15 kG design
Plasma current	90 kA warm 400 kA cold	45 kA
Pulse duration	>0.1 sec	15 msec in present experiments

hundreds of microamperes of 1- to 3-MeV electrons are required to account for the observed average x-ray flux, and if all of the charge represented by these fast electrons were circulating simultaneously, it would account for less than 5% of the total current. The possibility that a much larger fraction of the current was carried by not-so-energetic runaway electrons cannot, however, be ruled out.

The same behavior as has been seen in ORMAK has been observed in the T-6 experiment, which has about the same configuration. In addition the T-6 magnetic field is the same as in our first experiments. Table 3.1 presents a comparison of the two devices. There is an even greater similarity in results when we use only the capacitor bank. The T-6 group made poloidal beta (poloidal beta $\equiv \beta_p$ = ratio of kinetic pressure to poloidal magnetic field pressure) measurements⁴ which showed that along with the x rays, there was a sudden increase in transverse plasma pressure accompanying a burst. The T-6 data also showed the discharge shrinking in minor diameter with time. We infer, however, from inductance measurements at turnoff that the current-carrying cross section in ORMAK is at least two-thirds of the aperture size at this time in some cases. Also, position measurements showed only small outward shifts of about 1 cm along with smaller oscillating movements with amplitudes of ~ 2 mm. The quantity $\beta_p + l_i/2$ (l_i = plasma internal inductance) was calculated from the equilibrium condition of the plasma, showing an increase toward the end of this discharge which may imply a shrinkage of the plasma current channel. Figure 3.4 illustrates the outward shift and the quantity $\beta_p + l_i/2$ for a discharge whose characteristics I and V are also shown. We are unable to reconcile these observations with the interferometer results which show large fluctuations in line density along a vertical minor diameter. The ORMAK and T-6 both operate in about the same pressure range. ORMAK gives good results

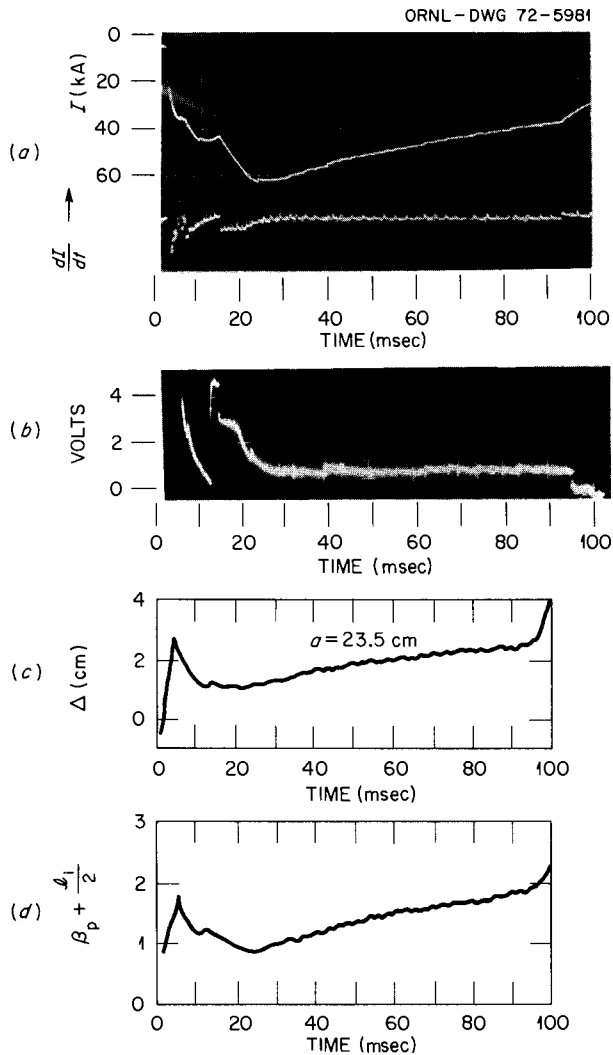


Fig. 3.4. Plasma column shift measurements. (a) Discharge current and current derivative. (b) Discharge loop voltage. (c) Measured radial outward shift. (d) Calculated $\beta_p + \frac{1}{2}$. $B_{\perp} = 17$ G for this discharge condition.

only for filling pressures below about 2×10^{-4} torr of H_2 . At higher pressure there is a breakdown, but the discharge goes out as soon as the capacitor voltage has fallen slightly.

At present, the process responsible for the burst phenomena is not understood. The question is whether or not the fast electrons carry the bulk of the current. On the one hand, there is sufficient time early in the discharge, when the loop voltage is high, for electrons to be accelerated to relativistic energies. It seems unlikely (but not impossible) that some roughly constant fraction of these electrons is lost in each instability burst. The evidence from the T-6 experiment, which showed a suddenly increased transverse plasma pressure, might indicate some instability which transfers

energy from the relativistic electron population to the rest of the plasma. Again, one would not expect this process to involve just a small fraction of the total population of the fast electrons in each burst. Unfortunately, we do not have reliable time-resolved x-ray intensity information which would show a dump of remaining relativistic electrons, if any, at the time of turnoff of the pulse. On the other hand, the electric fields present on the average during the main part of the discharge are much too small to accelerate cold electrons to relativistic energy *between* bursts. These latter fields are orders of magnitude below the critical electric field for production of runaway electrons. The possibility of very large electric fields within the plasma due to sudden changes in the current-carrying capability of a region in the plasma cannot be ruled out. This effect would not be seen outside of the liner. Another remarkable feature is the small fluctuation in loop voltage from burst to burst. If an electron temperature is responsible for the resistivity, one would expect rather large changes, but if most of the current is carried by fast electrons, the loop voltage might be low and nearly independent of the burst process. So the picture is obscure. There should be less tendency for this type of behavior at the higher magnetic fields and with the use of preionization. Some of our experiments did not show large x-ray emission during the main part of the discharge, and also, the Soviet T-6 team reports⁴ that there is an operating regime, dependent upon chamber conditions, in which these bursts do not occur.

3.4 RELATED THEORY

The effect of the electric fields on the ions produced by fast neutral injection has been of some interest this year. The radial electric fields produced by separation of the fast ion from its electron have been evaluated and are discussed in Sect. 1.3.3. The effect of the electric field driving the plasma current has also been investigated. We found that it could affect the slowing-down process significantly. Aside from the direct effect of accelerating or decelerating the fast ions, it also produces an electron drift (J/en) along the magnetic field which leads to an enhanced friction between the electrons and fast ions.^{7,8} In addition we found that the existence of a bootstrap current J_B in the plasma driven by density and temperature gradients also contributes to the electron-fast ion friction. We have

7. A. V. Gurevich, *Sov. Phys. JETP* **13**, 1282 (1961).

8. H. P. Furth and P. H. Rutherford, to be published in *Physics of Fluids*.

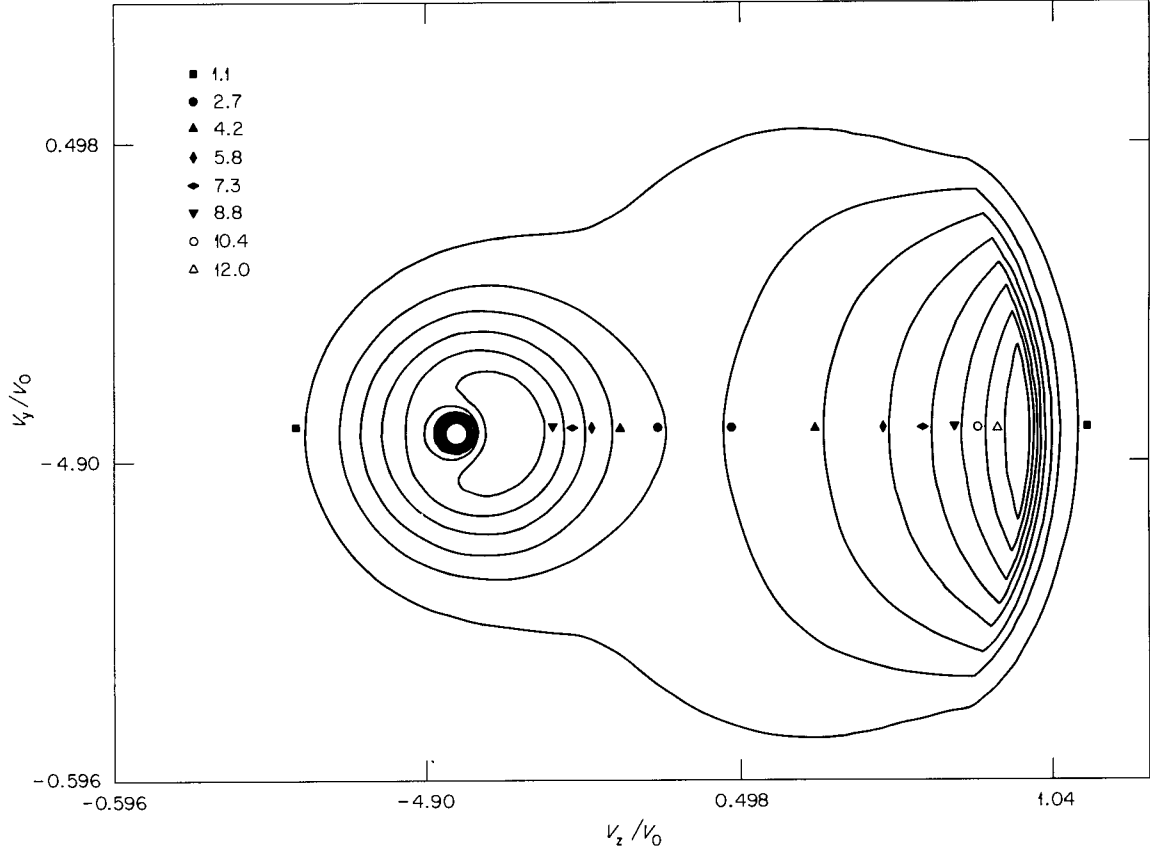


Fig. 3.5. Contour plot in velocity space for resultant distribution function f_α . $E = 30$ keV, $E^* = 0.8$ V/m.

shown that all three effects can be included in the calculation of fast-ion slowing down by introducing into the kinetic equation an effective electric field:

$$E^* = E \left[1 - \frac{Z_\alpha}{Z_i} \left(1 - 1.95 \sqrt{\frac{r}{R}} \right) \right] + \eta_{\parallel} J_B, \quad (1)$$

where from Rosenbluth et al.⁹

$$J_B = \frac{nT_e}{B_\theta} \sqrt{\frac{r}{R}} \left[-1.46 \left(1 + \frac{T_i}{Z_i T_e} \right) \frac{n'}{n} - \frac{T_e'}{T_e} + \frac{0.172 T_i'}{Z_i T_e} \right] \quad (2)$$

and η_{\parallel} is the Spitzer resistivity. The fast ions have charge Z_α , while the plasma ions are assumed to have charge $Z_i \gg 1$. If $Z_i = 1$ the coefficients of n' , T_e' , and T_i'

in Eq. (2) become 2.44, 0.69, and 0.42, respectively, since electron-electron collisions become significant.

We have solved the equation

$$eZ_\alpha \frac{E^*}{M_\alpha} \cdot \frac{\partial f_\alpha}{\partial \mathbf{v}} = C(f_\alpha, f_e^M) + C(f_\alpha, f_i^M),$$

where $C(f_\alpha, f_\beta)^M$ is the Landau collision operator and f_β^M is a Maxwellian; all non-Maxwellian effects are included in E^* . A contour plot of the resultant distribution function f_α is shown in Fig. 3.5, showing the peaking around the injection velocity v_0 . This peaking is very much enhanced by the action of E^* . Figure 3.6 shows one interesting consequence of the peaking of f_α . The plot shows the power deposited in the plasma by the fast ions relative to the injection power $I_0 W_0$ as a function of E^*/n .

The total current in the plasma increases because of the fast-ion current J . Since these fast ions are held in equilibrium mainly by the electron friction, the excess power is deposited in the electrons. At moderate

9. M. N. Rosenbluth, R. D. Hazeltine, and F. L. Hinton, to be published in *Physics of Fluids*.

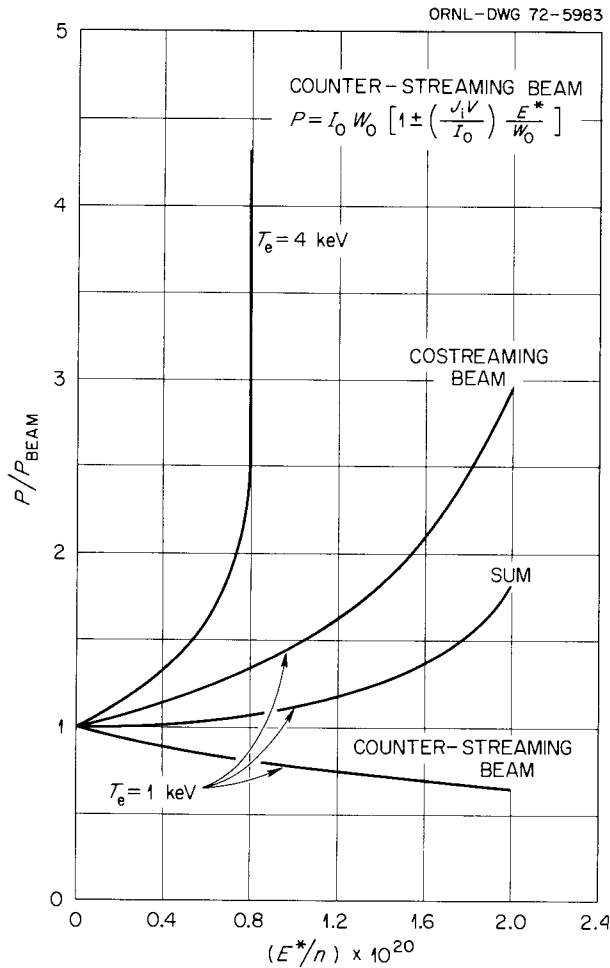


Fig. 3.6. Normalized power deposited in the plasma vs E^*/n . Costreaming refers to injection in the direction of the plasma current; counterstreaming to injection opposite to the direction of the plasma current.

densities this could lead to electron thermal runaway. In addition, if we reduce the plasma current in order to keep the total current constant, we will create a peaked current distribution in the plasma, since we can only affect the external layers of plasma current because of the skin effect. E^* inside the plasma is relatively fixed, especially that portion given by $\eta_{\parallel} J_B$. The net consequence of these effects is not clear, but together with the radial E field effects described in Sect. 1.3.3, they indicate the need for a vigorous and thorough experimental investigation of neutral injection heating.

3.5 DIAGNOSTICS

3.5.1 Thomson Scatter Experiment

During the low-magnetic-field experiments an attempt was made to measure the density and temperature of

the electrons with a simplified version of the Thomson scatter experiment previously described.¹⁰ Unfortunately, the high level of x rays emitted during a discharge produced noise signals which swamped any possible Thomson scatter signal. The ratio of x-ray-broadened signal to expected signal was in excess of 100 to 1. A lead shield structure has been constructed and installed to screen the detector system against both direct and scattered x rays.

The original design was simplified to a single spatial point measurement. This was done to permit alignment under vacuum at liquid-nitrogen temperatures, using a retractable alignment probe.

Under optimum conditions, Rayleigh scatter measurements, using nitrogen, have been made with a unity ratio of Rayleigh scattered signal to stray scattered signal for a filling pressure of 30 torr. For the current experimental configuration, which has no input baffles, this ratio is unity for a nitrogen pressure of about 450 torr. A reevaluation of expected scattered light intensity for this experiment suggests that for a plasma with a 500-eV electron temperature and a density in excess of $2 \times 10^{13} \text{ cm}^{-3}$, the measurements of temperature and density can be made with about 10 and 50% accuracy respectively.

An entirely new apparatus for Thomson scattering is now being designed which will permit alignment at liquid-nitrogen temperatures and movement to different spatial points between discharges. This new system is also expected to give a fivefold increase in scattered signal sensitivity.

3.5.2 Other Diagnostics and Plasma Production

The neutral-particle spectrometer device could not be tested during the first series of experiments because of very severe detector background produced by the x rays from the discharge.

The 2-mm Zebra-stripe microwave interferometer is installed and operational.

The optical spectroscopy equipment is installed, operational, and ready for plasma diagnostics.

The basic magnetic and electric plasma diagnostics were tested during low-field operation, and no major problems were encountered. A duplicate set of inputs has been interfaced into the PDP-8 computer. This addition is expected to improve the reliability of data acquisition.

10. *Thermonuclear Div. Annu. Progr. Rep. Dec. 31, 1970*, ORNL-4688, sect. 3.5.1, pp. 57-60.

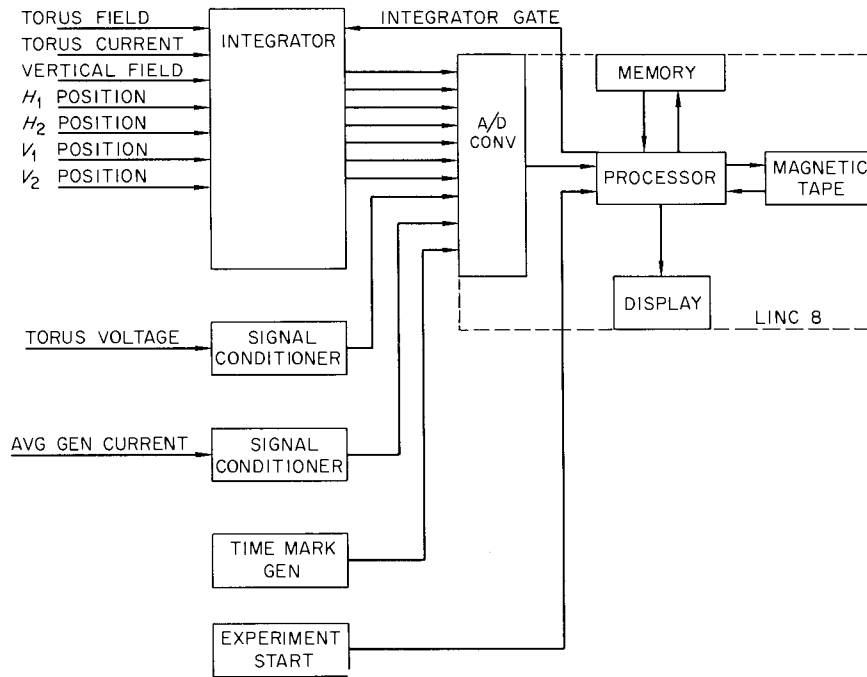


Fig. 3.7. Block diagram of LINC-8 diagnostic system.

Three additional schemes of preionization have been added to the existing loop voltage breakdowns for attempted operation at filling pressures higher than 2×10^{-4} torr. These three methods include applying a pulse of up to 40 kW of 8-mm microwave power to the gas, shining a low-power, dc ultraviolet light onto the gas, and exposing heated filaments to the gas.

3.5.3 Computer-Diagnostics Interfacing

The Linc-8 computer has been interfaced to ORMAK to measure and record the following parameters as a function of time during machine pulses:

1. toroidal magnetic field,
2. toroidal magnetic field coil current,
3. vertical plasma position,
4. horizontal plasma position,
5. vertical magnetic field,
6. toroidal loop voltage.

The maximum time difference for corresponding values of two variables is 0.5 msec. The raw data are displayed on the Linc-8 oscilloscope.

Software has been developed to record the data on magnetic tape and also recall the data from tape. Provision has been made for measuring eight additional

variables, using the computer A/D converter when sensors become available. Charge-exchange data accumulated by the Nuclear Data model 180 multi-channel analyzer can be recorded. All data are recorded with an identifying shot number and the date to provide correlation of data. Figure 3.7 illustrates the basic system. The use of this system eliminates one oscilloscope for each variable measured. Hardware is under development to add the laser scatter experiment to the computer interface. In addition, software is being assembled to permit on-line/off-line analysis of the stored data.

3.6 ENGINEERING

3.6.1 Toroidal Field Coil Power Supply

The primary problems in the initial generator regulator were electrical noises changing the state of the flip-flops in the logic circuitry and cross talk between turn-on and turn-off commands in the SCR switching associated with the generator fields. The first problem was corrected by adding pulse generating circuits that are level sensitive rather than trigger pulse time sensitive and then filtering the voltage levels before letting them into the regulator chassis. The second problem, however, required a complete reworking of the electronics

in parts of the generator field driving supply and switches. Closed-core pulse transformers were wound and used in the firing circuits for the SCR's, removing the cross talk.

Since ORMAK uses four times the rated drive voltage on the generator fields to achieve the necessary rate of current rise, the existing overvoltage protection relays were too slow to offer definite protection to the generator against flashover. A fast electronic sensor was built and installed and is to be checked out. The overcurrent protection circuit breakers were modified, calibrated, and set to trip at approximately $1\frac{1}{3}$ times the design current.

The primary circuit breakers between the generator and ORMAK were rebuilt twice, and adjustments were made several times to try to get them to close simultaneously. The closing scheme was also completely changed to get the breakers to close more nearly together, which necessitated changes in the experiment-finish circuitry in the generator regulator.

An instrument has been built and is now used to monitor the current through, and the voltage across, the six bus-bar pairs at the locations where each enters the vacuum tank. The primary purpose of the instrumentation is fault analysis, which is applied to the Ohmic heating and the vertical field as well as to the four generator systems.

Following the resolution of these difficulties, the set of four generators was successfully current regulated (each individual generator current is compared with the average) at about one-third the design current levels.

3.6.2 Control of Transistor-Battery Power Supplies

Large transistor-controlled storage battery supplies are used for inducing plasma current and for the production of the vertical magnetic field. We have had a higher failure rate of transistors in these supplies than we had hoped, but the trays in which these transistors are mounted are easily replaced individually, and from a practical point of view, the problem has not been a serious one. In the present arrangement the circuits are protected in such a way that failure of one component cannot cause other components to fail. These two systems were operated in open-loop fashion during the summer. We are prepared now to operate in a closed-loop mode which will permit the current wave shape to be controlled in an arbitrary manner within the limitations of the voltage available from the battery supplies. The capability for increasing the current from the plasma current supply is 10^7 A/sec.

3.6.3 Electrical Insulation

Two distinct schemes of insulation were used to isolate the various coil systems from adjacent conductors. The toroidal field coils (essentially 56 identical pieces) were wrapped with glass tape and coated with vacuum-impregnated epoxy applied with a precise mold. The plasma primary and vertical field coils (essentially 54 different shapes) were wrapped with glass tape and then hand coated with epoxy which was heat cured without any molds.

In practice, there have been no electrical breakdowns associated with the toroidal field coil insulation and many individual, localized breakdowns with the plasma primary coil insulation. Most of these latter coil difficulties have been associated with a breakdown from coil to torus through the epoxy insulation or near one of the joint areas where the coil insulation, of necessity, stops. Each of these individual breakdowns has been fixed by inserting insulation (Mylar or Nomex) at the proper place. In addition, the general occurrence of new breakdowns has been virtually eliminated by using the 9:1 turns ratio connection on the plasma primary coil rather than the higher-voltage 18:1 connection. The 9:1 ratio will be used until an improved insulation can be installed.

During initial excitation tests of all coils in combination, it was found that there were frequent occurrences of bus-to-bus shorts on the toroidal field coil feeders within the vacuum system. These high-energy shorts fortunately only damaged the cooling-line insulators on the bus feeder and not the coil leads themselves. The extent of the damage to the insulators was frequently enhanced by the bouncing of the main circuit breakers applying finite generator voltage to the low-level short. The shorts were apparently caused either by localized pressure bursts up into the critical range for voltage breakdowns around the insulators, or more likely by a reduction in insulation integrity by earlier plasma current coil breakdowns which faintly copper plated much of the surrounding insulation. In any case, removal of most of the possible gas sources, recoating the epoxy insulation, using Nomex sheet insulation at all critical locations, and carefully breaking up any breakdown paths resulted in a complete cessation of bus-to-bus breakdown.

3.6.4 Cooling

Vacuum leaks in the electrical insulators (~300 total) on the cooling lines inside the vacuum tank have been a

source of constant difficulty. The original insulator used a compression joint applied to a Lexan tube; this joint appears to require very precise installation and is susceptible to flexing. Following a considerable number of leaks and repairs, a copper-to-copper fitting with a cast epoxy insulator was tried as an answer to the vacuum leak. This insulator, unfortunately, was more susceptible to the electrical difficulties described above and was replaced with a standard glass-to-metal seal insulator. The glass insulator satisfied the electrical requirement and seemed to satisfy the vacuum required but was susceptible to breakage. A standard ceramic-to-metal seal was then tried, and it satisfied all the requirements, with the aggravating exception of occasional vacuum leaks at the metal-to-metal joint made at installation. All insulators are now the ceramic-to-metal seal type, and the last remaining difficulty appears to be associated solely with the procedure for making the joint and is being remedied with improved techniques and materials.

3.6.5 Injection-Related Changes

Design efforts have been concentrated in three areas: the neutral beam injectors and adaptations to the injectors to fit ORMAK; modifications to ORMAK to accept the injectors; and basic improvements to ORMAK that can best be accomplished at the time of the injection installation.

Although the basic injector has existed in the laboratory for some time, it was necessary to begin design studies aimed at supporting the injector in the horizontal plane, at providing a small amount of flexibility in the angle of injection, and at providing the necessary pumping to prevent excess gas from entering the plasma chamber. The injection angle flexibility should allow a test of the theoretical model (Sect. 1.2.3), which suggests varying degrees of success with injection as a function of the injection trajectory in ORMAK.

The primary modification to the machine is the remodeling of eight toroidal field coils to allow tangential access for the four 8.8-cm-diam neutral particle beams. Each of these modified coil pairs produces a maximum error field of about 100 G near the surface of the plasma with an extent comparable with the coil-to-coil spaces, that is, a few centimeters. Auxiliary coil compensation is being considered. Lesser modifications to the plasma primary and vertical field coils, torus, and vacuum tank ports are also necessary.

Since installation of the injectors necessitates demounting of all the toroidal field coils from the torus

and the removal of the liner, a few basic improvements to the machine are made feasible. One of the improvements is the building of a plasma liner with additional clearances, tighter tolerances on fabrication and assembly, and an improved, tested method for making the many demountable vacuum seals for diagnostic entry, in addition to the necessary changes for injection entry. A second change is in the scheme of insulation used to separate electrically the plasma primary and vertical field coils from the torus; an improved method of insulation based on experiences with the present epoxy-glass tape procedure is being investigated. A third item is the movement of many of the cooling pipes and electrical buses to positions allowing easier personnel movement and machine access.

3.6.6 Back Bias

The initial plan for back biasing the core of the plasma-driving transformer relied on remanence. In practice, air gaps in the core were too large for this system to work. A system which provides a steady back-bias current has been designed and installed. This supply is inductively isolated so that the bias current does not change during a discharge. The 0.72-V-sec capacity of the core was determined with an induction of 360 Oe. Using the steady-current system, a more practical back-bias level becomes 5 Oe, yielding a volt-second capability of 0.2 V-sec from the negative (back-bias) direction and 0.35 V-sec from the positive direction for a total flux change of about 0.55 V-sec.

3.7 FUTURE PLANS

We feel that we are close to having an operating device at full design levels and can begin experiments looking at some crucial questions concerning Tokamaks. Questions such as the effects of low aspect ratio and of operation in the regime of relatively low collision frequency can be investigated, and, perhaps, because of the relatively large bore and high temperature, we will begin to see the effect of finite penetration time of current changes in the plasma. We expect to be occupied with these questions until late 1972, at which time we intend a major shutdown for installation of two and perhaps four of the neutral-particle injectors developed by the EPI Group. The additional energy input from these sources will allow us to move further into the region of low collision frequency and should indicate the usefulness of neutral injection as a technique for heating still larger devices.

4. High-Beta Plasmas

4.1 HIGH-BETA RELATIVISTIC ELECTRON PLASMAS IN AXISYMMETRIC AND NONAXISYMMETRIC MIRRORS¹

R. A. Dandl² G. E. Guest
H. O. Eason C. L. Hedrick
P. H. Edmonds J. T. Hogan
A. C. England J. C. Sprott

Plasmas with $kT_e \sim 1$ MeV, $n \sim 10^{12}$ cm⁻³, and stored energies as high as 360 J in a volume of 2 liters have been produced and confined in a 2:1 mirror trap (ELMO) using simultaneous resonant (35-GHz) and off-resonant (55-GHz) continuous-wave microwaves. The stable, steady-state, relativistic electron plasma is confined in an axisymmetric annular region near the midplane of the mirror trap.

The self-consistent magnetic field has a minimum in the annular region, so that the main body of the plasma is in a magnetic well. The outer surface of the plasma is in a region of unfavorable curvature and is stabilized by line tying to conducting end walls. The amount of cold plasma required for particle equilibrium exceeds by two orders of magnitude that required for stability.

A new machine (the canted mirror) has been constructed to study the limitations on equilibrium and stability of a high-beta plasma ring resulting from deformation of the initially axisymmetric mirror trap into one sector of a "bumpy torus" geometry. In these experiments the mirror coils are mechanically rotated through equal angles in opposite directions about parallel axes which are perpendicular to the original axis of symmetry of the mirror. The effects of the high-beta plasma equilibrium on the nonaxisymmetric confinement geometry are being ascertained. This experiment is the first step in a program whose eventual goal is a toroidally confined plasma incorporating a set of mirror-confined high-beta plasma rings.

1. R. A. Dandl et al., abstract of Paper CN-28/G-4, IAEA Conference on Plasma Physics and Controlled Nuclear Fusion Research, Madison, Wis., June 1971.

2. Instrumentation and Controls Division.

4.2 THE ELMO BUMPY-TORUS EXPERIMENT³

R. A. Dandl² G. E. Guest
H. O. Eason C. L. Hedrick
A. C. England J. C. Sprott

4.2.1 Introduction

For many years, toroidal magnetic traps have been attractive from a fusion reactor standpoint because classical confinement in closed traps would permit an advantageous scaling of plasma loss rates with size, a scaling which is not possible in open-ended traps. The fact that single particles are not confined in simple toroidal fields has given rise to several distinct classes of closed traps: those using external windings to generate the necessary rotational transform, as in stellarators; those using internal conductors for this purpose, such as levitrons; those using induced plasma currents, as in Tokamak; and those using a periodic spatial modulation of the magnetic field, the so-called "bumpy torus." The first three types of field configurations have been studied theoretically and experimentally in sufficient depth to reveal serious problems which must be overcome before they can provide adequate confinement for a fusion power source. By contrast, the bumpy torus has received very limited attention, primarily because of anticipated magnetohydrodynamic (MHD) instability. In this paper we discuss a bumpy-torus device which circumvents the stability problem and permits combined experimental and theoretical studies aimed at determining the validity of certain possibilities described later which make this approach appealing for fusion reactors.

We propose a specific bumpy torus which is closely modeled after existing stable, steady-state, high-beta, hot-electron plasmas produced in open-ended traps with electron-cyclotron heating. This device will permit the study of equilibrium, stability, and plasma confinement required for assessment of the bumpy-torus approach.

3. Expanded abstract of ORNL-TM-3694.

In advance of such a study, we cite experimental and theoretical evidence to support our expectation of an optimistic conclusion. These arguments are summarized briefly in the body of this report. They do not permit a unique prediction of the outcome of the proposed experiment, but they do make plausible the expectation of adequate control for meaningful experiments. In this regard we shall discuss single-particle confinement on the drift time scale as well as loss rates on the longer scattering time scale. It is not possible to predict uniquely the high-beta equilibrium resulting from the interplay between particle creation, heating, and loss; but we do indicate the type of study being undertaken to facilitate a combined experimental and theoretical analysis and control of these observed equilibria. Similarly, stability cannot be discussed in depth until details of realistic equilibria are known, although several heuristic guidelines are presented here.

The key stability feature is interchange stability of the hot-electron shell, mirror confined in each sector of the bumpy torus. Here we have recourse to a long history of experiments^{1,4-11} and analysis, giving assurance of stability provided certain constraints are satisfied. We shall demonstrate that these are not unduly restrictive as we discuss heating techniques,

energy balance, and the estimated plasma parameters to be achieved in the proposed device.

The key equilibrium feature is a neoclassically confined toroidal component whose existence is based primarily on theoretical studies, and therefore is a central experimental objective of the present proposal. We bring to bear on this objective several important resources: a steady-state heating technology, tested diagnostic techniques, and several sensitive control parameters.

4.2.2 High-Beta Experiments in Open Traps

Mirror-confined, high-beta, hot-electron plasmas have been studied extensively in open-ended traps, both straight (i.e., with azimuthal symmetry) and canted so as to model one sector of a bumpy torus. The conclusions of this work are:

1. stability against flute modes is obtained if the ambient gas pressure exceeds a critical value of order 10^{-5} torr,
2. high-beta equilibrium results if the mirror ratio between resonant surfaces exceeds a critical value around 1.2,
3. high-frequency stability is achieved by off-resonant heating if the off-resonant power exceeds a value around 10% of the resonant power,
4. maximum values of β obtained experimentally are weakly dependent on the cant angle and $\beta > 0.5$ for the 15° cant chosen to model a 24-sector torus.

4.2.3 Particle Confinement and Equilibrium

It has been demonstrated by many workers that the bumpy torus confines single particles¹² for a wide range of magnetic parameters, allowing optimization with respect to the electron-cyclotron heating technology, stability considerations, and various other constraints. Because the character of the particle drift surfaces is independent of mass, no difficult space-charge problems seem likely to occur, and we can discuss the equilibrium from the standpoint of a charge-neutral guiding-center fluid. We cannot, however, ignore the plasma currents which are expected to make a significant modification of the magnetic field.

4. M. C. Becker, R. A. Dandl, H. O. Eason, Jr., A. C. England, R. J. Kerr, and W. B. Ard, *Nucl. Fusion: 1962 Supplement*, Pt. 1, p. 345.

5. W. B. Ard, R. A. Dandl, A. C. England, G. M. Haas, and N. H. Lazar, p. 153 in *Plasma Physics and Controlled Nuclear Fusion Research* (Proc. Conf., Culham, 1965), vol. II, IAEA, Vienna, 1966.

6. W. B. Ard, M. C. Becker, R. A. Dandl, H. O. Eason, A. C. England, and G. M. Haas, *Proc. Colloque Intern. sur l'Interaction des Champs H.F. Associés à un Champ Magnétique Statique Avec un Plasma* (Saclay, France, 1964), p. 38 (Paris, Presses Univ. de France, 1965; T. Consoli, ed.).

7. R. A. Dandl, *Bull. Amer. Phys. Soc.* 12, 461 (1967); R. A. Dandl, H. O. Eason, P. H. Edmonds, and A. C. England, p. 181 in *Relativistic Plasmas: The Coral Gables Conf.* (O. Buneman and W. B. Pardos, eds.) (Benjamin, New York, 1968); also, R. A. Dandl, H. O. Eason, P. H. Edmonds, and A. C. England, *2ème Colloque Intern. sur les Interactions entre les Champs Oscillants et les Plasmas* (Saclay, France, 1968), vol. I, p. 161 (T. Consoli, ed.).

8. R. A. Dandl, J. L. Dunlap, H. O. Eason, P. H. Edmonds, A. C. England, W. J. Herrmann, and N. H. Lazar, p. 435 in *Plasma Physics and Controlled Nuclear Fusion Research* (Proc. Conf., Novosibirsk, U.S.S.R., 1968), vol. II, IAEA, Vienna, 1969.

9. R. A. Dandl, W. B. Ard, H. O. Eason, P. H. Edmonds, A. C. England, and S. T. Nolan, *Bull. Amer. Phys. Soc.* 14, 1019 (1969).

10. R. A. Dandl, *Bull. Amer. Phys. Soc.* 14, 1270 (1969).

11. R. A. Dandl, H. O. Eason, P. H. Edmonds, and A. C. England, *Nucl. Fusion* 11, 411 (1971).

12. B. B. Kadomtsev, in *Plasma Physics and the Problems of Controlled Thermonuclear Reactions* (Pergamon, New York, 1959), vol. III, p. 340, and vol. IV, p. 417; G. Gibson et al., *Phys. Fluids* 7, 548 (1964); A. I. Morozov and L. S. Solov'ev, in *Reviews of Plasma Physics* (M. A. Leontovich, ed.), 2 267 ff. (1966); B. B. Kadomtsev, op. cit., 170.

These effects must be studied in close conjunction with the experiments, since there is no unique pressure profile which can be confined in the device. Our program is therefore to optimize the vacuum field at present, and to develop the analytical and experimental techniques for study and control of the equilibrium.

The most significant feature of the guiding-center drift surfaces is their inward shift, that is, toward the major axis of the torus. This shift is partially characterized by the ratio of the two radial points at which the drift surface intersects the equatorial plane of the torus, $\hat{r} \equiv r_{\text{outer}}/r_{\text{inner}}$, a measure of the fraction of the field volume occupied by the plasma. A second important measure of optimization is the radial position of the center of the drift surface, which can be moved outward by proper choice of coil design. Both indices depend on the particle pitch angle, given, for example, by v_{\parallel}/v , so that the relative probability that a particle will be lost (e.g., by striking the inner wall) depends strongly on pitch angle. It therefore seems unlikely that the energetic toroidal population will exhibit an isotropic pressure, and we place correspondingly little stress on criteria such as $\phi dl/B$ derived for scalar pressure models. Instead, we anticipate a pressure anisotropy approaching that obtained in open-ended traps and select a mirror ratio of 2:1 to avoid loss of equilibrium at high beta from the so-called "mirror instability."

In addition, we have attempted to select a coil design to minimize the loss of passing particles to the inner surface of the cavity, since particles should be confined for many 90° scattering times for energies above 1 keV, and hence must pass through this exit pupil many times. At sufficiently low energies, where the mean free path is less than the distance around the torus, the plasma is expected to be isotropic with constant pressure on surfaces of constant $\phi dl/B$. These surfaces are qualitatively similar to the drift surfaces for the coil design selected here and thus pose no additional constraints.

4.2.4 Stability

A key element of the present proposal is its scheme for circumventing interchange instability, anticipated because $\phi dl/B$ (for the vacuum field) increases monotonically away from a single minimum in the interior of the plasma. We propose to use the mirror-confined, high-beta, hot-electron plasma, itself stabilized as in ELMO, to produce an average minimum-B configuration for the toroidal plasma component. Since there is

no current along the magnetic field, kink modes are not a problem as in the Tokamak. The microinstability problem should be less severe than in the open-ended device, since the pressure anisotropy is lessened and the loss cone is at least partially filled. Thus the off-resonant heating techniques which gave microstability in open traps should be more than adequate to stabilize the toroidal plasmas.

A particularly sensitive question in these studies is the continued stability of the hot-electron plasma. The observed stability has been ascribed to various forms of "line-tying," although there is evidence to indicate that conducting end plates are not necessary for stability. In fact, there is considerable evidence suggesting that the stabilization stems from the electrostatic confinement of a cold-electron component produced by ionization of the ambient background gas. We propose to investigate, theoretically and experimentally, the conditions necessary for stability of the plasma surface. At present we are encouraged by the many observations of stability in straight and canted mirrors so long as the pressure exceeds its critical value.

4.2.5 Plasma Heating and Confinement

Our immediate proposal is to heat the plasma with microwave power, just as in the ELMO and earlier experiments; although additional heating techniques such as neutral injection might merit serious consideration at a later date. With microwave heating, the steady-state plasma parameters are determined by the competition between heating and loss, the electrons being heated directly by the microwave power, the ions indirectly via Coulomb collisions with the electrons, just as in Tokamaks. The loss processes are not yet well understood, since no definitive confinement experiments have yet been performed in similar toroidal devices. Here we shall assume the electrons to be lost at the neoclassical rate (i.e., at the rate inherent with realistic toroidal geometry and classical collisions with no turbulent enhancement). Ions near the surface of the plasma are lost mainly by charge exchange, while the inner ions may exhibit the neoclassical loss rate. With microwave power density around 1 W/cm^3 , a toroidal plasma of 10^{13} cm^{-3} with $T_e \gtrsim 1 \text{ keV}$ and $T_i \sim 0.5 \text{ keV}$ can be sustained. A significant feature of the microwave technology is the degree of control possible by the use of resonant and off-resonant frequencies, since the off-resonant power is absorbed almost entirely by the high-energy electrons.

4.2.6 Extension to High Magnetic Field

Given affirmative answers to the questions of stability and confinement to be studied in the present device, it is important to consider the eventual extension of this scheme to higher magnetic fields capable of confining energetic ions for long times. Two questions immediately arise: (1) will synchrotron radiation from the relativistic electron annulus become prohibitive from an economic standpoint, and (2) can one realistically foresee a technology for producing the necessary surface current. Calculations have shown that the synchrotron radiation remains a negligible energy burden in plasmas above the Lawson criterion. In response to the second question, we advance a supplementary scheme in which charged reaction products could provide the surface current, should fields beyond the existing microwave technology be desirable. The control required for shaping the surface current via an array of skimmer probes is being developed in conjunction with the study of the high-beta equilibrium.

4.2.7 ELMO Bumpy-Torus (EBT) Technology

The proposed experiment has been designed to take advantage of as much existing technology and equipment as possible. EBT will use existing microwave systems at a great cost saving and little compromise in the experimental objective. The same is true of hollow copper magnetic-field coils, 10 MW of dc generator power, integral cavity-vacuum sections, and existing control room and diagnostics of the ELMO mirror experiment. The hot-electron plasma diagnostic capability and the microwave plasma production technology developed over the last decade are in themselves distinct carry-over assets. In general we feel that we can mount a program to investigate a very interesting toroidal confinement regime with a rather impressive experimental vehicle achievable at modest cost and small extension of our existing technological capability.

4.3 MACROSCOPIC INSTABILITY STIMULATION

F. R. Scott¹³ R. A. Dandl²

Because of the large energy storage in relativistic electrons under steady-state conditions in ELMO, a rapid but controlled method of releasing this energy could be very useful. We have been examining several methods. Previously reported work¹⁴ demonstrated

13. Consultant, University of Tennessee, Knoxville.

14. R. A. Dandl et al., *Plasma Phys.* **12**, 235 (1970).

acceleration of electrons to at least 10 MeV and deuterons to at least several hundred kilo-electron volts when the high-beta ring went violently unstable as the base pressure in the system was lowered. Recently we have been able to initiate several types of anomalous hot-electron ejections by pulsing a current through a single-turn water-cooled coil 6 cm in diameter placed on axis at the midplane of the ELMO cavity. Preliminary data on x rays detected on an axially collimated detector indicate that a rapid increase in the loss of high-energy electrons occurs axially during the first 3 μ sec of the 10- μ sec current pulse. The amplitude of these x-ray signals increases faster than linearly with the initiating current pulse, indicating that with a modest increase in the current amplitude a much larger axial loss of electrons can be triggered. So far, only minor energy losses have been observed.

One hypothesis presented to explain this rapid axial loss of high-energy electrons involves the initiation of an instability in the cold background plasma in ELMO. This instability grows to a limit controlled by the magnitude of the initiating current pulse, and then decays by Landau damping. During the growth and decay of this instability the relativistic electrons scatter off the cold-plasma fluctuations. In addition to this anomalous axial loss during the current pulse, additional x-ray signals are seen later on detectors observing the radial walls of the cavity as well as the detectors observing axial losses. These signals are intense and are accompanied by observed particle energy losses in flux loops. Further work is planned, including magnitude and period changes in the initiating coil circuit, the use of different diagnostics, and an examination of the character of the ejected plasma.

4.4 PULSED MICROWAVE HEATING EXPERIMENTS IN ELMO

R. A. Dandl² R. L. Livesey
H. O. Eason M. W. McGuffin
A. C. England J. C. Sprott

A high-power (200-kW), pulsed ($\sim 1 \mu$ sec at 1000 pulses/sec), 9375-MHz (3-cm) microwave source was used to produce and to heat plasmas in ELMO. The plasma properties were similar to those obtained with continuous-wave sources of the same average power. Enhanced axial losses were observed with pulsed lower-off-resonance power just as with continuous-wave power. A fast diamagnetic loop showed a resonant heating rate consistent with 100% absorption as expected theoretically and $\lesssim 1\%$ absorption when the pulsed power was applied below resonance.

4.5 NUMERICAL CALCULATIONS OF OFF-RESONANCE HEATING¹⁵

J. C. Sprott

The off-resonance heating that is observed in hot-electron plasmas at Oak Ridge and elsewhere is explained in terms of harmonic resonances, appropriately modified to include relativistic and Doppler effects. A theoretical expression for the heating rate is proposed and is found to agree with the results of a computer simulation over a range of parameters. The theoretical heating rate is evaluated numerically for several special cases, including a uniform magnetic field, a mirror field with a 2:1 mirror ratio, and a large-aspect-ratio bumpy torus. The enhanced axial loss observed experimentally with heating below the cyclotron frequency is explained by absorption at harmonics of the electron-bounce frequency.

4.6 POLARIZATION OF FREE-FREE BREMSSTRAHLUNG FROM MAGNETICALLY CONFINED PLASMAS

R. A. Dandl² R. L. Livesey
H. O. Eason M. W. McGuffin
A. C. England J. C. Sprott

The bremsstrahlung radiation arising from electron-ion collisions is not emitted isotropically and is polarized. In a magnetically confined plasma, where an anisotropic electron distribution is found, there can be a net polarization of the radiation emitted normal to the field. Measurements made on ELMO at several photon energies between 100 and 400 keV have shown a polarization of less than 1%. Subsequent numerical calculations, based on the theoretical calculations of Gluckstern and Hull,¹⁶ have shown that the expected polarization from a high-temperature ($T_e \sim 1$ MeV) plasma in a 2:1 mirror should be less than 1%, consistent with the measurements. This is to be contrasted with the large polarization expected at lower temperatures, as has been observed by Greene et al.¹⁷ for $T_e \sim 20$ keV in a 1.2:1 mirror field and by Von Goeler et al.¹⁸ for a 100-keV plasma in the ST Tokamak. Theoretical calculations based on the Gluck-

15. Abstract of paper submitted for publication in the *Physics of Fluids*.

16. R. L. Gluckstern and M. H. Hull *Phys. Rev.* 90, 1030 (1953).

17. D. G. S. Greene et al., *Phys. Rev. Lett.* 27, 90 (1971).

18. S. Von Goeler et al., *Bull. Amer. Phys. Soc.* 16, 1231 (1971).

stern and Hull formulation qualitatively confirm the high polarization observed in these cases. The technique could easily be applied to ORMAK and possibly to the target plasma experiments where the mirror ratio is smaller.

4.7 OFF-RESONANCE EFFECTS ON ELECTRONS IN MIRROR-CONTAINED PLASMAS¹⁹

R. A. Dandl² P. H. Edmonds
H. O. Eason A. C. England

Resonant heating by microwave power has been used to produce high-beta plasmas with electron temperatures near 1 MeV. Typically, plasmas are produced with $\omega_{pe} \sim \omega_{ce}$. Further experimental heating studies described here have shown that a large increase in stored plasma energy is produced by microwave power with a frequency higher than the cold-electron resonance frequency. This increase, caused by off-resonance heating, is attributed both to stochastic heating and to the control of an instability through changes in the electron distribution function. Alternatively, a decrease in the stored plasma energy is produced by microwave power at a frequency below the cold-electron resonance frequency. This effect is attributed in part to enhanced diffusion into the loss cone. However, a small fraction of the plasma is heated to high energies.

4.8 COMPUTER CALCULATIONS OF ELECTRON-CYCLOTRON HEATING IN A NONUNIFORM MAGNETIC FIELD²⁰

J. C. Sprott P. H. Edmonds

A computer is used to calculate the trajectories of a collection of noninteracting, nonrelativistic electrons near the axis of a spatially sinusoidal, dc magnetic field in the presence of a spatially homogeneous, perpendicular rf electric field. The computed heating rate is in good agreement with the prediction of various equivalent stochastic models for a wide variation of parameters. The distribution is approximately Maxwellian, and the particles tend to turn at the resonance surface. Departure from the stochastic theory is observed for high-energy particles that turn near the resonance surface, and a condition for stochasticity is derived.

19. Abstract of published paper: *Nucl. Fusion* 11, 411 (1971).

20. Abstract of published paper: *Phys. Fluids* 14, 2703 (1971).

5. Turbulent Heating

Igor Alexeff
L. A. Berry
K. G. Estabrook¹

A. Hirose
R. V. Neidigh
W. R. Wing²

5.1 INTRODUCTION

Turbulent heating is a means of heating plasma ions or electrons to many kilovolt average energies via plasma-generated radio-frequency oscillations from a dc input. Theoretical studies and basic experiments in turbulent heating, and the operation of the large, successful, ion-heating device, Burnout VI, were terminated in June 1971. All equipment, except the magnet coils, has since been either transferred to other devices or salvaged, and the personnel have dispersed. This is a final report and includes an extrapolation to a "next-generation" turbulent heating device.

5.2 REVISIONS TO TURBULENT HEATING THEORY

5.2.1 Introduction

Our most advanced theory of the turbulent heating of plasma electrons and ions had been accepted for publication in *Nuclear Fusion*.³ This introduction contains only a summary paragraph of that paper. The theory in this report is an advanced version of that which appeared in the previous annual report.⁴

The plasmas of turbulent ion-heating experiments are characterized by the presence of strong, high-frequency electric fields driven by a dc electric field applied, in the Burnout experiments, perpendicular to the magnetic axis. This $E \times B$ configuration would normally make

the plasma rotate azimuthally with a velocity cE/B . However, since the plasma has a finite mass, the centrifugal force acting on the plasma must be counterbalanced by a centripetal force. This centripetal force is created by an azimuthal current, j_θ , which is generated by the retarded ion drift with respect to electron drift.

5.2.2 Advanced Theory

Three ion-heating mechanisms are depicted in Fig. 5.1. The velocity difference between ion drift and electron drift is about 10^7 cm/sec. It is not great enough to trigger electrostatic instabilities in a homogeneous plasma, so initial ion heating is by the collisional instability. This is the first stage in the heating. In the now warm plasma, the presence of a density gradient makes the lower hybrid oscillation unstable, with a growth rate having an e -folding time shorter than 10^{-9} sec. In the plasmas of Burnout V and Burnout VI, the heating rate was then on the order of 10^9 eV/sec.

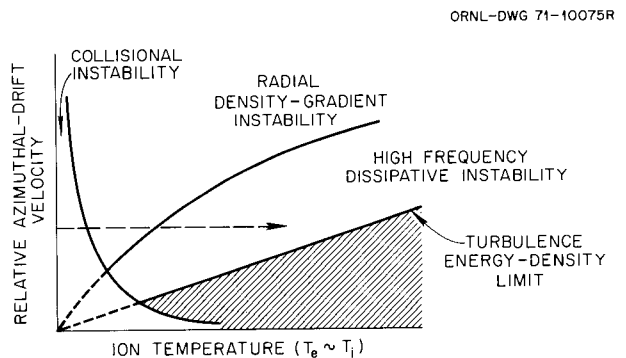


Fig. 5.1. Three ion-heating mechanisms. The energy density limit was not reached in Burnout VI. Ion heating was numerically greater than 2.5 times the centrifugal splitting velocity and limited only by electrical breakdown of the plasma source insulation.

1. Oak Ridge Associated Universities Fellow from the University of Tennessee.

2. Oak Ridge Associated Universities Fellow from the University of Iowa.

3. A. Hirose and I. Alexeff, "Theory of Turbulent Heating," paper to be published in *Nuclear Fusion*.

4. *Thermonuclear Div. Annu. Progr. Rep. Dec. 31, 1970*, ORNL-4688, pp. 77-89.

As the ion temperature increases, the cold-plasma model ceases to be valid; but as we have seen experimentally, the lower-hybrid instability still persists. Theoretically, we understand that this is due to finite ion Landau damping. Experimentally, we have observed average ion velocities six times greater than the relative drift velocity. The relative drift velocity is therefore *not* an upper limit on the achievable ion temperature, as suggested by Mikhailovskii and Tsypin,⁵ but the achievable ion temperature is related to the turbulence energy density and is numerically proportional to the square of the relative drift velocity. So we find that, for a given relative azimuthal-drift velocity, ions are heated through three instabilities, and the temperature is limited only by the turbulence energy density.

5.3 DIAGNOSTICS ON BURNOUT VI

5.3.1 Correlator Studies on Burnout VI

Use of a correlator on Burnout VI was prompted by the well-known fact that the Fourier transform of a correlation function recovers the spectral density of the correlator input. By using signals from probes sensitive to the fluctuating electric field in the Burnout plasma, the spectral density tensor of this fluctuating electric field, $S_E(k, \omega)$, could be recovered. Since this fluctuating (turbulent) electric field was responsible for the heating, knowledge of its spectral density (which contains the dispersion relations of the waves) would allow the physical mechanism of the heating to be verified.

The correlation function of the electric field has been measured at selected points throughout the accessible volume of Burnout VI. The measurements show the heating instability to be strongly confined to the plasma volume near the core of the machine ($r < 2.0$ cm) in the region of steepest density gradient and strongest radial electric field.

Limited experimental data prevented direct recovery of the spectral density; therefore, the problem was inverted. The predicted dispersion relations and power spectra³ were used to generate spectral densities which in turn were computer transformed to yield computer-generated correlation functions. The process and the results are illustrated in Figs. 5.2 and 5.3. The figures illustrate the two dispersion relations³ which were the most likely candidates for the heating instability, the

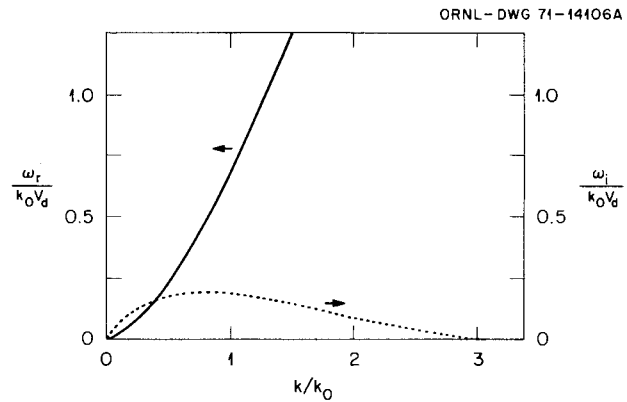


Fig. 5.2. Dispersion relation for the high-frequency dissipative drift mode.

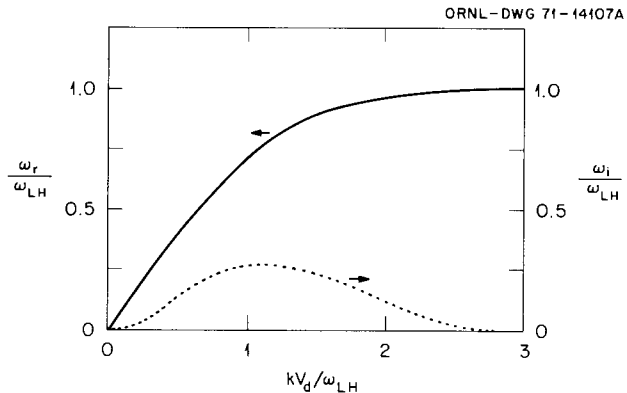


Fig. 5.3. Dispersion relation of collisional mode.

high-frequency dissipative drift mode, and the collisional mode. As can be seen, both predict very broad power spectrums. Figure 5.4 compares the results of the computer transforms of these dispersion relations (spectral densities) with the measured correlation function. Since the correlator measures the correlation function as a function of time for fixed probe spacing, the program was written to display the computed transform the same way. The figure also shows the measured correlation function for three azimuthal probe separations: 0, +0.13, -0.13 mm. The top two photographs illustrate the computed transforms. As can be seen, the agreement between the measured function and the one computed on the basis of the dissipative drift mode is quite good.

5.3.2 Off-Axis Plasma Source on Burnout VI

It has been very difficult to measure particle lifetime in the Burnout experiments. Turnoff experiments routinely gave e -folding times of less than 100 μ sec for

5. A. B. Mikhailovskii and V. S. Tsypin, *Zh. Eksp. Teor. Fiz. Pis'ma Redakt.* 3, 247 (1966); *JETP Lett.* 3, 158 (1966).

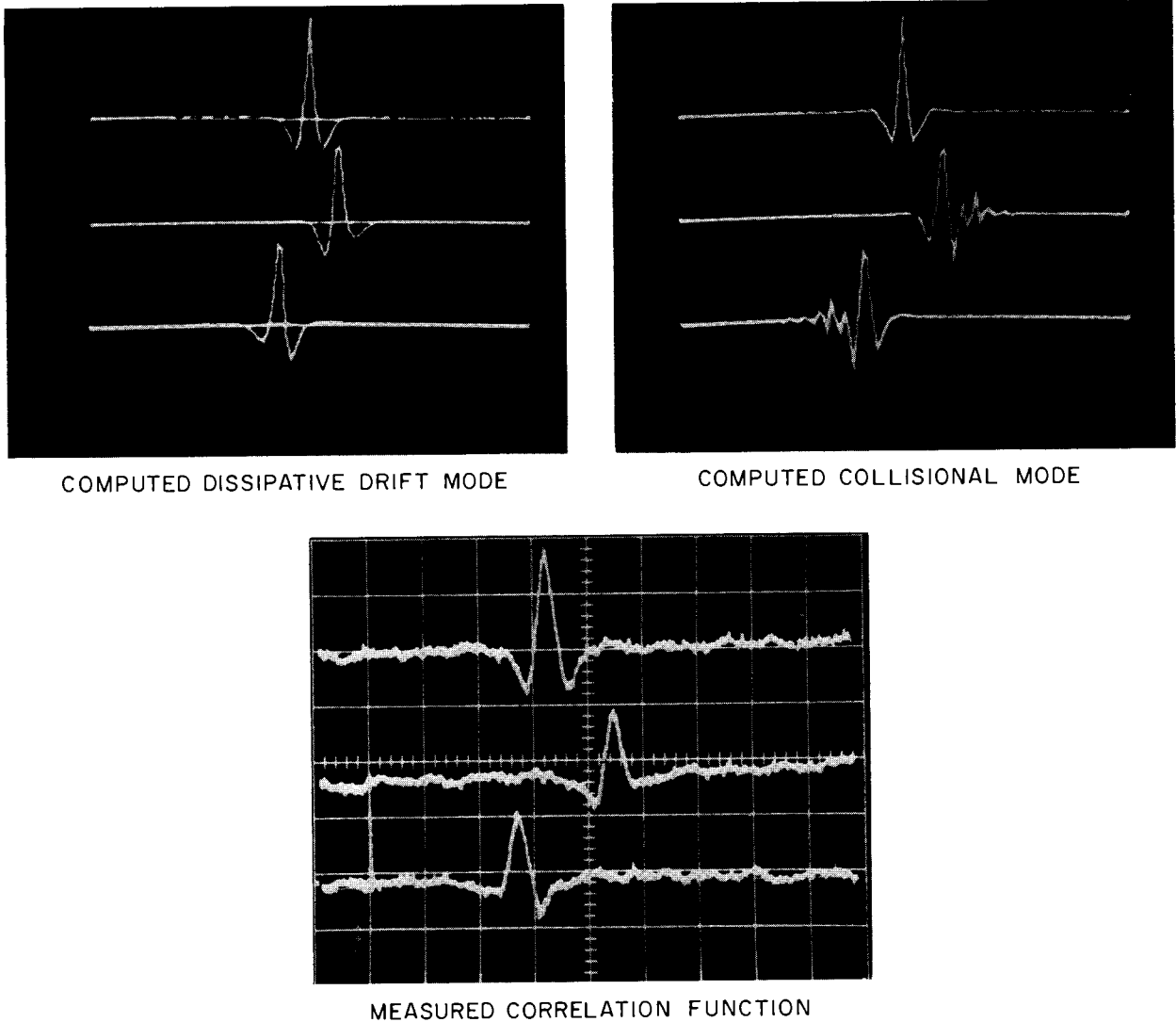


Fig. 5.4. Correlation functions. The measured function for three values of azimuthal probe separation: 0, +0.13, -0.13 mm, is compared with two computed functions. The time scales in the computed functions have been chosen to allow direct comparison with the 1 nsec/cm scale of the experimental traces.

decay of the plasma density. Yet, energy balance and estimates of heating efficiency always seemed to indicate that the dynamic-particle lifetime in the plasma core was much longer.⁴ The ion energy distribution also implied a longer lifetime.⁴

A dynamic-particle lifetime can be estimated if the plasma source is located off the magnetic axis. The plasma will then drift around the axis due to the magnetic-field gradient, and the rate of its intensity falloff may be measured. This is not an easy measurement to make, since one must look through the plasma, but the data can be unfolded. Our results are shown in Fig. 5.5.

Positive conclusions may not be drawn from this

scant data. We note (1) lifetimes were more than twice those obtained from turnoff measurements; (2) at radii greater than 2 cm the relation of particle lifetime to energy shows the typical charge-exchange dependence $1/\sigma v$; and (3) at less than 2 cm for particles below 1 keV, charge exchange again dominates. From 1 to 3 keV, however, the direction of the curve changes. The collisional dependence, $T^{3/2}$, is shown by the dashed line for comparison. The only claim here is that the particle lifetime did increase with energy near the axis in this energy interval, giving the experimental indication that the interior of a larger or denser plasma can be shielded from charge exchange in a Burnout device.

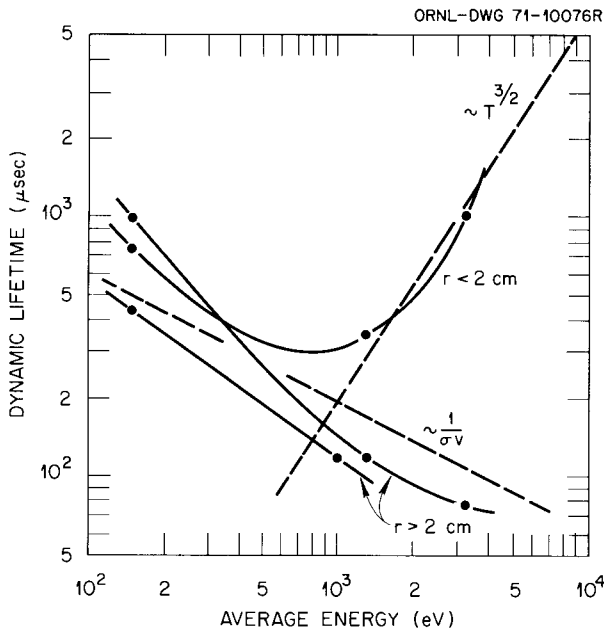


Fig. 5.5. Dynamic particle lifetime. The two $r > 2$ cm curves are different runs. Error in this data may be as great as a factor of 2, but the change in direction of the $r < 2$ cm curve is real.

5.3.3 Power Pulsing of the Plasma Source Bias

Power input to Burnout VI as adjusted for the correlation measurements and off-axis arc experiments described above is typically 40 kW (10 kV/4 A). Ion temperature is about 2 keV.⁴ Atomic beam attenuation and an observed decrease of spectral light emission from neutral atoms on axis lead one to believe that the maximum density is $4 \times 10^{12} \text{ cm}^{-3}$ to 10^{13} cm^{-3} . Particle lifetime in this stable ion-heating mode is mostly limited by charge exchange on molecular deuterium. It is possible to raise the power input to 80 kW for a few seconds before anode overheating, by simply hand-switching the plasma source bias supplies.

We find that doubling the input power nearly doubles the ion temperature. Analysis was by velocity selection of the charge-exchanged deuterons. Analyzer readout is shown in Fig. 5.6. Note that there is an increase in neutral current as well as a shift to higher energy. Since there was no change in gas feed rate, an increase in the density of the higher-energy deuterons is indicated.

It is necessary to unfold the velocity-analyzed neutral flux $I(nv\sigma_{01}\sigma_{10})$ to obtain $I(n)$ and subsequently $n(\epsilon)$. Further, the analyzer resolution is energy dependent (resolution $\sim 1/v^2$). This additional v^2 dependence, however, is partially compensated for by the stripping cross section which increases steeply with energy. To arrive at the values for the density vs energy plot of Fig.

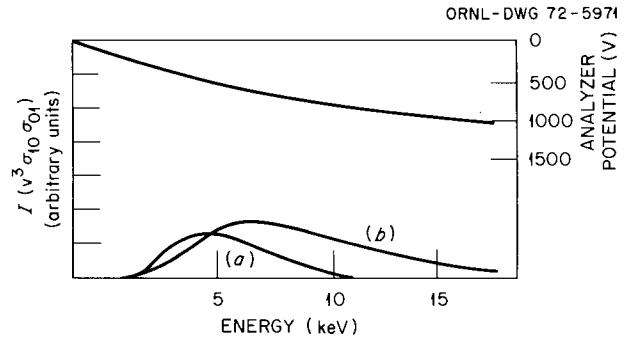


Fig. 5.6. Velocity selector analyzer readout. The upper curve with zero at the top is the voltage applied to the velocity selector analyzer. The two lower curves are analyzer currents as functions of energy for: (a) 40 kW input steady state and (b) 80 kW input of several seconds duration. Note the increase in current of deuterons with energy > 10 keV. Heavy impurity ions miss the collector and therefore do not contribute to the above data.

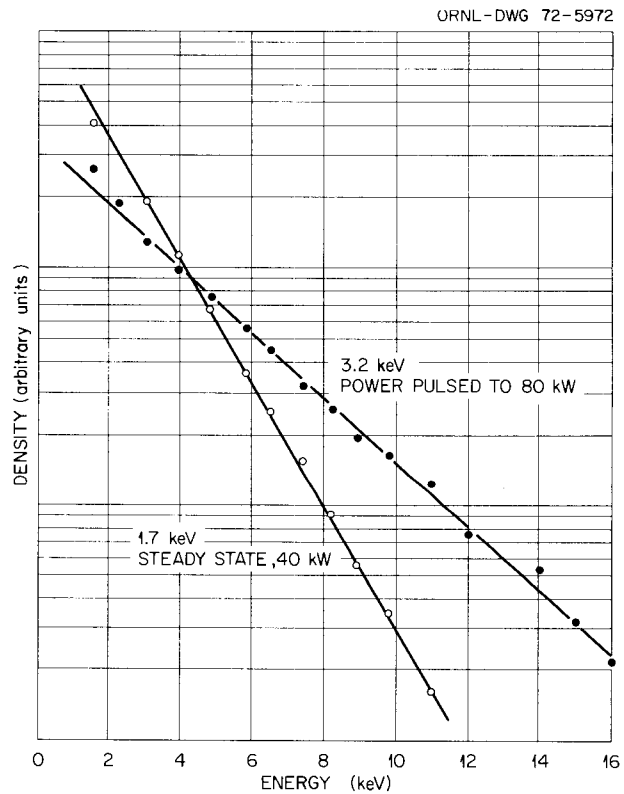


Fig. 5.7. Energy density distribution. The power-pulsed distribution (80 kW) has nearly twice the temperature of the steady-state plasma. Note that the total particle count under the low-temperature curve is about twice the high-temperature curve if one assumes the curves extrapolate to zero. However, deuterons above 4.5 keV are more abundant in the power-pulsed mode.

5.7, we divided the analyzer current by $v^3\sigma_{10}\sigma_{01}$, where σ_{10} is the cross section for charge exchange on

molecular deuterium, and σ_{01} is the stripping cross section on molecular deuterium. That we have chosen the appropriate compensating dependences is attested by the semilogarithmic relation which persists over two orders of magnitude in density for one in energy.

This experiment indicates that we have not yet experimentally observed any ion temperature limits to this turbulent heating process. The experimental limit was one of anode heat dissipation and subsequent electrical breakdown.

5.3.4 Stabilization by Inherent Positive Plasma Potential

Measurements concerning the behavior of the Burnout VI plasma after power turnoff have demonstrated that some plasma survives for quite long periods of time (5 msec) before an instability, tentatively identified as the flute instability, dumps it.⁶ Thus the plasma seems inherently stable against the flute instability. A possible explanation of this unexpected stability is that the plasma is experimentally observed to be everywhere *positive* with respect to the source, as demonstrated in Fig. 5.8. Thus the stabilizing mechanism predicted for a mirror-confined plasma with a positive plasma potential is possibly at work here. The positive potential⁷ would be expected to disappear late in the afterglow, due to electron cooling, and the stabilization mechanism would disappear.

5.3.5 Mirror Stopping by Plasma Rotation

Measurements made during the past year have demonstrated that centrifugal force in a machine such as Burnout provides a considerable force which tends to aid in closing the mirror. Alternately, it provides an effective mirror ratio greater than B_{\max}/B_{\min} . That is, for a plasma (in a simple mirror) undergoing solid body rotation (under the influence, say, of an $\mathbf{E} \times \mathbf{B}$ drift), there is an additional confining force

$$m\omega^2 r \frac{\bar{r} \cdot \nabla \bar{B}}{\bar{B}}$$

directed toward the midplane. Adding this to the usual force $\bar{\mu}_m \cdot \nabla \bar{B}$, and solving the equations of motion, we get an enhanced mirror ratio:

6. *Thermonuclear Div. Annu. Progr. Rep. Dec. 31, 1970*, ORNL-4688, p. 83, sect. 5.2.3.5.

7. G. E. Guest and E. G. Harris, *Phys. Rev. Lett.*, 27, 1500 (1971).

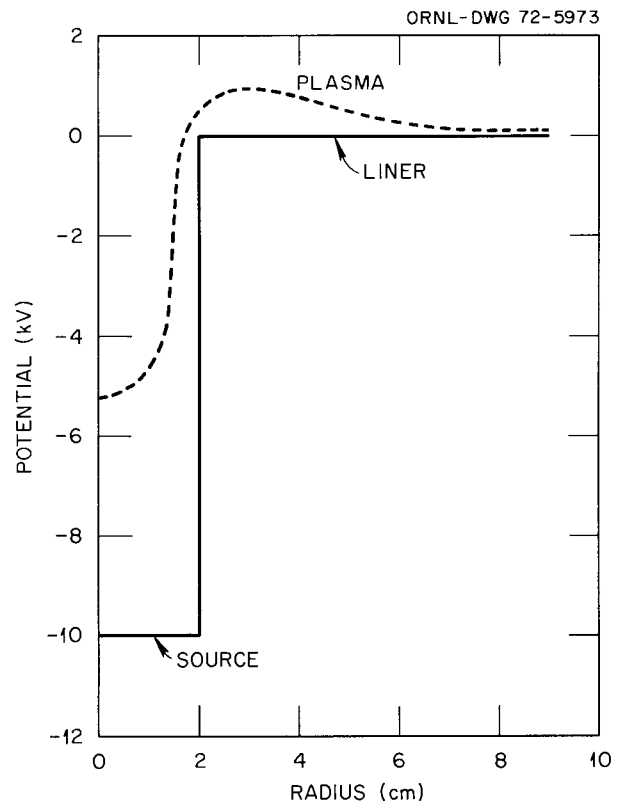


Fig. 5.8. Plasma potential. The potential of the Burnout plasma is always positive with respect to the end wall it sees along magnetic field lines. In the plasma source region it is kilovolts positive with respect to the source. Outside the source region it is hundreds of volts positive with respect to the liner wall.

$$MR_{\text{enh}} \approx MR_{\text{nominal}} \left(1 + \frac{m r^2 \omega^2}{kT} \right).$$

For typical Burnout parameters, $v_{+n} \approx 4 \times 10^7$ cm/sec and $v_{\text{rot}} \approx 2 \times 10^7$ cm/sec, which yields an enhancement of 25%.

5.4 EXTRAPOLATION TO A NEXT-GENERATION EXPERIMENT

5.4.1 Ion Temperature Exceeds Centrifugal Splitting

We have discovered, both experimentally and theoretically, that the conventionally expected limit to turbulent ion heating in machines like Burnout VI can be greatly exceeded. Conventionally, one expects the heating process to cease when the ion thermal velocity

becomes comparable with the velocity difference between the azimuthally precessing ions and electrons.^{5,8} However, as pointed out in our paper at the Fourth International Conference on Plasma Physics and Controlled Nuclear Fusion Research,⁹ the instability merely changes its form as the ion thermal velocity exceeds the relative ion-electron motion. Landau damping, instead of quenching the instability, is theoretically found to enhance it! Experimentally, the average ion velocity is found to be over six times higher than the relative ion-electron velocity. In addition, our theory predicts that the factor of 6 is *not* an intrinsic limit. The limit is determined by the rate of power input into the plasma.

5.4.2 Next-Generation Turbulent-Heating Experiment

5.4.2.1 Introduction. This projection of a next-generation turbulent-heating experiment is extrapolated from experimental experience, local magnet technology, and with scaling based upon an understanding of the heating mechanism. It is intended to describe, in terms of n , T_i , τ , what sort of plasma may be attained with the coils and source bias power supplies that remain of the Burnout VI apparatus. The goal, of course, is a "classical plasma" (mirror-contained loss-cone distribution).

8. L. I. Rudakov, *Discussion in the Autumn School of Plasma Physics*, Tbilisi, U.S.S.R., 1970; E. Ott, et al. *Phys. Rev. Lett.* 28, 88 (1972).

9. Madison, Wisconsin, June 17-23, 1971.

5.4.2.2 Magnetic field strength. If the Burnout VI coils, capable of 50-25-50 kG dc fields at 8500 A, were relocated so that the ORMAK generator control system for raising and lowering the current could be used, and the mirror ratio reduced to 1.6, by moving the coils closer together, they would provide a field strength of 80-50-80 kG for a 1-sec rise, 1-sec hold, and 1-sec fall time. Circuit breaking, as it is done on ORMAK, would not be necessary since cooling is less of a problem. The 50-kG midplane field strength should permit a density of $2 \times 10^{14} \text{ cm}^{-3}$ ($\omega_{pe} < \omega_{ce}$), Fig. 5.9; and the flatter midplane field provides a trapped volume of about 2 liters.

5.4.2.3 Power pulse. Let us assume that the voltage available in the four calutron supplies can, with some modification, bias a nest of seven plasma sources outside each mirror to 50 kV. Bias will, of course, have to be held near maximum with capacitors during the power pulse. Charging can be during a period of low field strength when the source bias current is less than 1 A. We anticipate that four phases will complete the power pulse cycle. (1) *Charging*: ~30 sec, midplane field strength ~10 kG, maximum capacitor charging current ~10 A, plasma current 1 A, weakly turbulent plasma, capacitors charge to 50 kV; (2) *Power up*: 1 sec, magnetic field increases to 50 kG in midplane, gas pulse to sources, bias current and turbulence increase to maximum; (3) *Hold*: 1 sec, magnetic field steady 80-50-80 kG, bias voltage and current drop as capacitors discharge, gas pulse off; (4) *Power down*: 1 sec, magnetic field lowers, bias current falls, ready for charging phase to begin.

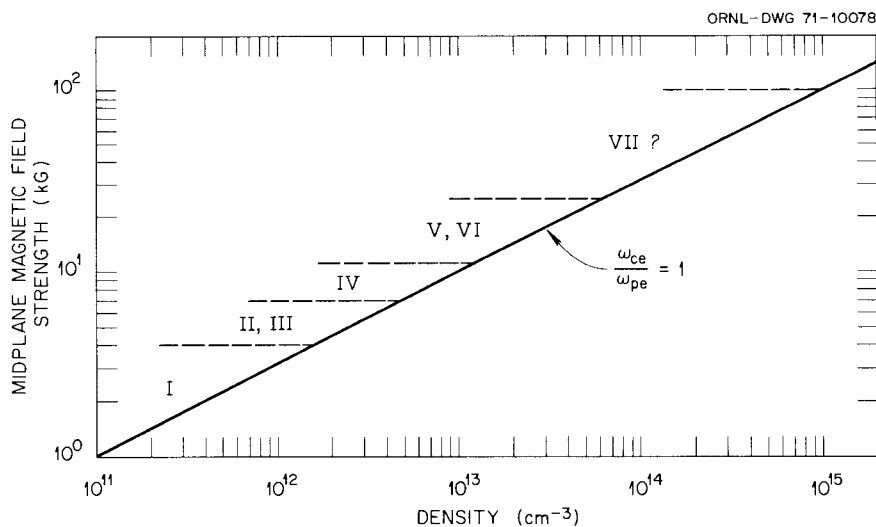


Fig. 5.9. Magnetization requirement. Turbulent heating of ions requires that in the region of contained plasma, the electrons be magnetized, that is, $\omega_{ce} = \omega_{pe}$ line.

5.4.2.4 Predicted ion energy. Our experience gives us confidence that the radio-frequency electric field will be proportional to the applied bias voltage. No violation of this was found in Burnout V or Burnout VI. The 50 kV used in this extrapolation is the upper limit of the available calutron supplies. We scale the azimuthal drift velocity by $v_d = cE/B$, and the density by the electron magnetization limitation, $\omega_{ce} = \omega_{pe}$, and get an ion energy as a function of density and the applied bias voltage,

$$T_i = \frac{E^2 M}{8\pi m n k}.$$

Here, m and M are the electron and ion masses. If $n = 2 \times 10^{14} \text{ cm}^{-3}$, and $E = 50 \text{ kV cm}^{-1}$, then $T_i = 12.5 \text{ keV}$. The family of curves is displayed in Fig. 5.10.

Centrifugal splitting gives a relative velocity proportional to E^2/B^3 . The maximum average particle energy observed on Burnout VI was 4 keV with a 10-kV/cm electric field and 25-kG midplane magnetic field. If we extrapolate this to 50 kV/cm and 50 kG, we get an ion energy of about 12.5 keV. This family of curves is displayed in Fig. 5.11. This extrapolation must be considered a lower limit, since, experimentally, ion energy has always exceeded this splitting velocity.

We would like to know how ion energy will scale with particle lifetime. A larger volume of trapped plasma will

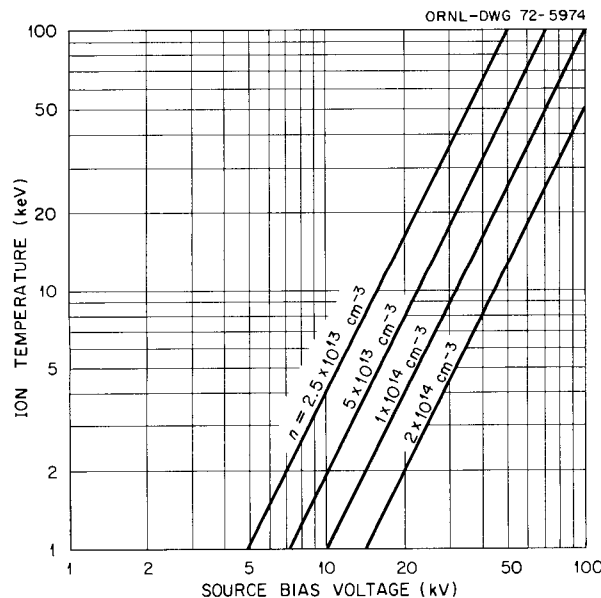


Fig. 5.10. Ion temperature scaling, variable n . These curves assume that the rf electric fields which heat ions will be proportional to the applied plasma source bias voltage, and that $\omega_{ce} = \omega_{pe}$.

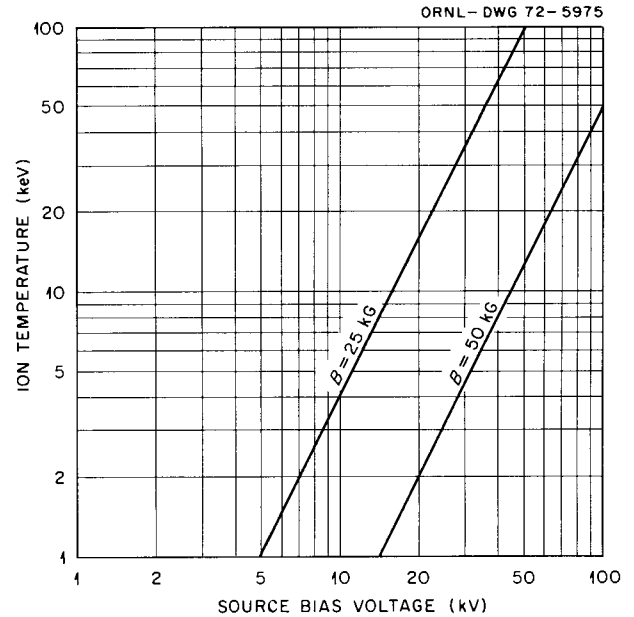


Fig. 5.11. Ion temperature scaling, variable B . These curves assume that the rf electric fields which heat ions will be proportional to the applied plasma source bias voltage, and that the "centrifugal splitting" velocity varies as E^2/B^3 .

increase the particle lifetime in its core by shielding against charge exchange. Ion heating rates are ample to provide a linear dependence with lifetime through any classical scattering time we can imagine for an open-ended system.

About all we can say from experience is that as the applied plasma-source bias was increased, the average ion energy increased more steeply than the square of the increase in ion source bias (see Fig. 5.12).

5.4.2.5 Plasma volume. Using a single source in Burnout VI, the volume of the hot trapped plasma in the midplane was about 150 cm^3 . In the proposed system, the inside diameter of the coils will permit a nest of seven sources with a plasma radius of 6 cm and a trapped plasma length of 20 cm due to the lower mirror ratio. The trapped plasma volume will have a football shape and be about 2 liters. This plasma would be well shielded in all directions from Franck-Condon neutrals. The Franck-Condon mean free path is 0.6 cm when $n = 2 \times 10^{14} \text{ cm}^{-3}$ and $T_e = 100 \text{ eV}$.

Impurity density (mainly copper and titanium in Burnout V and Burnout VI) would be much lower. The 3-sec total "on time" would not give the walls opportunity to heat, and sputtering by 12.5-keV, charge-exchanged fast neutrals would be reduced.

5.4.2.6 Stability against flutes. The plasma in a Burnout device has always been everywhere positive with respect to the walls which it sees along magnetic

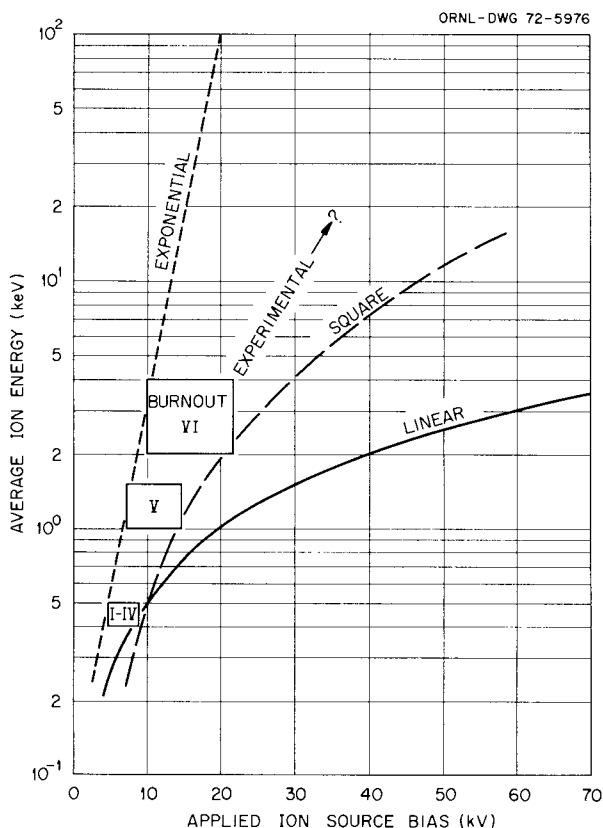


Fig. 5.12. Extrapolation of the ion energy. The wide range of parameter values makes narrow limits in the extrapolation impossible. The only thing that seems obvious in a next-generation experiment is that average ion energy will be numerically greater than the square of the source bias.

field lines (see Fig. 5.8). In the proposed plasma $T_i > 10 T_e$, and therefore it is not likely that there will be gross energy dumping by flutelike instabilities.⁷

5.4.2.7 Power requirement. The power required for plasma heating will come from the source bias supply and is, of course, unrealistic for this extrapolation unless one restricts the experiment to a few scattering times. Using $\tau = 6 \times 10^{-3}$ sec, $T_i = 12.5$ keV, $V = 2 \times 10^3$ cm³, and 10% efficiency, the power required equals

$$\frac{nkT_iV}{10^7 \text{ eff}} = 1.3 \text{ mJ/sec.}$$

If the bias were constant for 30 msec, the total energy would be 40 kJ. Of course, the bias will not be constant but will fall continuously during the "hold" phase. Capacity required at 50 kV is 33 μ F. Divided between seven sources, this would be about 5 μ F per source. A 33- μ F, 50-kV capacitor bank is reasonable. One calutron

supply for each source could be used to keep the plasma alive during the charging phase and to charge the capacitors.

Experiments and an understanding of the heating mechanism have allowed one to predict with confidence that an experimental 2-liter plasma, with density $>10^{14}$ cm⁻³, composed of >10 -keV deuterons, having at least a classical lifetime, is obtainable in an ORNL mirror machine for which nearly all of the most expensive parts are already in hand.

5.5 BASIC PLASMA PHYSICS

5.5.1 Simulation of Pseudowaves and Ion Acoustic Waves

The experimental study of ion acoustic waves in a laboratory plasma involves a very nonlinear boundary value problem if the plasma disturbances to be studied are launched by electrodes. Linear theory fails to describe the inherent sheath effects about an electrode.

We approach the problem by numerically solving the nonlinear Vlasov-Poisson equations by a finite difference technique.¹⁰⁻¹² The electrons are assumed to be in thermal equilibrium. An example of the results is shown in Fig. 5.13. In this example, a transparent grid at the position marked "grid" had a negative sinusoidal potential applied of bias $-15 kT_i/e$, amplitude $15 kT_i/e$, and frequency of one-fourth of the ion plasma frequency. The initial plasma was a Maxwellian. From time zero to the moment of this snapshot, the potential oscillated from zero to $-30 T_i$ three times. As the grid potential was driven negative, ions filled the phase space volume about the grid to about $\pm\sqrt{2e\Phi(\text{grid})/M_i}$ in velocity space and $\pm\sqrt{k\Phi(\text{grid})n_e^{-2}}$ in position space. As the potential is made increasingly positive, the fast ions in the sheath are released to form the fast ion bursts. The tails of the first two bursts and the head of the third (at about $10 \lambda_D$) may be seen in Fig. 5.13. An ion acoustic wave may be seen in the central parts of the velocity distributions. Numerical plots of $n(\text{fixed } x, t)$ have been made and are in good agreement with oscillograms of both ion acoustic waves and pseudowaves taken in the laboratory.³

For these parameters of frequency and amplitude, the ion acoustic waves marginally dominate the pseudo-

10. K. Estabrook, Ph.D. Thesis, University of Tennessee, August 1971.

11. K. Estabrook and I. Alexeff, paper to be submitted to *Physics of Fluids*.

12. K. Estabrook, M. Widner, I. Alexeff, and W. D. Jones, *Phys. Fluids* 14, 1792 (1972).

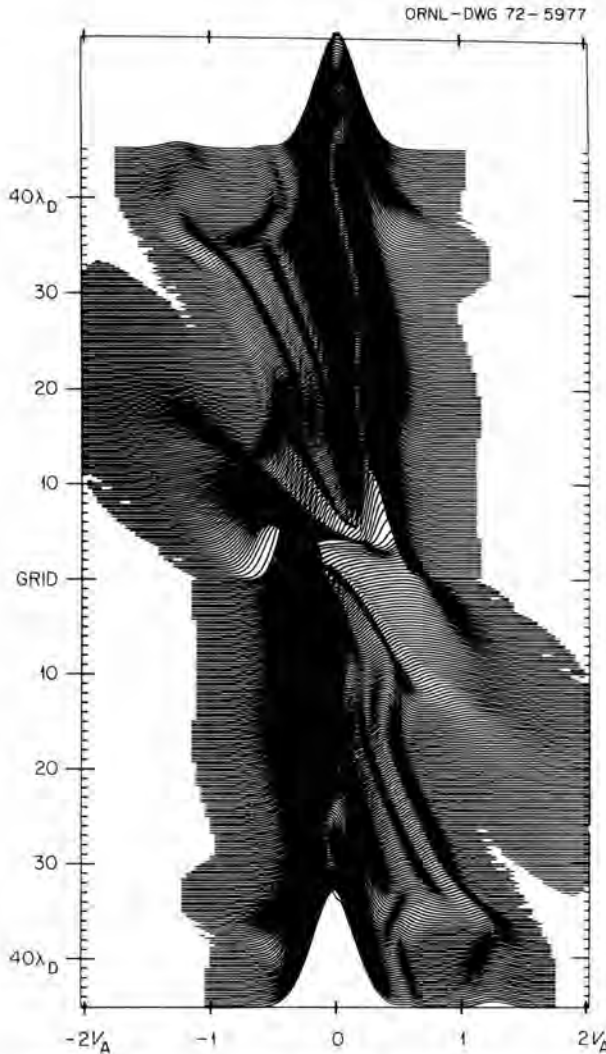


Fig. 5.13. Phase space plot of the ion distribution function at a single point in time. The ordinate measures the distance from the grid in Debye lengths. The abscissa measures the velocity in units $v_A = \sqrt{kT_e/M_i}$. Each line is a velocity distribution at a fixed distance from the grid. The height of the line above the distance intercept is the normalized phase-space density.

waves (ion bursts). However, for frequencies above f_{pi} , the pseudowaves dominate the ion acoustic waves. The pseudowaves may beat with the ion acoustic waves to produce what may erroneously appear to be regrowth due to nonlinear Landau damping.

5.5.2 Pseudowaves – Cerenkov Radiation Form

Some time ago we demonstrated that a grid placed in a plasma and pulsed strongly negative produced fast bursts of ions.¹³ These ion bursts produced results that

13. I. Alexeff, W. D. Jones, and K. Lonngren, *Phys. Rev. Lett.* **21**, 878 (1968).

appeared to be waves, and so were called “pseudowaves.” Subsequent experiments showed that pseudowaves were almost always associated with grid excitation of waves, causing ambiguities in wave propagation experiments.

We have now found that the fast ion burst can itself launch ion acoustic waves,¹⁴ without the confusing effects due to grids. The fast ion burst corresponds to a positive test particle moving through the plasma at a velocity well above the ion-acoustic velocity, and so generates a cone of ion-acoustic Cerenkov radiation.

5.5.3 Isotope Separator Studies

We have consulted with J. M. Googin in an attempt to find if there exists some fundamental limit to the throughput of uranium in a calutron (conventional mass spectrograph) type of isotope separator. We have, in fact, found that such a limit exists. It is due simply to the particulate nature of the ion beam, and does not depend on any plasma instabilities or waves whatever. Essentially, we find that, although the ion beam of a calutron is extracted from the ion source at some tens of kilovolts, the *relative* energy of the $^{235}\text{U}^+$ ions to the $^{238}\text{U}^+$ ions is only a fraction of 1 eV. This small relative energy produces the slow radial relative drift of ^{235}U to ^{238}U that results in isotope separation.

However, when one charged particle drifts very slowly through an environment of other charged particles, it is extremely susceptible to *multiple scattering*. Thus the directed relative velocity is easily lost. Reducing the beam voltage reduces this relative velocity and increases the undesired scattering. Increasing the beam current increases the number of scattering centers and also increases the undesired scattering. We can easily show that for a fixed, tolerable degree of multiple scattering, the minimum extractor voltage (volts) and the maximum beam current density j (amperes/cm²) are related by the following equation:

$$V^2/j = \text{a constant}.$$

Thus, reducing the voltage a factor of 2 means that the current density must be reduced by a factor of 4 to keep the scattering tolerable. The exact value of the constant is difficult to compute, and my own (I. Alexeff) value may be in error, but I find a value of 3×10^{10} (an easy number to remember) for uranium in a typical calutron field of ~ 5 kG. We wish to acknowledge several helpful discussions with the Isotopes

14. K. Estabrook and I. Alexeff, *Phys. Lett.* **36A**, 95 (1971).

Division of ORNL. A publication on this work is in preparation.

5.5.4 High-Z Ion Source

We have produced theoretical and experimental evidence¹⁵ that high-Z heavy ions can be produced in a

hot-electron plasma. The ions apparently are produced by multiple impacts, which enhance the yield of high-Z ions relative to low-Z ions. The plasma is produced by beam-plasma interaction, and special techniques are used to segregate the desired high-Z ions from the more numerous low-Z ions produced directly by the electron beam.

15. I. Alexeff and W. D. Jones, paper presented at the International Conference on Multiply Charged, Heavy-Ion Sources and Accelerating Systems, Riverside Motor Lodge, Gatlinburg, Tenn., Oct. 25-28, 1971, and to be published in the *IEEE Transactions on Nuclear Science*.

6. Energetic-Particle Injection

R. C. Davis	O. B. Morgan
H. K. Forsen ¹	G. Schilling ²
R. R. Hall	L. D. Stewart
T. C. Jernigan	W. L. Stirling

Producing and heating a plasma are essential both for present plasma confinement studies and future reactor systems. Present multiampere (equivalent) neutral-particle injectors can be used either for injection filling of open-ended devices or for injection heating of toroidal devices.

The multiampere beams used for these injectors are obtained from the duoPIGatron ion source. Detailed discussions of this ion source have been published.³⁻⁵ The source consists of a duoplasmatron ion source feeding a PIG discharge system. The extraction electrodes are multiaperture and are placed in an accel-decel arrangement with up to 5 cm diameter. The source is simple, flexible, and efficient.

Hydrogen ion beams of ~ 1 A are extracted with steady-state operation with ion energies of from 1.5 to 5 keV. These sources are now being utilized as injection diagnostic devices for target plasma studies in the magnetic mirror experiments INTEREM and IMP. The sources will also be used to fill these devices with hot ions in the energy range 2 to 10 keV. Experiments are continuing in an effort to more optimally match the beam divergence and gas and beam efficiency of the source to these particular plasma experiments. It has been shown that by changing the electrodes of the duoPIGatron ion source one can easily shift the performance over a broad range of beam parameters.

Source electrodes are being built based on previous plasma and ion optical studies³⁻⁵ for evaluation that should correspond more closely to the future IMP injection requirements.

The second major application of the duoPIGatron ion source is to create multiampere ion beams for energetic-particle injection heating of plasmas in toroidal devices. A detailed discussion of this new heating technique has been accepted for publication.⁶ The motivation for this work is to attain ion temperatures corresponding to the collisionless regime where reactors will operate. This is essential for extending the encouraging confinement results in Tokamak devices and to further establish scaling laws. Ohmic heating used in the present devices is self-limiting, since the plasma resistance drops as the temperature increases. Neutral injection is a supplemental heating scheme that is efficient and not self-limiting. This heating technique could not make a significant contribution to Tokamak plasma research until injectors capable of adding energy comparable to the energy gained from Ohmic heating were developed. These injectors have now been developed, and detailed discussions of their performance have been published.³⁻⁶ Two or four of these injectors will be installed on the ORMAK experiment during 1972.

These injectors also used the duoPIGatron ion source from which 4-A beams are extracted for 0.1 sec and 10% duty cycle at ion energies of 20 to 40 keV. In the energy range of 30 to 40 keV, $\sim 60\%$ of the ion beam is within a half-angular divergence of 1.2° with no magnetic lens. The source is used with a hydrogen gas cell, as indicated in Fig. 6.1, and produces 2.6 A (equivalent) of 17.5- and 35-keV H^0 particles within a

1. Consultant, University of Wisconsin, Madison.
2. On leave from the Institute for Plasma Physics, Garching, Munich, Germany.
3. R. C. Davis et al., to be published in *Review of Scientific Instrumentation*, February 1972.
4. O. B. Morgan, *Proc. Symp. on Ion Sources and Formation of Ion Beams, Brookhaven National Laboratory, Oct. 19-21, 1971*, BNL-50310, p. 129.
5. W. L. Stirling et al., *ibid.*, p. 167.

6. G. G. Kelley et al., to be published in *Nuclear Fusion*, February 1972.

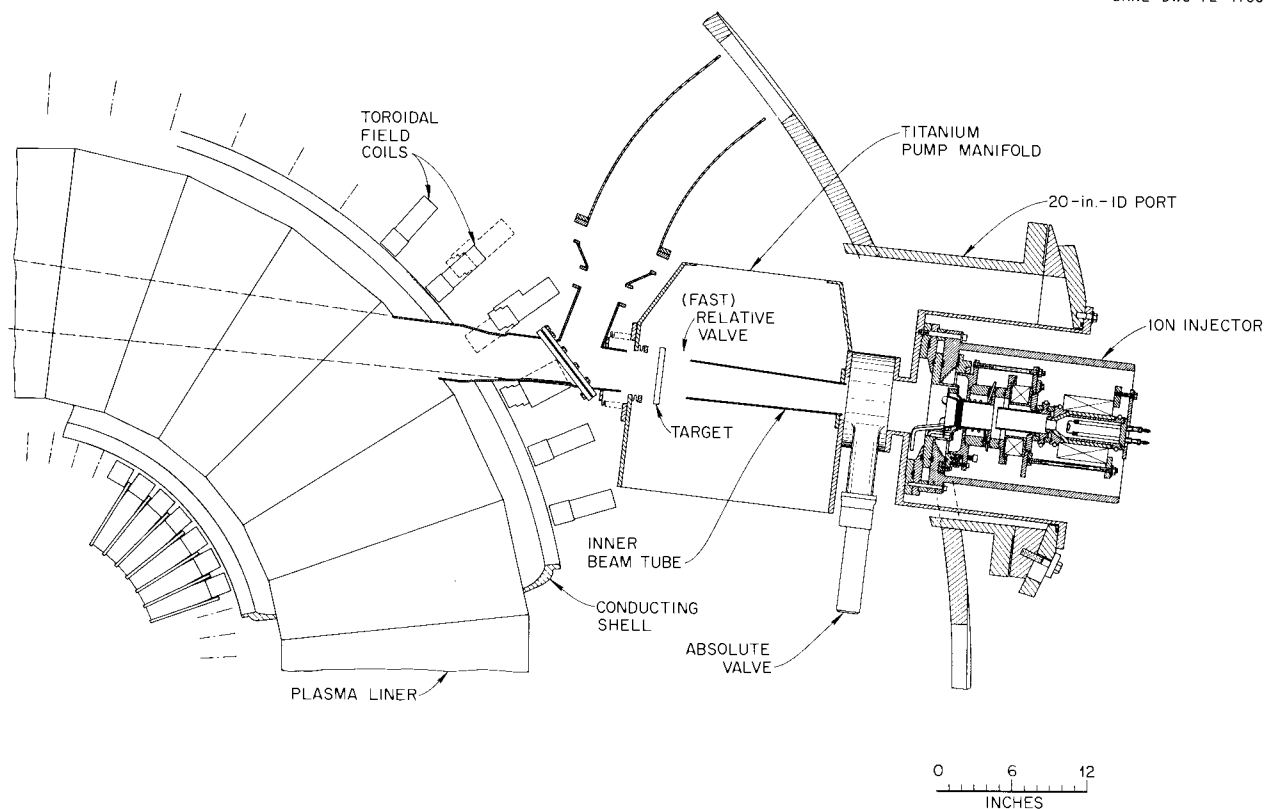


Fig. 6.1. ORMAK injection heating system.

half-angular divergence of 1.2° . The majority of the parameters essential to utilizing these injectors on ORMAK have been studied.³⁻⁶

The efforts of the Energetic-Particle Injection Group during the next year will be to further understand and increase the capability of either the present or new sources of particles for doing pertinent plasma research. The 4-A, 100-kV test stand is being used to determine the impurity content of these multiampere ion beams. This test stand will also be used for ion optical studies based partially on computer studies now in progress. There will simultaneously be a continuous program to scale these injectors to the 10-A module level relevant for future large-scale devices. The primary limitation in this scaling has been the 3.5-A, 100-kV power supply. Two new 5-A, 80-kV power supplies are being purchased and are scheduled to be delivered by March 1972. Studies are also in progress to improve the voltage stability, pulse length, and possibly the duty cycle of these sources.

A second test stand has been modified, Fig. 6.2, and is now equipped with a 4-A, 20-kV power supply.

Initial work on this device is concentrating on plasma studies on the duoPIGatron ion source. The density uniformity of this plasma has been shown to be essential to good source performance.³⁻⁶ Present studies include examining the plasma density, uniformity, and oscillations, and determining the role that these parameters play in the resulting ion beam. Based on the results obtained, modifications of this plasma source or new plasma sources will be studied. This test stand has also been equipped with a series high-voltage tube that will be used for switching and energy regulation of multiampere ion beams. The 4-A, 20-kV power supply can also be isolated to ~ 80 kV, which will allow studies of two-stage-multiampere, ion-beam accelerators.

The effort of this group during 1972 will also include participating in the design, installation, and utilization of these injectors on both the IMP and ORMAK devices.

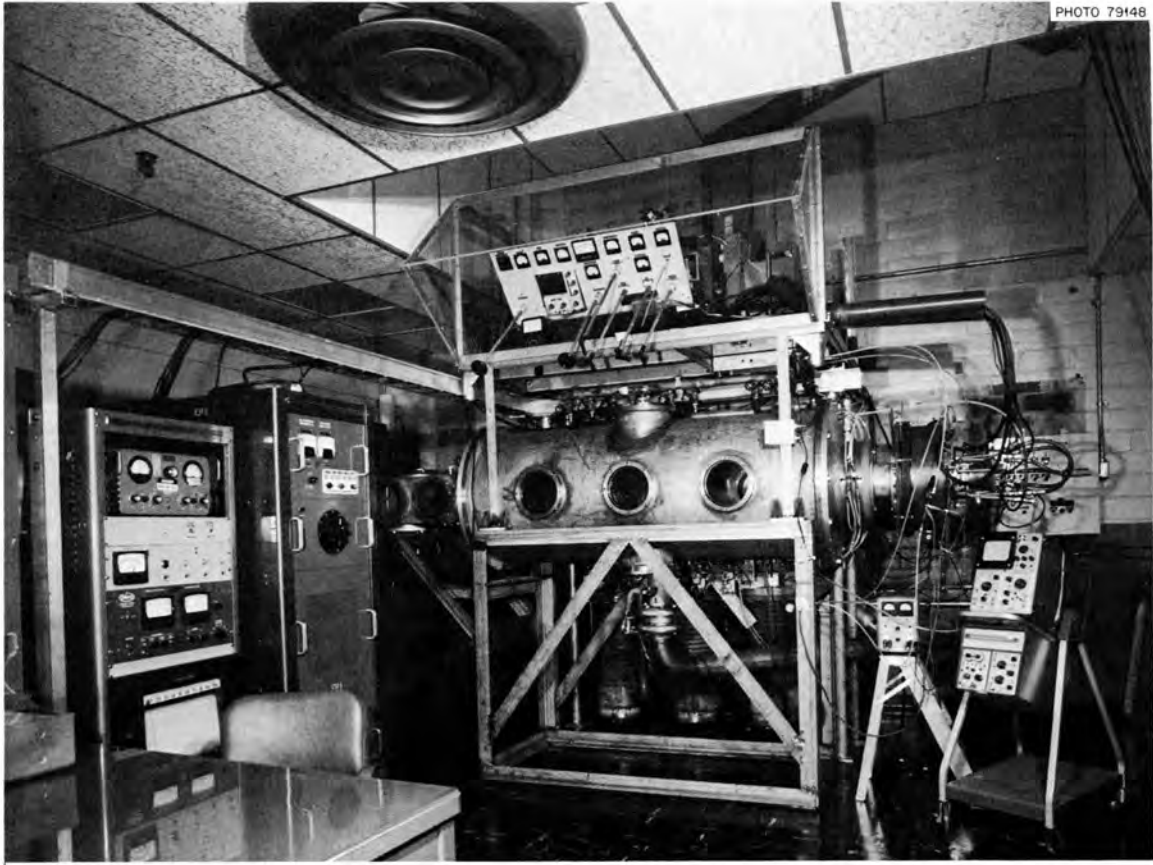


Fig. 6.2. New ion beam test stand.

7. Atomic Physics and Plasma Diagnostics

C. F. Barnett R. Berisch¹ J. A. Ray

7.1 HIGHLY EXCITED STATES OF HYDROGEN MOLECULES²

Highly excited states of hydrogen molecules have been formed by electron capture collisions of 50- to 450-keV diatomic ions in hydrogen gas. Populations of the excited states ($n \geq 10$) have been determined by passing the molecules through an intense electric field which strips the excited electron from the molecule. The fraction of molecules in states $n \geq 10$ was approximately 10^{-3} , with D_2^* being a factor of 2 greater than H_2^* . The fractional yield of H_2^* varied as the stripping electric field to the three-fourths power. Results are presented for molecular autoionization, excited-state population dependence on ion-source electron energy, and state-mixing measurements.

Present theory fails to explain these measurements. A. Russek (Consultant, University of Connecticut) has uncovered a level-crossing phenomenon between the $1-\sigma_g$ ground electronic state and the $1-\sigma_u$ excited state which has a profound effect on the electron capture process for H_2^+ , the detection of H_2 in high Rydberg states, and on the autoionization lifetimes. Further experimental work is dependent on theoretical developments.

7.2 ENERGY LOSS IN CARBON AND ALUMINUM FOILS

The conventional method to measure energy dispersion of energetic hydrogen atoms escaping a plasma entails stripping the electron from the hydrogen atom by passing it through a gas cell and then electrostatically analyzing the proton. Plasma contamination results from the stripping gas streaming from the gas

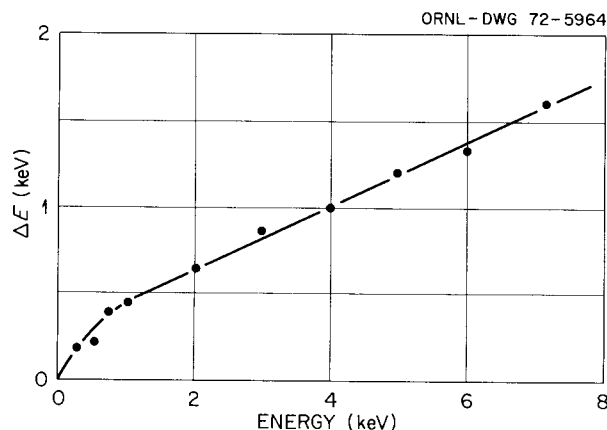


Fig. 7.1. Energy loss of protons passing through a 75-Å carbon foil.

cell to the plasma region. Ideally, the gas cell could be replaced with a thin metallic foil such that particles would be transmitted through the foil in the 100-eV energy range. A series of measurements have been made to determine the energy loss of protons through carbon and aluminum foils. The proton energy, after passing through the foil, was determined by an electrostatic-parabolic analyzer. Figure 7.1 shows the most probable energy loss in kilo-electron volts as a function of the incident proton energy for a 75-Å carbon foil. The behavior was as expected, with the energy loss decreasing with particle energy down to 250 eV, where the energy loss was 170 eV.

The most serious problem encountered in using the 75- to 100-Å foils is illustrated in Fig. 7.2, where the particle energy spectrum is plotted for protons after passing through the foil. The lower broad peak *A* arises from the protons interacting with the carbon lattice, resulting in energy loss whose most probable value was plotted in Fig. 7.1. The higher energy peak *B* results from 4-keV protons passing through the foil without

1. Solid State Division.

2. Abstract of paper accepted for publication in *Physical Review*.

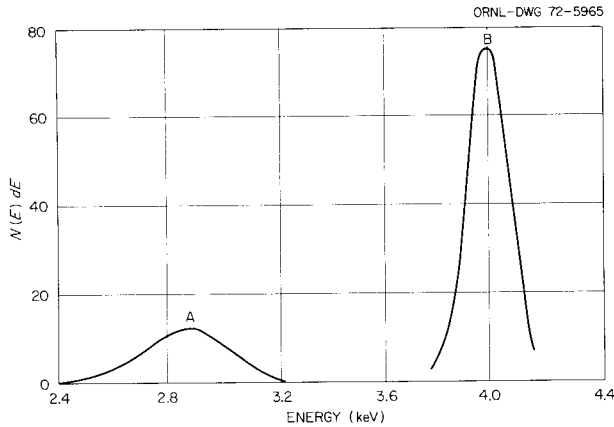


Fig. 7.2. Energy spectrum of protons after passing through a 75-Å carbon foil. Peak A results from particle energy loss in the foil; peak B results from particles passing through "cracks" without energy loss. Incident energy, 4 keV.

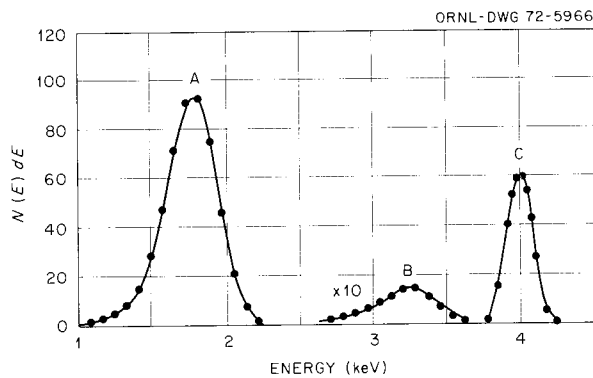


Fig. 7.3. Energy loss of protons after passing through a 300-Å aluminum foil. Peak A results from particle energy loss with lattice; peak B results from particle energy loss in which particles are channeled; peak C is energy spectrum of incident 4-keV proton beam.

collisions. During the preliminary work it was believed that this peak was due to pinholes in the foil. However, visual and 200-power microscopic observations failed to show any evidence of pinholes. Examination of the foils by electron microscopy revealed microscopic cracks. At present we have been unable to obtain foils free of cracks.

A spectrum obtained by passing 4-keV protons through a 300-Å aluminum foil is shown in Fig. 7.3. The lower peak *A* again arises from particle interaction with the aluminum lattice. The full energy peak was absent for this foil. Removing the foil gave the upper trace *C* for the spectrum of incident protons. The middle trace *B* represents an energy loss which we have

interpreted as the phenomenon of channeling. If the lower trace represents energy loss from a 300-Å foil, then the effective thickness of the foil for the energy loss observed in the center trace is 100 Å. The amplitudes of peaks *A* and *B* may be compared directly, but normalization has not been made for the upper trace. Work is continuing to develop foils that are uniform and free of defects.

7.3 HYDROGEN PARTICLE INTERACTION WITH SURFACES

Measurements have been initiated to obtain quantitative data for hydrogen atoms or ions colliding with metallic surfaces. Attempts will be made to determine the energy and angular dependence of reflected H and H⁺, the ratio of H/H₂, and the reflection coefficient in the energy range 10 eV to 50 keV for various angles of incidence. Shown in Fig. 7.4 are preliminary data obtained for 50-keV protons reflected from copper. Two curves are shown, the number of particles reflected plotted on a linear scale and the other on a logarithmic scale. The upper and lower limits of the abscissa are 50 and 10 keV respectively. The lower limit was determined by the noise of the solid-state detector used in determining the spectrum. The linear curve indicates that most of the particles are reflected at low energies;

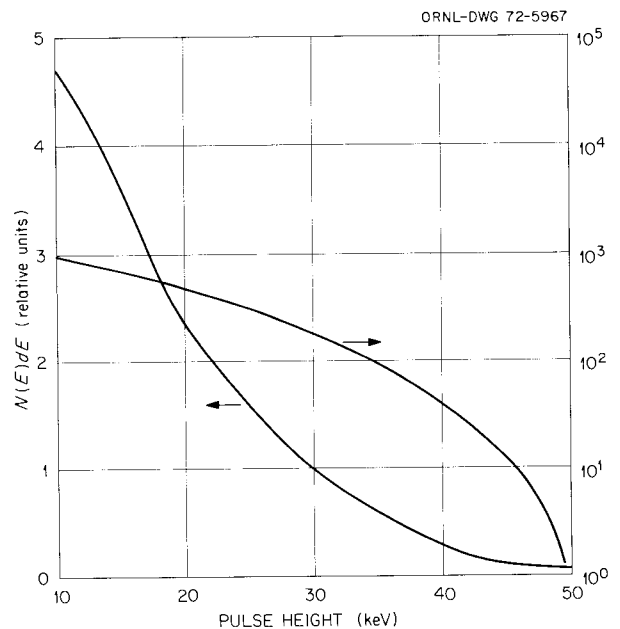


Fig. 7.4. Energy spectrum as determined by a silicon barrier detector of total H + H⁺ reflected from a copper surface. 50-keV protons incident on the surface.

the logarithmic curve indicates a considerable fraction reflected at near-incident energies. In the energy range 1 to 10 keV, we plan to use foil stripping and an electrostatic energy analyzer to obtain the reflected energy spectrum. A quadrupole spectrometer will be used to obtain energy and mass spectra at lower energies. Presently, a large scattering chamber pumped by turbo and titanium-gettering pumps has achieved an ultimate vacuum of 6×10^{-10} torr. Targets and detection systems that can be rotated are now being installed.

7.4 DIAGNOSTICS

In plasmas such as those in ORMAK it is desirable to have a neutron counter capable of differentiating neutrons arising from the D-D reaction and those from disintegration of the deuterons by runaway electrons. The characteristics of 2.5- and 10-cm-diam, 30-cm-long ^3He counters have been investigated using the neutrons produced by 400-keV D^+ impinging on a deuterium target. A solid-state detector, mounted in the vacuum chamber which also contains the deuterium target, is used to determine the proton recoil from the proton-triton branch of the D-D reactions. The ^3He counter outside the vacuum system measures the neutron from the (n, He) branch of the D-D reaction. By knowing the solid angle subtended by the two detectors, the branching ratio of the D-D reaction, and the angular distribution of the neutrons and protons, the absolute efficiency for 2.5-MeV neutrons can be determined. Preliminary measurements with the ^3He counters indicate that (1) the counting efficiency was low for energetic neutrons, (2) the counter was essentially "black" for thermalized neutrons, and (3) great difficulty was encountered when trying to separate the thermal and the energetic neutron spectrum. Since the counter is "black" for thermal neutrons, it will be used to determine the time history of plasma ion tempera-

tures by surrounding the ^3He counter with a moderator. Measurements are continuing, using an organic scintillator with pulse-shape discrimination techniques.

Further developments have been made to determine the feasibility of using a pyroelectric detector to measure the total (particle and photon) energy escaping a plasma. A strontium-barium-niobate crystal has given a responsivity of 60 V/W, using a low-power He-Ne laser beam. Further tests will be made to determine the responsivity for neutral beam impact.

Preliminary design and calculations have been made for the use of a high-power CO_2 laser beam and a high-energy heavy-ion beam in measuring the poloidal field produced by the discharge current in ORMAK.

7.5 CONTROLLED FUSION ATOMIC DATA CENTER

During the past year three books or monographs have been sent to John Wiley and Sons for publication. *Theory of Charge Exchange* by R. A. Mapleton has been completed and will appear in February 1972. *Dissociation by Heavy Particles* has gone through the galley and page-proof stage and will appear in April 1972. *Excitation by Heavy Particles* has gone through the galley-proof stage and will appear in June 1972. Two other books, *Ionization by Heavy Particles* and *Experimental Charge Exchange*, are in the stages of data extraction and evaluation.

Literature searching was resumed during 1971. The 1970 bibliography has been completed and will be published soon. Composite bibliographies for particular reactions, such as charge exchange, are being prepared for the interval 1950 to 1970. Plans are to have these published by July 1972. Extra effort is being expended in updating and reissuing the compilation, *Cross Sections of Interest to Thermonuclear Research*.

8. Magnetics and Superconductivity

R. L. Brown H. M. Long
 K. R. Efferson M. S. Lubell
 W. F. Gauster¹ J. N. Luton
 J. E. Simpkins

8.1 SUPERCONDUCTING COILS FOR IMP

Performance tests of the IMP superconducting coil system were completed on January 7, 1971. These tests demonstrated that the Nb₃Sn quadrupole coils could be operated simultaneously with the NbTi mirror coils to at least ($I = 605$ A) 74% of their design value [$I_{\text{quads}}(\text{design}) = 815$ A, $H_{\text{quads}}(\text{design}) = 85$ kG at windings, $I_{\text{mirrors}}(\text{design}) = 383$ A, $H_{\text{mirrors}}(\text{design}) = 69$ kG at windings]. Upon reaching 605 A the automatic energy dump engaged and discharged the coils. No attempt has been made to exceed 605 A since this test. It is not known whether a normal-state transition occurred in the coils (in which case we think it would have been due to conductor movement) or whether the automatic dump circuit was activated by a line transient (the susceptibility of this circuit to line transients was discovered later).

At the completion of these tests, the coils were turned over to the engineering staff for installation in the IMP system. The system was completed, and coil checkout began on May 28, 1971. During the checkout, problems were encountered with a power supply, a switch in the current circuit, and an automatic energy dump circuit which triggered when subjected to line transients. These problems were corrected, and the coils have been operated routinely by members of the IMP Group to 71% of design values (coils were energized 32 times during 1971). The coils will be charged to higher currents as required by plasma experiments. At present, we see no reason why the coils should not reach their design values. However, if the normal transition which occurred at 605 A was due to conductor movement, then a series of "training" transitions may be encountered as the conductor settles due to the increasing forces with increasing fields.

1. Consultant.

8.2 ORMAK CRYOGENICS

The ORMAK cryogenic system is required to accomplish the three tasks shown in Table 8.1. The expected liquid-nitrogen requirements for these tasks are shown in Table 8.2. Liquid nitrogen for these tasks is obtained through a building supply system serviced by two 17,000-liter trailers from the central Y-12 supply.

Table 8.1. ORMAK cooling requirement

1. Cooldown	
10,000 kg Iron	773×10^6 J
4500 kg Stainless steel	348×10^6 J
4000 kg Aluminum	844×10^6 J
1800 kg Copper	132×10^6 J
	<hr/>
	2097×10^6 J
2. Operation	
10^7 J per pulse at 10-min intervals	16.7 kW
Internal radiation from lines	1.0 kW
External heat leak	1.5 kW
	<hr/>
	19.2 kW
3. Standby	
External heat leak	1.5 kW

Table 8.2. ORMAK liquid-nitrogen requirement

1. Cooldown	
2.1×10^9 J = 9700 kg = 12,000 liters, considering 50% recovery of enthalpy	
2. Pulsed mode	
19.2 kW = 116 g/sec = 517 liters/hr, considering 85% recovery of heat of vaporization	
3. Standby	
1.5 kW = 9 g/sec = 40 liters/hr, considering 85% recovery of heat of vaporization	

The initial sizing of the cryogenic system was set by the requirement to remove the operational heat of 19.2 kW by circulating liquid nitrogen in a closed circuit comprised of the internal cooling passages in ORMAK and an external heat exchanger, where the heat is transferred to boiling liquid nitrogen. The internal cooling passes in ORMAK consist of:

Primary coils	56 coils with 0.635-cm bore and 26.4-m length, all in parallel
Pulse coils	18 coils with 0.762-cm bore and 10-m average length arranged in 36 parallel cooling paths
Vertical field coils	8 coils with 1.118 × 0.610 cm elliptical bore and 10 m average length arranged in 16 parallel cooling paths
Bus connectors	10 leads traced with 0.483-cm bore tubing 22.9 m long in two parallel paths
Aluminum ring and plate	8 tubes with 0.622-cm bore and 6.1-m length in parallel

The pulse energy of 10^7 J is deposited in 1.5 sec in the primary coils, resulting in a temperature rise of 30 K in the copper conductors filled with nitrogen. Since this energy could cause rapid boiling of the nitrogen and possible uncontrollable high pressures or liquid discharge from the coils, the nitrogen is pressurized above 14.6 atm (the vapor pressure at 110 K) to prevent vaporization.

This requirement of a single liquid phase in the ORMAK coils dictated that all flow controlling valves be placed downstream from the coils, since throttling through the valves could produce two-phase mixtures. This also alleviated any maldistribution of flow between the parallel paths due to two-phase flow.

The earlier calculations by Luton (documented in ORMAK design memorandum) showed that all of the coils were of sufficient length that liquid nitrogen flowing in the turbulent regime would thermally equilibrate with the metal so that the liquid nitrogen leaving the primary coils after a pulse would be at 110 K. The centrifugal pump, purchased for an earlier system, was capable of circulating 450 liters/min of nitrogen against a back pressure of 2.85 atm — sufficient flow to ensure turbulence. The problem in design was to size a heat exchanger to reduce the temperature of the flowing nitrogen from 110 to 80 K so that the copper coils would be cooled back to 80 K in a 10-min period, while at the same time coping with the additional heat loads from the liner and external heat leaks — a total heat load of 19.2 kW.

To be sure that the centrifugal pump remained primed, it was necessary to maintain a net positive suction head of 3 m at the inlet. A survey of several possible arrangements indicated that the most favorable one placed the heat exchanger in the inlet line to the centrifugal pump, since this would maintain a nearly constant temperature at the suction, and simple pressurization could be used to produce the net positive suction pressure, provided that the pressure drop through the heat exchanger was not too great.

The boiling side of the heat exchanger requires sufficient area to ensure that the surface remains wetted with liquid at all times. Since the peak nucleate heat flux for liquid nitrogen is 20 W/cm^2 , this theoretically requires only 1000 cm^2 ; but since the temperature difference for this heat flux is 10 K, leading to a base temperature of 88 K, a much larger area is needed if the final temperature of the circulating liquid is to approach closely to 78 K, the normal boiling temperature of liquid nitrogen.

In the final design, a total boiling surface of $61,000 \text{ cm}^2$ is provided, yielding a boiling heat flux of 0.300 W/cm^2 and a temperature difference of about 2 K. The boiling nitrogen is on the shell side of the heat exchanger to allow the high-pressure circulating liquid to be inside seven parallel tubes which are 3.8 cm in diameter by 7.6 m long. Since it was desirable to keep the space around ORMAK as clear as possible, the heat exchanger was installed vertically, with the centrifugal pump located on the ground floor 6.1 m below ORMAK. The liquid feed and the vapor discharge for the boiling side were connected via a vapor/liquid-phase separator to provide recirculation (reflux) of the liquid in an arrangement known as a vertical thermosyphon reboiler, as shown in Fig. 8.1. The system is designed for a reflux ratio of 5, and the average density of the liquid vapor mixture is 0.027 g/cc (about $\frac{1}{30}$ liquid), giving a static pressure of 0.05 atm at the bottom of the heat exchanger, equivalent to a boiling temperature increase of 0.2 K.

Having sized the heat exchanger for the desired pulsed operation, the other modes were considered. For standby operation, the total heat exchanger duty is 1.5 kW, leading to a boiling heat flux of 0.025 W/cm^2 and a temperature difference of less than 1 K. For this mode of operation the pump is operated at the low speed of 1750 rpm, the flow rate is reduced to 100 liters/min, and the head is reduced to about 0.2 atm. The overall heat loss from the system is kept at a tolerably low level with foam-in-place-urethane insulation on the cold box and the external piping and with aluminized Mylar

ORNL-DWG 72-5968

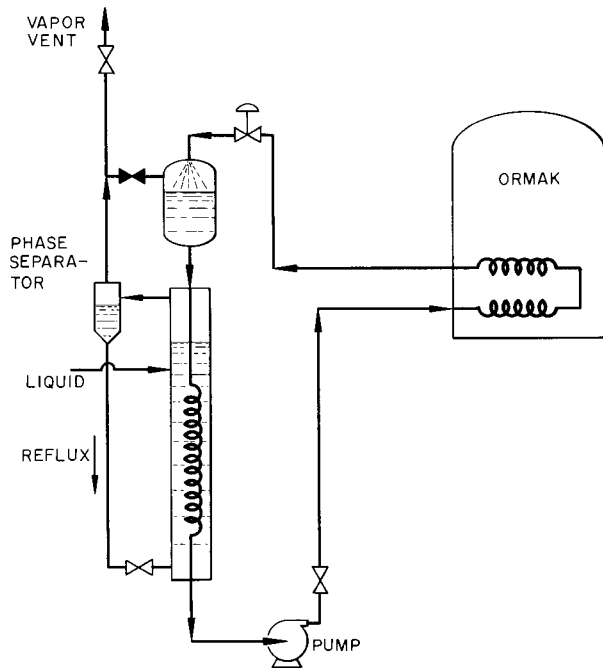


Fig. 8.1. Pulsed operating mode for ORMAK.

multilayer insulation on the interior surface of the vacuum vessel. Without this insulation, the standby refrigeration loss would be nearly 9 kW.

For cooldown, a stream of gaseous nitrogen is required at temperatures varying from just below room temperature to liquid-nitrogen temperature. This is achieved by mixing liquid with a flow of dry nitrogen gas from the building supply. The mixture is produced by flowing the gas upward through liquid falling down the casing side of the heat exchanger, as shown in Fig. 8.2. For this mode the flow through ORMAK is reversed, and the spent nitrogen is discharged to the atmosphere.

During the cooldown the overall rate is set by the requirement that internal temperature differences between major components must be no greater than 30 K in order to avoid mechanical interference which would crush insulation or stresses which would rupture supports. The rate for each component is controlled by adjusting the flow through that component by setting the pneumatically controlled valves in the circuit. Since much of the structure is cooled indirectly from other components, there is a complex interrelation which defies precise analysis, and operating settings, flows, and cooling rates must be set by trial and error. A cooldown rate of 5 K per hour was achieved in an early cooldown, but since there was evidence of insulation

ORNL-DWG 72-5969

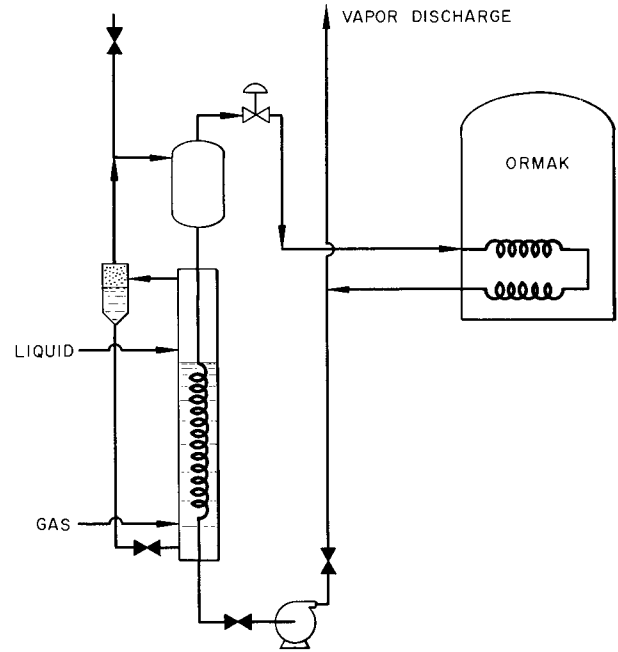


Fig. 8.2. Cooling mode for ORMAK.

damage after warmup, the latest cooldown rate was held to 2.5 K per hour.

The aluminum ring and plate cooling passes were not initially provided in the ORMAK design, but were added after the first cooldown tests when this cryogenic system showed that the heat transfer to these relatively large structures was insufficient to provide adequate rate of cooldown and control of temperature differences between the various components of ORMAK. The cooling passes were made from 0.95-cm-OD copper tubing welded to 5-cm-square copper lugs which were bolted to the aluminum ring and plate at each primary coil location, giving 112 lugs altogether. A bench test of heat transfer in vacuum between a pair of lugs bolted together showed that for the expected range of nitrogen flow, the heat transfer was 14 W per degree Kelvin for bare joints and 18 W per degree Kelvin for joints with 0.005-cm indium foil. The ORMAK lugs were installed with indium foil, and thus in total should provide cooling of up to 2 kW per degree Kelvin.

The system is operated from a panel in the ORMAK console, where the pneumatically operated valve controllers and solenoid switches are located. During the pulsed operation and standby modes with continuous nitrogen circulation, the supply to the phase separator is automatically controlled by liquid-level sensors in the phase separator. Liquid makeup to the pressurizer vessel

is automatically controlled from level sensors in the pressurizers.

Provision has been made for future installation to reduce the temperature to 64 K by using a heat exchanger after the pump. A higher-pressure pump will, however, be required, and the liquid in the heat exchanger shell will have to boil at a reduced pressure.

The system has generally operated satisfactorily to date. During shakedown, trouble was encountered with several ball valves which were delivered by the manufacturer with incorrect gaskets and seats. Some difficulty has occurred with the original ultrasonic level sensors. In fact, we have not had the pressurizer sensors working properly. Substitute thermistor level sensors have been selected and ordered.

While the operation has been satisfactory, the system has not been called upon to operate in a pulsed mode to cool the primary coils after a pulse, and the nitrogen consumption appears to be high. We cannot be sure of the latter point, however, since we do not have means to separate ORMAK consumption from that in the rest of the building.

In addition to the design of the cryogenic system, the group has investigated solutions to the high-vacuum-low-temperature leaks encountered during shakedown of ORMAK. A gold "O"-ring seal was designed to correct leakage in the Varian copper gasket flanges used on the liquid-nitrogen headers, and an epoxy-to-copper-insulated connector was designed to replace the Lexan connectors in the cooling line to coil assemblies. Bench tests of ruggedness and leak-tightness under repeated thermal shocking and vacuum-pressure cycling were conducted prior to installation in ORMAK.

Subsequently, the Varian flanges were welded together to provide a permanent seal, and the epoxy-insulated connectors were replaced by either glass-Kovar or ceramic-Kovar connectors which were bench tested to the same specifications as the epoxy fittings.

8.3 COILS WITH AZIMUTHALLY VARIABLE CURRENT DENSITY FOR EBT

In the course of the coil design work on the ELMO Bumpy Torus (EBT),² it became clear that the requirements on field shape might be better met by coils which were not perfectly symmetrical but had a winding cross section which, on the side nearest the torus axis, was compact and carried high-current density, while its opposite side was radially expanded with a low-current density. In particular, the flux lines nearest the torus axis will be lengthened and thus more nearly equalized with those at the extremity of the midplane. The configuration mentioned above can be approximated by providing an adjacent coil of larger bore at each end of the main coil, the auxiliary coil axis being shifted outward from the torus axis so that the winding cross sections nearest the axis are as close together as possible. This latter arrangement will probably be used for the EBT because of its simplicity and use of proven-design features, even though it is somewhat wasteful of space and, therefore, power. However, since a coil with azimuthally variable current density would consume less power, and power will be an important limitation for EBT as it is for ORMAK, an effort has been commenced to develop such a coil.

2. See Sect. 4.2 of this report.

PHOTO 79274



Fig. 8.3. Test coil with azimuthally varying winding depth.

Figure 8.3 shows a successful model coil cut along its symmetry plane, that is, the torus midplane. The hollow extruded conductor is uniformly 0.635 cm ($1/4$ in.) square, but partial-turn filler bars of solid copper have been wound along with the conductor, giving nearly step variations in the total conductor section. The filler bars have tapered ends, and their lengths are chosen so that bars at successively larger radii span successively larger azimuths, and the cross-sectional area of the winding thus changes smoothly with azimuth. In a test coil, the soft-solder joints between the filler bars and the hollow conductors were made by heating the entire coil after the pretinned conductor and fillers were insulated and wound, thus reducing the labor involved. One test coil successfully carried 4000 A, even though subsequent destructive inspection showed that the solder joints were not well made. The later coil of Fig. 8.3 was soldered at a higher temperature, and the joints appeared satisfactory.

8.4 COILS FOR THE TARGET PLASMA GROUP LONG-FIELD EXPERIMENT

A design of coils for the Long-Field Experiment (LFX), based on the extensive earlier work of the Target Plasma Group, has been made. In the schematic of Fig. 8.4 a central pair of disk coils are used to extend the distance between the racetrack-shaped mirrors (while maintaining a mirror ratio of 2) and to provide

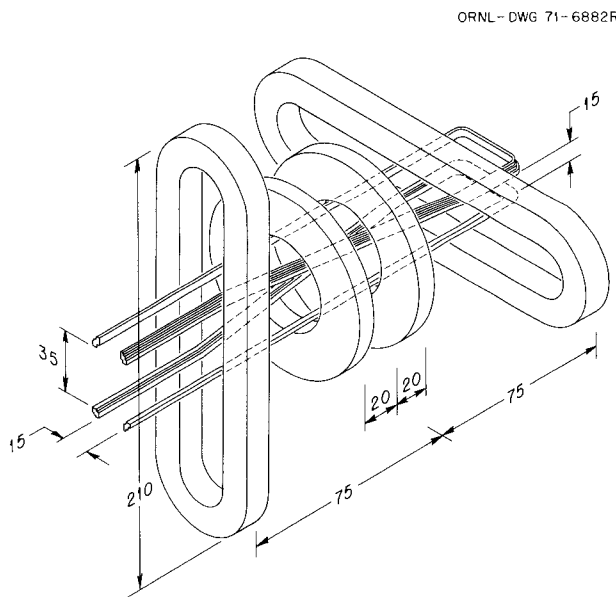


Fig. 8.4. Coil arrangement for the Long-Field Experiment.

operational control of the field shape. The mirror coils are shown elongated and rotated so that the flux lines, as distorted into fans by the Ioffe bars, will still exit through their throats. The mirrors are to be composed of three "pancakes," each wound of hollow conductors arranged in ten parallel water paths. All electric and hydraulic terminations are at the U-bends so that they will not interfere with the Ioffe bars or the enclosed double fan-shaped vacuum chamber. Half the terminations are inside the bore, thus giving each more room and eliminating the troublesome hydraulic "cross-overs." The Ioffe bars are to be assembled in place, one turn at a time, by means of bolted joints which need not carry cooling water. The bars are thus expected to be easy to install or modify. They are shown skewed in order that they will remain close to the flux lines of interest and so require a small current.

8.5 THIN FILM TARGETS

Thin, self-supporting foils have been made for use in determining the energy of charged particles by measuring their energy loss through the foils. Such films are being used in IMP and are being investigated for possible diagnostic use in ORMAK. Despite many difficulties encountered in this work, some progress has been made.

Both carbon and aluminum films have been used in IMP, and, at present, carbon films having a thickness of 500 Å are favored. The films need to be pinhole free and homogeneous with a known and reproducible thickness. The qualifications are being met in carbon films having a thickness of 500 Å or more. The most serious problem remaining unsolved is that of mounting, since the film must cover a 1.27-cm-diam hole. Various grid-supporting structures have been tried, but most have been unsuccessful, since almost all grids cause the films to stretch severely and crack. Recently, a film was successfully supported on 100-mesh electron microscope screening.

The diagnostics group has obtained encouraging results with aluminum foils. These films also must be absolutely pinhole free and the thickness known precisely. Microcracks have been a serious problem, but an aluminum film with a thickness of 300 Å showed no cracks. Island formations which occur during an early phase of film growth, just before the film becomes continuous, are believed to be the source of the microcracks, and thus these cracks should occur in all films below some minimum thickness. We are attempting to find this minimum value for aluminum films and

will attempt to produce reproducible film having only a slightly greater thickness.

Coatings of tantalum and molybdenum have been sputtered onto copper electrodes for use in ion sources. These coatings are being tested to determine their ability to minimize secondary electron emissions.

The vacuum tank which was used to coat the first ORMAK vacuum liner is being modified for ion plating. This modification will include the installation of two 10-kW electron-beam evaporation sources in order that the new ORMAK liner can be plated with both platinum and gold during one vacuum run. The undercoat of platinum is intended to prevent diffusion from the stainless steel liner through the gold film. After the new ORMAK liner is completed, this facility may be used to produce very adherent coatings of various metals having thicknesses of up to a few tenths of a millimeter.

8.6 SUPERCONDUCTOR STABILIZATION STUDIES

The central question which had to be answered prior to final design of the IMP superconducting quadrupole coils was how to cope with the dynamic instabilities created by the magnetic-field component perpendicular to the surface of the Nb_3Sn ribbon superconductor. This question was answered by testing various stabilization schemes with relatively large pairs of coils operated with opposing fields and in a variable background field. These "cusp-coil" tests showed that stabilization could be achieved by co-winding aluminum ribbon along with the Nb_3Sn ribbon.

Similar instabilities can be directly observed in magnetization experiments on small cylindrical samples (1 cm in diameter by 7 cm long) which require only a few feet of conductor (albeit in the form of small disks). We have performed experiments on samples of Nb_3Sn ribbon used in IMP with the object of determining whether or not the number of large cusp-coil tests might be minimized by performing the smaller-scale magnetization experiments. We are looking for correlation between magnetization measurements and the IMP cusp-coil tests.

8.7 INVESTIGATION OF FLUCTUATIONS OF LIQUID-HELIUM SURFACES

The availability of a continuous, fast-responding, linear, liquid-helium level indicator³ has made possible

3. K. R. Efferson, "A Superconducting (Nb-Ti) Liquid Helium Level Detector," p. 124 in *Advances in Cryogenic Engineering*, ed. by K. D. Timmerhaus, vol. 15, Plenum, New York, 1970.

the measurement of fluctuations of the surface of a liquid helium bath. Liquid-level fluctuations can be caused by such things as mechanical vibrations, thermoacoustic oscillations, boiling effects due to constant and nonconstant heat leaks, and Dewar pressure changes. The observation of changes in the liquid surface is important, particularly in large superconducting magnet Dewars, where one needs as many clues as possible to indicate the state of the system.

To aid in intelligently interpreting the reason for the fluctuations occurring at the liquid-helium surface, experiments have been performed to determine the speed with which one can expect the detector to respond to a disturbance, and the size and nature of the surface movement caused by various amounts of heat dissipated within the bulk of the liquid. Preliminary results indicate that the superconducting detector responds to a rising liquid surface at rates up to 25 cm/sec and to falling surfaces at rates up to 4 cm/sec. This is more than adequate to detect the usual disturbances occurring in helium systems.

The effect of sudden constant heat input below the helium surface has been found to result in an initial linear rise of the helium surface due to the volume of bubbles formed within the bulk liquid. The surface rise rate is directly proportional to the heater power. The linear region is followed by a random series of fluctuations starting when the bubbles reach the surface. The size of the random fluctuations depends on heater power and depth. Quantitative measurements have shown fluctuations of 1 to 2 mm at 1 W and ~7 mm at 16 W for a heater depth of 32 cm in a 10-cm-ID Dewar.

8.8 A 7.6-cm-DIAMETER, 100-kG COIL

In the final design of the IMP quadrupole coils, the superconductor packing factor λ was reduced from 0.7 to 0.43 in order to accommodate the aluminum ribbon required to stabilize the General Electric Nb_3Sn superconductor purchased for the coils. Thus a large quantity of the conductor (1.27 by 0.02 cm of Nb_3Sn) was left over. While much of this material was in short pieces (less than 60 m) and in used lengths from various test coils, there was considerable usable material in lengths greater than 150 m. After reviewing various possibilities, we decided to use the bulk of the material to build a 7.6-cm clear-bore solenoid. This size of magnet has the advantage of being a useful laboratory device while serving as a reservoir for material in the event that major repairs are ever needed in IMP.

An outside diameter of 24.1 cm was chosen so that the coil would fit inside our two largest Dewars. The

clear bore of 7.6 cm was chosen to give us the largest possible access while still allowing the possibility of achieving 100 kG. A 100-kG coil is rather common these days; however, the largest field now available in our laboratory is 80 kG, and 100 kG is considered a logical first step to higher fields. The solenoid will consist of 16 pancakes containing more than 2750 m of Nb₃Sn ribbon. Turn-to-turn insulation will be an Al₂O₃ and graphite mixture such as was used in IMP. Pancake-to-pancake insulation will be a specially designed lattice of G-10 epoxy fiber glass formed into 0.02-cm-thick disks. Aluminum ribbon will be added to the end pancakes for stabilization in regions of high radial magnetic field. The amount and position of the stabilizing aluminum will be based on our experience in designing the IMP coils as well as our recent magnetization experiments. This coil will be a good test of the efficacy of using small-sample magnetization measurements to grade material for stabilization.

The probability of this coil reaching its design point is heavily dependent on extrapolation of our short-sample data from fields below 80 to 100 kG. We used data furnished by General Electric for this extrapolation and have no way of verifying its accuracy at this time.

8.9 RIBBON COIL ENDURANCE TESTING

Previous reports⁴ have described the development of water-cooled magnet coils consisting of a grooved strip conductor interleaved with an insulating ribbon. Such coils are capable of overall current densities of 30 kA/cm² (200 kA/in.²). Because of the high power densities involved and the possible weakness of the coils due to the possible movement of the conductor and the exposure of wetted insulator to electrical and mechanical stress, endurance testing of prototype coils was considered necessary. Several coils were fabricated for testing. "Transverse Ribbon Coil No. 4" has been installed in the bore of another coil in the Magnet Laboratory and tested at full current for nearly 200 hr, as indicated in Table 8.3. The total field with both coils energized was 101.5 kG in a 4.8-cm (1.9-in.) bore. The coil was disassembled and inspected twice during the course of the testing; after the second inspection a fatigue-cracked end segment of the conductor was replaced, and the mating surfaces of a joint outside the winding were repolished. This prototype coil has been sufficiently tested to illustrate its ruggedness, and therefore it has been released for routine operation for

4. *Thermonuclear Div. Semiannu. Progr. Rep. Apr. 30, 1966, ORNL-3989, pp. 110-113.*

Table 8.3. Transverse ribbon coil No. 4 endurance testing

Inside diameter	4.8 cm
Outside diameter	12.2 cm
Length	3.8 cm
Current	8000 A
Voltage	71 V
Power	0.57 MW
Self-field	44 kG
Ambient field	57 kG
Total field	101 kG
Overall current density	22,000 A/cm ²
Cooling water velocity	~80 fps
Coolant pressure drop	~160 psi
Time at $I \geq 7000$	191 hr
Number of cycles to full current	75
Additional time in flowing water	~250 hr
Time in stagnant water	~4 months
Test period	1966 to September 1971 (includes dry storage, 1967 through 1970)

those experiments which will fit in its restricted bore. Other ribbon coils will be built should their use be advantageous.

8.10 FUSION FEASIBILITY

We participated in the International Working Session on Fusion Reactor Technology which was held at the Oak Ridge National Laboratory from June 28 to July 2. Talks were given in the session on Engineering Design of Magnet Systems on (1) The State-of-the-Art of Superconducting Magnet Technology, which included a detailed discussion on the latest results in high-field superconducting materials research, a fairly detailed summary of all high-field and large-magnet developments, an analysis of the overall magnet current density compatible with very large completely stabilized coils, a summary of the available experimental information on radiation damage, and a discussion of some strength of materials properties useful for superconducting magnets; (2) the testing and performance of the IMP superconducting quadrupoles (Sect. 8.1); (3) the engineering design study of a superconducting magnet system for a power reactor (see the details in Sect. 9.1.1); (4) the cryogenic problems associated with large superconducting magnet systems — the very useful empirical data and curves of Strowbridge pertaining to cryogenic refrigerators were shown to be still valid. In addition, the session on Engineering Design of Magnet Systems was reviewed in the summary session of the conference. Two main features of superconducting magnet technology pertinent to fusion reactor technology emphasized in the summary are that no magnet

built or even being considered for construction comes anywhere near the sizes and fields which will be required for a full-scale fusion plant, and that a complete magnet system for the presently envisioned fusion reactors will be expensive. For example, in the ORNL study, the preliminary design of a magnet system with the maximum field less than 80 kG indicated that the magnet would contribute approximately \$30/kW(e) to the cost of a 2500-MW(e) fusion power reactor. Other reactors discussed at the meeting required magnets of comparable size operating at higher fields, with some requiring fields not yet achieved in superconducting magnets. Although detailed cost estimates were not made for these magnet systems, their cost at present would be higher than \$30/kW(e).

8.11 CRYOGENIC TEST FACILITY

The vacuum tank fabricated to test the IMP coils has been modified to be used as a cryogenic test facility to obtain electrical, mechanical, and heat transfer data in high vacuum at temperatures down to 4.5 K.

The 1.37-m-diam by 0.91-m-deep tank has been outfitted with a "10-in." trapped diffusion pump to provide rapid pumpdown. Liquid nitrogen from the building supply is available at the test site, and liquid helium is available from Dewars or possibly from the IMP helium liquefier/refrigerator. The output from two dc generators may be series connected to give 7000 A at 7000 V, or paralleled to give 14000 A at 350 V. The exciters of these generators are driven by amplidyne to

give good regulation and rapid ramping from zero to full load in 3 sec.

Initial tests on nitrogen-cooled copper coils such as used in ORMAK are being planned. The facility will also be used to provide the required high-vacuum bakeout for the new ORMAK liner prior to the successive platinum-gold plating.

8.12 POWER-TRANSMISSION TECHNOLOGY

Cryoelectrical power transmission systems are under development in the U.S. and several foreign countries. A review⁵ of these programs and other nonconventional means for power transmission in the U.S. was undertaken to provide background information for possible ORNL programs in this area. In the review the present status of the electric power transmission in this country is summarized, and conventional, semiconventional, and unconventional electric power transmission systems are characterized. The development of UHV and HVDC overhead power transmission is reviewed, and a short discussion of the various underground power transmission systems is presented. Compressed-gas-insulated cables and cryoresistive and superconducting electric power transmission are considered. As a result of this study and a review of the facilities and capabilities in the Thermonuclear Division, a program for the investigation of dielectric breakdown in cryogenic fluids and solids was developed. If funding can be secured, this program will be implemented during the coming year.

5. Technical memorandum in preparation, *Unconventional Electric Power Transmission in the U.S.A.*

9. Fusion Reactor Technology

K. R. Efferson	J. N. Luton	W. C. T. Stoddart ²
A. P. Fraas ¹	J. R. McNally	M. L. Tobias ¹
W. F. Gauster	O. B. Morgan	J. S. Watson ³
H. M. Long	C. E. Parker	F. W. Wiffen ⁴
M. S. Lubell	Don Steiner ¹	O. O. Yarbro ³

9.1 PUBLISHED WORK

9.1.1 Magnet Design

K. R. Efferson	M. S. Lubell
A. P. Fraas	J. N. Luton
W. F. Gauster	C. E. Parker
H. M. Long	Don Steiner
W. C. T. Stoddart	

The magnet design group has completed an engineering study on a superconducting toroidal field system for a 5000-MW(t) Tokamak fusion reactor.⁵ The study is based upon (1) a conservative value for the reactor power density (3.5 MW/m² at the vacuum wall) and (2) commercially available superconducting material (NbTi operating at a maximum field strength of 80 kG in the windings). Cost estimates were made for the entire magnet system, and the economic effects of varying reactor power density were investigated. The results of this study are presented in the following abstract.

A detailed engineering study has been made of a superconducting magnet system for a full-scale tokamak fusion reactor. For economic reasons, the main toroidal field must be produced by superconducting coils. We decided to employ compound conductors with twisted, thin filaments and a sufficiently high

copper-to-superconductor ratio to provide both static and dynamic stability. Commercial superconductors which satisfy these criteria are NbTi compound conductors. The use of this material restricts for our design the maximum magnetic field strength (which results from the d.c. main toroidal field and the pulsed poloidal field) to about 80 kG.

We assumed a total power $P_T = 5000\text{-MW(t)}$, a wall loading $P_w = 3.5\text{-MW/m}^2$, a vacuum chamber minor radius $r_w = 3.5\text{-m}$, a pressure ratio $\beta_\Theta = 3$, and a stability margin $q = 1.4$. These values and the maximum field strength $B_M = 80\text{-kG}$ yield a toroidal magnetic field $B_\phi = 37\text{-kG}$, a major radius $R = 10.5\text{-m}$, a minor coil radius $r = 5.59\text{-m}$, and a plasma aspect ratio $A = 3.75$, if we consider a blanket thickness $w = 2\text{ m}$ and a ratio $y = 0.8$ between plasma and vacuum chamber radii. The stored magnetic energy is about 40,000-MJ and about $1.45 \times 10^6\text{-m}$ of compound conductor is required. The design of the mechanical structure is based on detailed force and stress calculations. The net radial force on each of the 48 coils is 10,580 tons, requiring massive reinforcement of the bobbins. The cryogenic calculations consider all sources of heat loads, and in the worst case about 75% of the total loss is due to the nuclear radiation. The structural design takes into consideration the assembly as well as maintenance and repair difficulties arising from radiation damage and neutron activation. Detailed cost estimates were made. We summarized the kind of major technological research and development work which is necessary for optimized realistic designs. Finally, an economic comparison is given between a 5000-MW(t) and a 1000-MW(t) reactor with the result that while the magnet system for the latter would cost only 43% as much, the unit cost in $\$/\text{kW(e)}$ would be about double.

9.1.2 The Blascon – An Exploding-Pellet Fusion Reactor⁶

A. P. Fraas

A fusion reaction can be initiated by directing an intense laser beam with a short pulse duration at a

1. Reactor Division.
2. General Engineering Division.
3. Chemical Technology Division.
4. Metals and Ceramics Division.

5. M. S. Lubell et al., "Engineering Design Studies on the Superconducting Magnet System of a Tokamak Fusion Reactor," paper presented at the 4th IAEA Conference on Plasma Physics and Controlled Nuclear Fusion Research, Madison, Wis., June 1971.

6. Abstract of ORNL-TM-3231 (July 1971).

pellet of a frozen deuterium-tritium mixture. A study of the application of this approach to a series of conceptual designs has yielded some surprisingly attractive systems. Analyses and tests indicate that the explosion can be contained in a pressure vessel, and that, if pellets can be exploded at about 10-sec intervals, a reactor and pressure vessel assembly can be obtained at a modest unit cost for central stations or ship power plants having outputs as low as 100 MW(t). A reactor of this type would require no large magnets, activation of the structure would be negligible, thus easing afterheat and hazard problems, and the problems of fast-neutron damage to the reactor structure would be avoided. The exploding-pellet concept might also be applied to give a spacecraft propulsion system that might reduce the propellant weight requirements for an Earth-Mars-Earth mission to about 10% of that for a Rover-type nuclear rocket.

An examination of the principal problems of these systems indicates that the major uncertainty in each case is the feasibility of obtaining a practical laser that will ignite D-T pellets of the required size to yield a much greater energy output than the laser energy input. An analysis of the problem of laser ignition indicates that there is a reasonably good chance that this problem can be solved, and that analysis has been supported by an experiment that appears to have given 10^4 neutrons from a 130- μ -diam D-D pellet heated with a 40-J laser beam. The report concludes that, in view of the tremendous potential payoff and the relatively low cost of some definitive experiments, a small experimental program to investigate this type of reactor deserves a high priority.

9.1.3 Environmental Considerations⁷

Don Steiner

The emergency cooling and radioactive waste-disposal requirements anticipated for fusion reactors are compared with those requirements posed by fission reactors. A reference fusion reactor is used as the basis for comparison. This reactor is based on the D-T fuel cycle and employs a blanket consisting of niobium as the structural material, lithium as the coolant, and graphite as the neutron moderator and reflector.

Relative to fission reactors, the reference fusion reactor exhibits the following advantages with respect to emergency cooling requirements: (1) a lower hazard

potential associated with radioactive inventories, (2) lower nuclear power densities during operation and for many hours following shutdown, (3) no potential for nuclear energy insertions resulting from loss of coolant or meltdown, and (4) a more favorable coolant passage geometry. The management of radioactive wastes should require fewer operations for fusion reactors than for fission reactors, and therefore the associated economic penalty should be less.

The effects of alternate fusion fuel cycles and alternate blanket structural materials are summarized. Fusion reactors operating on the D-³He fuel cycle would exhibit less-stringent emergency cooling and radioactive-waste disposal requirements than would reactors operating on either the D-T or D-D fuel cycles. Of the several blanket structural materials considered, vanadium has the most desirable characteristics with regard to emergency cooling and radioactive-waste disposal.

9.2 WORK IN PROGRESS

9.2.1 Radiation Damage Experiment

F. W. Wiffen

Tensile specimens and microscopy disks were placed in the HFIR during the early part of October 1971. The purpose of this experiment (conducted by the Metals and Ceramics Division) is to evaluate the effects of fluence, temperature, and helium concentration on the properties of niobium and niobium-1% zirconium. Fluence values will approach $\sim 2 \times 10^{22}$ neutrons/cm² (>0.1 MeV), and temperatures will vary between 450 to 950°C. The helium production anticipated under fusion reactor conditions will be simulated by alpha injection and by ¹⁰B(*n*, α)⁷Li transmutation. Irradiation time will be between six months to one year, and postirradiation examination will include microscopy, immersion density measurements, and some tensile tests to evaluate ductility.

9.2.2 Tritium Handling and Recovery

J. S. Watson O. O. Yarbro

The Thermonuclear Division in cooperation with the Chemical Technology Division has initiated a detailed paper investigation of alternate methods for recovering tritium from the breeding blanket of a fusion reactor. The methods under investigation include (1) cold trapping, (2) distillation, (3) gas stripping, (4) chemical gettering, and (5) permeable membranes. In evaluating the alternate methods, consideration is being given to

7. Abstract of "Emergency Cooling and Radioactive Waste-Disposal Requirements for Fusion Reactors," paper presented at the 4th IAEA Conference on Plasma Physics and Controlled Nuclear Fusion Research, Madison, Wis., June 1971.

(1) economics, (2) recovery effectiveness, and (3) the extent to which tritium diffuses into the steam system of the fusion power plant. The results of this paper study will be the basis on which we shall build an experimental program.

9.2.3 Neutron Cross-Section Requirements for Fusion Reactor Design

M. L. Tobias

In order to calculate the neutronic behavior of fusion reactors with a high degree of confidence, it is necessary that accurate nuclear data be available.⁸ To ensure that the neutron cross-section needs for fusion reactor design are met, the Thermonuclear Division in cooperation with the Reactor Division has initiated a comprehensive program consisting of the following components:

1. Evaluation. Existing data will be critically evaluated over the entire energy range of interest.
2. Preparation. Evaluated data will be put into a form which is useful and easily available.
3. Recommendation. Sensitivity tests will be performed in order to recommend to data-measuring groups our critical cross-section needs and accuracy requirements. This input is most essential, since, in many instances, existing data are not adequate for meaningful calculations.

9.2.4 Fusion Reactor Blanket Benchmark Calculations

Don Steiner

At the Neutronics Session of the International Working Sessions on Fusion Reactor Technology (Oak Ridge National Laboratory, June 1971) it was noted that the ${}^7\text{Li}(n, \alpha n' t)$ reaction rate calculated by a discrete-ordinates transport-theory method was ~18% lower than that calculated by a Monte Carlo method. In order to identify the source of this discrepancy, it was agreed that the neutronics of a standard fusion reactor blanket model be evaluated by several groups, that is, that a benchmark calculation be undertaken. It was hoped that all groups could employ the same cross-section data so that the only variable in the calculations would be the method, either discrete ordinates or Monte

8. D. Steiner, "Neutron Cross Section Requirements for Fusion Reactor Design," paper presented at the Third Conference on Neutron Cross Sections and Technology, University of Tennessee, Knoxville, March 1971.

Carlo. Ten neutronics groups are participating in this exercise (including groups both in the United States and abroad). This effort is being coordinated by the groups at ORNL and at Harwell, England.

9.2.5 Fusion Reactors as Radioactive-Waste Burners (RWB's)

Don Steiner

The management and control of the long-lived radioactive wastes associated with a fully developed fission power economy will present a formidable problem. These radioactive wastes must be stored for centuries to permit long-lived fission products such as ${}^{90}\text{Sr}$ and ${}^{137}\text{Cs}$ to decay to nontoxic levels. Long-lived fission products such as ${}^{99}\text{Tc}$ and some of the actinides require thousands of centuries to decay to nontoxic levels. Present schemes for the management and control of the long-lived radioactive wastes include conversion of the aqueous wastes to solids, followed by long-term storage in man-made vaults or disposal in deep geological formations such as salt mines. Although the economic penalty associated with such schemes is not great, that is, estimated to be about 1% of the total electrical power cost, public opposition to the establishment of a long-term radioactive legacy could limit the growth of fission power. A possible solution to this dilemma may be the use of excess neutrons from fusion reactors to burn out long-lived radioisotopes by neutron-induced reactions, that is, to employ fusion reactors as RWB's.

The strategy of the RWB would be (1) to transmute the long-lived fission products to short-lived radionuclides which decay to stable isotopes and (2) to induce fission in the actinides and then handle the resulting long-lived fission products as in (1). Such a scheme would require extremely efficient chemical processing to separate the desired radionuclides and a cheap and abundant source of neutrons. ORNL's interest in the concept of an RWB is largely motivated by the expectation that fusion reactors will provide a cheap and abundant source of neutrons. Currently we are assessing the requirements imposed on the RWD concept by neutronic considerations.

9.2.6 Blanket-System Studies

A. P. Fraas

These studies include: (1) an assessment of the problems associated with employing a direct-cycle gas turbine as a topping cycle in a fusion reactor, (2) an analytical study of the heat transfer limitations imposed

on liquid lithium by magnetic field effects, and (3) the evolution of a lithium circulation scheme which appears to require much less pumping power than earlier schemes.

9.2.7 Engineering Requirements for Scatter-Dominated, Mirror-Confined Plasmas

J. R. McNally

Various parametric requirements for attaining high-beta, scatter-dominated, mirror-confined plasmas have been developed. The demands on injected current, gas loading, and pumping speed vary as $E^{-7/2}$, and beam power varies as $E^{-5/2}$. Thus it appears that the engineering requirements for generating interesting mirror-confined plasmas are most easily met by utilizing very high-energy (multi-MeV) injection, a point first made by Budker in 1954.⁹

9.2.8 Beam Technology

O. B. Morgan

As part of their effort, the injection group has been considering (1) the developmental effort necessary to bring present beam technology up to the requirements of fusion reactors and (2) the usefulness of present beam capabilities for producing detectable 14-MeV neutron damage. The latter effort is being pursued together with members of the Solid State Division.

9. G. I. Budker, p. 111 in *Plasma Physics and the Problems of Controlled Thermonuclear Reactions*, ed. by M. A. Leontovich, Pergamon, New York, 1959.

9.2.9 Use of Synchrotron Radiation to Provide Ionization of Wall-Originated Impurities in a Thermonuclear Reactor¹⁰

H. K. Forsen¹¹

A method is proposed for shielding a thermonuclear plasma from neutral wall reflux by filling the region between the plasma and wall with a warm tenuous plasma which ionizes the neutrals and allows them to be collected by a divertor. It is shown that the synchrotron radiation from the plasma core is adequate to sustain such a plasma against ionization losses.

9.3 INTERNATIONAL WORKING SESSIONS ON FUSION REACTOR TECHNOLOGY

Several members of the ORNL staff were involved in the organization of the International Working Sessions on Fusion Reactor Technology held at ORNL June 28 to July 7, 1971. This meeting was jointly sponsored by ORNL and the ANS Technical Group on Controlled Nuclear Fusion. There were about 150 attendees, including representatives from Canada, France, Germany, Italy, Japan, Russia, the United Kingdom, and the United States. The Proceedings of the Working Sessions have been edited and typed at ORNL and will be distributed early in 1972.

10. Abstract of paper to be published in *Nuclear Fusion*.

11. Consultant, University of Wisconsin, Madison.

Publications, Papers, and ORNL Reports

OPEN LITERATURE

Author(s)	Title of Article	Journal (or Book)
I. Alexeff, L. A. Berry, J. M. Dudley, ¹ K. G. Estabrook, ² A. Hirose, ³ W. D. Jones, ⁴ R. V. Neidigh, J. N. Olsen, ⁵ F. R. Scott, ⁶ W. L. Stirling, M. M. Widner, ⁵ and W. R. Wing ⁷	Understanding Turbulent Ion Heating in the Oak Ridge Mirror Machine, "Burnout V"	P. 221 (vol. II) in <i>Proceedings Fourth Conference on Plasma Physics and Controlled Nuclear Fusion Research, 1971</i> , IAEA, Vienna, 1971
W. B. Ard, R. A. Blanken, ⁸ R. J. Colchin, J. L. Dunlap, G. E. Guest, G. R. Haste, C. L. Hedrick, N. H. Lazar, and D. J. Sigmar ⁸	Use of a Hot-Electron Target Plasma for Accumulation of Energetic Ions in Stabilized Magnetic Mirror Traps	P. 619 (vol. II) in <i>Proceedings Fourth Conference on Plasma Physics and Controlled Nuclear Fusion Research, 1971</i> , IAEA, Vienna, 1971
W. B. Ard, W. A. Hogan, ⁹ and R. F. Stetson ⁹	Electron Distribution Measurements in a Hot-Electron, Mirror Contained Plasma	<i>Phys. Fluids</i> 14, 2038 (1971)
D. E. Baldwin, ¹⁰ C. O. Beasley, Jr., H. L. Berk, ¹⁰ W. M. Farr, ¹¹ R. C. Harding, ¹⁰ J. E. McCune, ⁸ L. D. Pearlstein, ¹⁰ and A. Sen ¹²	Loss-Cone Modes in Inhomogeneous Mirror Machines	P. 735 (vol. II) in <i>Proceedings Fourth Conference on Plasma Physics and Controlled Nuclear Fusion Research, 1971</i> , IAEA, Vienna, 1971
C. F. Barnett, J. F. Clarke, R. C. Davis, R. A. Dory, P. H. Edmonds, J. T. Hogan, G. G. Kelley, M. J. Lubin, ¹³ J. R. McNally, O. B. Morgan, M. Murakami, M. Roberts, L. D. Stewart, W. L. Stirling, M. M. Widner, ⁵ H. K. Forsen, ¹⁴ and J. M. Soures ¹³	Oak Ridge Tokamak Research	P. 347 (vol. I) in <i>Proceedings Fourth Conference Plasma Physics and Controlled Nuclear Fusion Research, 1971</i> , IAEA, Vienna, 1971
R. J. Colchin	Target Plasma Trapping	<i>Nucl. Fusion</i> 11, 329 (1971)

-
1. Colby College.
 2. ORAU Fellow, University of Tennessee.
 3. University of Saskatchewan.
 4. University of South Florida.
 5. Sandia Laboratories.
 6. Consultant, University of Tennessee.
 7. ORAU Fellow, University of Iowa.
 8. Consultant, Massachusetts Institute of Technology.
 9. Florida Atlantic University.
 10. Lawrence Radiation Laboratory.
 11. University of Arizona.
 12. University of Tennessee.
 13. University of Rochester.
 14. Consultant, University of Wisconsin.

Author(s)	Title of Article	Journal (or Book)
D. L. Coffey, ¹⁵ W. F. Gauster, and M. S. Lubell	Comparison of NbTi with Nb ₃ Sn Material Tests with the Actual Performance of Coils	<i>J. Appl. Phys.</i> 42, 59 (1971)
R. A. Dandl, H. O. Eason, P. H. Edmonds, A. C. England, G. E. Guest, C. L. Hedrick, J. T. Hogan, and J. C. Sprott	High-Beta Relativistic Electron Plasmas in Axisymmetric and Non-Axisymmetric Mirrors	P. 607 (vol. II) in <i>Proceedings Fourth Conference on Plasma Physics and Controlled Nuclear Fusion Research, 1971</i> , IAEA, Vienna, 1971
R. A. Dandl, H. O. Eason, P. H. Edmonds, and A. C. England	Off-Resonance Effects on Electrons in Mirror-Contained Plasmas	<i>Nucl. Fusion</i> 11, 411 (1971)
K. R. Efferson, D. L. Coffey, ¹⁵ R. L. Brown, J. L. Dunlap, W. F. Gauster, J. N. Luton, and J. E. Simpkins	The IMP Superconducting Coil System	<i>IEEE Trans. Nucl. Sci.</i> NS-18(4) (1971)
K. Estabrook, ² M. Widner, ⁵ I. Alexeff, and W. D. Jones ⁴	Simulation of Pseudowaves and of Plasma Sheath Formation about a Grid by Computer Solution of the Ion Vlasov Equation	<i>Phys. Fluids</i> 14, 1792 (1971)
K. Estabrook, ² I. Alexeff, W. D. Jones, ⁴ and K. Lonngren ¹⁶	Reflection of Pseudowaves	<i>Phys. Fluids</i> 14, 185 (1971)
G. E. Guest and E. G. Harris ⁶	Flute Stabilization Via Electrostatically Confined Cold Electrons	<i>Phys. Rev. Lett.</i> 27, 1500 (1971)
G. E. Guest and D. J. Sigmar ⁸	Stability of Microwave-Heated Plasmas ORMAK Facility	<i>Nucl. Fusion</i> 11, 151 (1971) <i>IEEE Trans. Nucl. Sci.</i> NS-18(4) (1971)
W. Halchin, J. F. Clarke, S. M. DeCamp, P. H. Edmonds, J. C. Ezell, J. E. Francis, R. E. Hill, ¹⁷ G. G. Kelley, S. O. Lewis, ¹⁷ J. R. McNally, Jr., M. Murakami, M. Roberts, M. J. Lubin, and J. M. Soares ¹³		
A. Hirose ³ and I. Alexeff	Anomalous Rapid Skin Current Penetration and Heating in Pulsed Plasma Experiments	<i>Phys. Rev. Lett.</i> 26, 949 (1971)
S. Krishan, ¹² and J. Fukai ¹²	Three-Wave Interaction and Non-linear Wave Particle Scattering	<i>Phys. Fluids</i> 14, 1158 (1971)
N. H. Lazar and G. R. Haste	Effect of Electron Heating on Overall Efficiency of Conceptual Mirror Fusion Reactors	<i>Plasma Phys.</i> 13, 433 (1971)
M. S. Lubell, W. F. Gauster, K. R. Efferson, A. P. Fraas, ¹⁹ H. M. Long, J. N. Luton, C. E. Parker, D. Steiner, ¹⁹ and W. C. T. Stoddart ¹⁷	Engineering Design Studies on the Super- conducting Magnet System of a Tokamak Fusion Reactor	P. 433 (vol. III) in <i>Proceedings Fourth Conference on Plasma Physics and Controlled Nuclear Fusion Research 1971</i> , IAEA, Vienna, 1971
M. S. Lubell and R. H. Kernohan ²⁰	Comparison of Calculated and Measured Lower Critical Field for Some Nb-Ti Alloys	<i>J. Phys. Chem. Solids</i> 32, 1531 (1971)
M. S. Lubell and D. M. Kroeger ²¹	Evidence to Support the Rigidly Pinned Vortex Model for the Peak Effect	<i>Physica</i> 55, 394 (1971)
O. B. Morgan, Jr	Intense Ion and Neutral Beams with Extraction Energies Above 10 keV	P. 129 in <i>Proc. Symp. on Ion Sources and Formation of Ion Beams</i> , Brook- haven National Laboratory, Oct. 19- 21, 1971, BNL-50310

15. American Magnetics, Inc.

16. University of Iowa.

17. General Engineering Division.

18. Consultant, University of Rochester.

19. Reactor Division.

20. Solid State Division.

21. Metals and Ceramics Division.

Author(s)	Title of Article	Journal (or Book)
M. Murakami and J. F. Clarke	A Method of Measuring the Poloidal Magnetic Field in Diffuse Toroidal Pinches	<i>Nucl. Fusion</i> 11, 147 (1971)
J. Rand McNally, Jr.	Autocatalytic Burning of ^6LiD Nuclear Fuel via the $p + ^9\text{Be}$ Resonance Reaction	<i>Nucl. Fusion</i> 11, 554 (1971)
J. Rand McNally, Jr., and R. V. Neidigh	Cu D in Burnout V	<i>J. Quant. Spectrosc. Radiat. Transfer</i> 11, 125 (1971)
J. Rand McNally, Jr.	Fusion Chain Reactions – I	<i>Nucl. Fusion</i> 11, 187 (1971)
	Fusion Chain Reactions – II	<i>Nucl. Fusion</i> 11, 189 (1971)
	Fusion Chain Reactions – III. The Production of MeV Plasmas	<i>Nucl. Fusion</i> 11, 191 (1971)
Rodger V. Neidigh and W. R. Wing ⁷	A Rapid Abel Inversion	<i>Amer. J. Phys.</i> 39, 760 (1971)
John N. Olsen ⁵	Fractional Fringe HCN Laser-Interferometer	<i>Rev. Sci. Instrum.</i> 42, 104 (1971)
Herman Postma	Engineering and Environmental Aspects of Fusion Power Reactors	<i>Nucl. News</i> 14, 57 (1971)
J. A. Ray and C. F. Barnett	Secondary Electron Emission of Metals Bombarded with 120 eV and 5 keV Protons	<i>J. Appl. Phys.</i> 42, 3260 (1971)
J. E. Robinson ²² and J. F. Clarke	Time Resolution of Plasma Potential Using Gridded Electrostatic Analyzers	<i>Rev. Sci. Instrum.</i> 42, 434 (1971)
David J. Rose ⁸	Controlled Nuclear Fusion Status and Outlook	<i>Science</i> 172, 797 (1971)
D. J. Sigmar ⁸ and J. D. Callen ⁸	Wave-Particle Energy Transfer and Wave-Amplitude Limiting Effects for a Flute-Like High-Frequency Mode	<i>Phys. Fluids</i> 14, 1423 (1971)
D. J. Sigmar ⁸ and Glenn Joyce ¹⁶	Plasma Heating by Energetic Particles	<i>Nucl. Fusion</i> 11(5), 447 (1971)
J. C. Sprott and P. H. Edmonds	Computer Calculations of Electron Cyclotron Heating in a Non-Uniform Magnetic Field	<i>Phys. Fluids</i> 14, 2703 (1971)
D. Steiner ¹⁹	Neutron Irradiation Effects and Tritium Inventories Associated with Alternate Fuel Cycles for Fusion Reactors	<i>Nucl. Fusion</i> 11, 305 (1971)
	Long-Lived Activities and Radioactive Waste Management Associated with D-T Fusion Reactors	<i>Nucl. Fusion</i> 11, 307 (1971)
	The Radiological Impact of Fusion	<i>New Sci.</i> , p. 168–171, Dec. 16, 1971
	Neutron Cross Section Requirements for Fusion Reactor Design	P. 514 in <i>Proceedings Third Conference on Neutron Cross Sections and Technology, University of Tennessee, Knoxville, TN, March 15–17, 1971</i> , vol. II; CONF-710301
	Emergency Cooling and Radioactive Waste-Disposal Requirements for Fusion Reactors	P. 447 (vol. II) in <i>Proceedings Fourth Conference on Plasma Physics and Controlled Nuclear Fusion Research, 1971, IAEA, Vienna, 1971</i>
W. L. Stirling, R. C. Davis, O. B. Morgan, and L. D. Stewart	The ORNL Multi-Ampere Ion Source	P. 167 in <i>Proceedings of Symposium on Ion Sources and Formation of Ion Beams, Brookhaven National Laboratory, Oct. 19–21, 1971, BNL-50310</i>
E. R. Wells, J. L. Dunlap, and J. S. Culver	The Mechanical Aspects of the IMP Mirror-Quadrupole Facility	<i>IEEE Trans. Nucl. Sci.</i> NS-18(4) (1971)

22. Massachusetts Institute of Technology.

Author(s)	Title of Article	Journal (or Book)
M. M. Widner, ⁵ R. A. Dory, and J. T. Hogan	Anomalous Electron Thermal Losses in Tokamaks	<i>Phys. Lett.</i> 36A, 217 (1971)
M. M. Widner, ⁵ I. Alexeff, and W. D. Jones ⁴	Plasma Expansion into a Vacuum	<i>Phys. Fluids</i> 14, 795 (1971)
M. M. Widner, ⁵ G. E. Guest, and R. A. Dory	Energy Transfer to Ions from Modulated Electron Beams	<i>Phys. Fluids</i> 11, 2547 (1971)

PAPERS PRESENTED AT SCIENTIFIC AND TECHNICAL MEETINGS

Third Conference on Neutron Cross Sections and Technology, University of Tennessee, Knoxville, Tennessee, March 15–17, 1971 [CONF-710301, vol. II, p. 514 (1971)].

D. Steiner,¹ “Neutron Cross-Section Requirements for Fusion Reactor Design.”

Annual Sherwood Theory Meeting, New York University (Courant Institute), New York, New York, March 22–23, 1971 (Proceedings will not be published.)

C. L. Hedrick, Jr., “Suppression of the Whistler Instability by Relativistic Effects.”

Fourth Symposium on Engineering Problems of Fusion Research, Naval Research Laboratory, Washington, D.C., April 20–23, 1971 [IEEE Trans. Nucl. Sci. NS-18 (1971)].

K. R. Efferson, R. L. Brown, D. L. Coffey,² J. L. Dunlap, W. F. Gauster, H. M. Long, and J. E. Simpkins, “The IMP Superconducting Coil System.”

W. Halchin, “Ormak Facility.”

E. R. Wells, J. L. Dunlap, and J. S. Culver, “The Mechanical Aspects of the IMP Mirror-Quadrupole Facility.”

Canadian Association of Physicists, Ottawa, Canada, June 21–24 1971 [Bull. Can. Ass. Phys. 27 (1971)].

I. Alexeff,³ L. A. Berry, R. V. Neidigh, and A. Hirose,⁴ “The Absence of Relative Drift Velocity Limitations on Ion Heating in the BO-VI Mirror Machine.”

A. Hirose⁴ and I. Alexeff,³ “Rapid Penetration of Electron Skin Current in Tokamak and Other Pulsed Plasma Experiments.”

Fourth IAEA Conference on Plasma Physics and Controlled Nuclear Fusion Research, Madison, Wisconsin, June 17–23, 1971.

I. Alexeff,³ L. A. Berry, J. M. Dudley,⁵ K. G. Estabrook,⁶ A. Hirose,⁴ W. D. Jones,⁷ R. V. Neidigh, J. N. Olsen,⁸ F. R. Scott,³ W. L. Stirling, M. M. Widner,⁸ and W. R. Wing,⁹ “Understanding Turbulent Ion Heating in the Oak Ridge Mirror Machine, ‘Burnout V.’ ”

W. B. Ard, R. A. Blanken,¹⁰ R. J. Colchin, J. L. Dunlap, G. E. Guest, G. R. Haste, C. L. Hedrick, N. H. Lazar, J. F. Lyon, and D. J. Sigmar,¹⁰ “Use of a Hot-Electron Target Plasma for Accumulation of Energetic Ions in Stabilized Magnetic Mirror Traps.”

-
1. Reactor Division.
 2. American Magnetics, Inc.
 3. Consultant, University of Tennessee.
 4. University of Saskatchewan, Saskatoon, Canada.
 5. Colby College.
 6. University of Tennessee.
 7. University of South Florida.
 8. Sandia Laboratories.
 9. University of Iowa.
 10. Consultant, Massachusetts Institute of Technology.

C. F. Barnett, J. F. Clarke, R. C. Davis, R. A. Dory, P. H. Edmonds, H. K. Forsen,¹¹ J. T. Hogan, G. G. Kelley, M. J. Lubin,¹² J. R. McNally, O. B. Morgan, M. Murakami, M. Roberts, J. M. Soures,¹² L. D. Stewart, W. L. Stirling, and M. M. Widner,⁸ "Oak Ridge Tokamak Research."

D. E. Baldwin,¹³ C. O. Beasley, Jr., H. L. Berk,¹³ W. M. Farr,¹⁴ R. C. Harding,¹³ J. E. McCune,¹⁰ L. D. Pearlstein,¹³ and A. Sen,⁶ "Loss Cone Modes in Inhomogeneous Mirror Machines."

R. A. Dandl, H. O. Eason, P. H. Edmonds, A. C. England, G. E. Guest, C. L. Hedrick, J. T. Hogan, and J. C. Sprott, "High-Beta Relativistic Electron Plasmas in Axisymmetric and Non-Axisymmetric Mirrors."

M. S. Lubell, W. F. Gauster, K. R. Efferson, A. P. Fraas,¹ H. M. Long, J. N. Luton, C. E. Parker, D. Steiner,¹ and W. C. T. Stoddart,¹⁵ "Engineering Design Studies on the Superconducting Magnet System of a Tokamak Fusion Reactor."

D. Steiner,¹ "Emergency Cooling and Radioactive Waste-Disposal Requirements for Fusion Reactors."

International Working Sessions on Fusion Reactor Technology, Oak Ridge, Tennessee, June 28–July 2, 1971. (Proceedings to be published.)

A. P. Fraas,¹ "Engineering Design of Blankets."

M. S. Lubell, "Superconducting Magnets – State-of-the-Art" (invited paper).

M. S. Lubell, "Summary of Session 7 – Engineering Design of Magnet Systems" (invited paper).

F. W. Wiffen,¹⁶ "Radiation Damage – State-of-the-Art."

Fourth U.N. Conference on the Peaceful Uses of Atomic Energy, Geneva, Switzerland, September 6–16, 1971. (Proceedings to be published.)

H. Postma, A. P. Fraas, D. Steiner,¹ R. G. Mills,¹⁷ R. J. Post,¹³ and F. L. Ribe,¹⁸ "Engineering and Environmental Aspects of Fusion Reactors."

Symposium on Ion Sources and Formation of Ion Beams, Brookhaven National Laboratory, Upton, New York, October 19–21, 1971. [Proceedings, BNL-50310 (1971).]

O. B. Morgan, Jr., "Intense Ion and Neutral Beams with Extraction Energies above 10 keV" (invited paper).

W. L. Stirling, R. C. Davis, O. B. Morgan, and L. D. Stewart, "The ORNL Multi-Ampere Ion Source."

USSR Academy of Sciences Symposium on Plasma Theory, Kiev, USSR, October 19–23, 1971.

R. A. Dory, G. E. Guest, E. G. Harris,³ J. T. Hogan, and M. M. Widner, "Containment in Tokamak and Bumpy Torus."

International Conference on Multiply Charged Heavy-Ion Sources and Accelerating Systems, Gatlinburg, Tennessee, October 25–27, 1971.

I. Alexeff³ and W. D. Jones,⁷ "Production of Highly Stripped Heavy Ions in Hot-Electron Plasmas."

11. Consultant, University of Wisconsin.

12. Consultant, University of Rochester.

13. Lawrence Radiation Laboratory.

14. University of Arizona.

15. General Engineering Division.

16. Metals and Ceramics Division.

17. Princeton University.

18. Los Alamos Scientific Laboratory.

American Physical Society, Southeastern Section, Columbia, South Carolina, November 4–6, 1971. [Bull. Amer. Phys. Soc. II 17(2) (1971).]

C. F. Barnett, "Excited State of H₂ Molecules" (invited paper).

R. J. Colchin, "The Use of Target Plasmas to Study Mirror Confinement" (invited paper).

American Physical Society, Division of Plasma Physics, Madison, Wisconsin, November 15–18, 1971. [Bull. Amer. Phys. Soc. II, 16(11)(1971).]

I. Alexeff,³ "Turbulent Heating in Beam-Plasma Experiments" (invited paper).

I. Alexeff³ and K. Estabrook,⁶ "Cerenkov Ion-Acoustic Wave Radiation from Ion Bursts."

C. O. Beasley, A. Sen,⁶ and J. D. Callen,¹⁰ "Microinstabilities in Inhomogeneous Plasmas: Finite Beta Effects."

J. D. Callen¹⁰ and J. F. Clarke, "Possible Limitations on Neutral Beam Injection into a Tokamak Plasma."

J. F. Clarke and R. H. Fowler,¹⁹ "Fast Ion Slowing Down in Tokamak Plasmas."

R. J. Colchin, "Adiabaticity in a Mirror Quadrupole."

E. C. Crume²⁰ and H. K. Meier, "Simulation of High Frequency Flute-Like Instabilities in Multicomponent Plasmas."

J. L. Dunlap, W. B. Ard, R. J. Colchin, and N. H. Lazar, "'Target' Plasma Experiments in the Superconducting Mirror-Quadrupole System IMP."

A. C. England, R. A. Dandl, H. O. Eason, and J. C. Sprott, "Recent High-Beta Canted Mirror Experiments."

K. G. Estabrook⁶ and I. Alexeff,³ "Simulation of Pseudowaves and Ion Acoustic Waves in a Plasma."

W. M. Farr,¹⁴ C. O. Beasley, J. D. Callen,¹⁰ J. E. McCune,¹⁰ and A. Sen,⁶ "Electrostatic Microinstabilities in Inhomogeneous Plasmas."

G. E. Guest, C. L. Hedrick, and J. T. Hogan, "Self-Consistent, High Beta, Hot-Electron Equilibria in Canted Mirrors."

E. G. Harris,³ "Diffusion in a Bumpy Torus."

G. R. Haste and N. H. Lazar, "Axial Distribution of Plasma Pressure in an ECH Plasma."

J. T. Hogan, "The Establishment of Bootstrap Currents in Tokamak."

G. G. Kelley, L. A. Berry, J. F. Clarke, P. H. Edmonds, J. R. McNally, Jr., M. Murakami, R. V. Neidigh, and M. Roberts, "Early Results from the ORMAK."

J. F. Lyon and N. H. Lazar, "Energetic Particle Measurements Using Neutral Beam Injection into an Electron-Cyclotron-Heated 'Target' Plasma in a Magnetic Well."

J. R. McNally, Jr., "Fusion Chain Reaction – A New Type of Nuclear Reaction Process for Violent Astrophysical Explosions."

O. B. Morgan, "Multi-Ampere Neutral Beams" (invited paper).

R. V. Neidigh, I. Alexeff,³ L. A. Berry, K. Estabrook,⁶ A. Hirose,⁴ W. L. Stirling, M. M. Widner,⁸ and W. R. Wing,⁹ "Turbulent Heating in the ORNL Mirror Machines Burnout V, VI."

D. J. Sigmar,¹⁰ "Feasibility of Stationary Tokamak by Neutral Injection."

J. C. Sprott, "Numerical Simulation of Off-Resonance Heating."

L. D. Stewart, R. C. Davis, G. G. Kelley, O. B. Morgan, Jr., and W. L. Stirling, "Neutral Injection Heating of the ORMAK Plasma."

W. L. Stirling, R. C. Davis, O. B. Morgan, Jr., and L. D. Stewart, "The ORNL DuoPIGatron Ion Source."

M. M. Widner,⁸ R. A. Dory, and J. T. Hogan, "Computer Models for Electron Thermal Losses in Tokamaks."

W. R. Wing,⁹ I. Alexeff, L. A. Berry, K. Estabrook,⁶ A. Hirose,⁴ and R. V. Neidigh, "The Ion-Heating Turbulence in the Oak Ridge Turbulent Heating Device, Burnout VI."

19. Mathematics Division.

20. On loan from Y-12.

Fifth Annual Conference on Numerical Simulation of Plasmas, Iowa City, Iowa, November 19–20, 1971.

H. K. Meier and E. C. Crume,²⁰ “Quieter Starts.”

American Physical Society, Cambridge, Massachusetts, December 27–29, 1971. [Bull. Amer. Phys. Soc. II 16 (1971).]

H. Postma, “Probable Engineering and Environmental Aspects of Fusion Reactors” (invited paper).

ORNL REPORTS

Author(s)	Title	Number
A. P. Fraas ¹	The Blascon – An Exploding Pellet Fusion Reactor	ORNL-TM-3231
W. B. Ard, W. A. Hogan, ² and R. F. Stetson ²	Electron Distribution Measurements in a Hot Electron, Mirror Contained Plasma	ORNL-TM-3302
W. L. Stirling	Lifetime of the Hot-Ion Plasma in the Oak Ridge Mirror Machine, Burnout V	ORNL-TM-3340
Philip B. Burt ³	Perturbation Theory in Toroidal Plasma	ORNL-TM-3351
D. J. Sigmar ⁴ and Glenn Joyce ⁵	Plasma Heating by Energetic Particles	ORNL-TM-3354
R. A. Dandl, H. O. Eason, P. H. Edmonds, and A. C. England	Off-Resonance Effects on Electrons in Mirror-Contained Plasmas	ORNL-TM-3356
J. C. Sprott and P. H. Edmonds	Computer Calculations of Electron Cyclotron Heating in a Non-Uniform Magnetic Field	ORNL-TM-3405
Owen Eldridge ⁶	Electron Cyclotron Heating as Resonant Diffusion	ORNL-TM-3417
J. D. Callen ⁴ and R. A. Dory	MHD Equilibria in Sharply Curved Axisymmetric Devices	ORNL-TM-3430
C. F. Barnett and J. A. Ray	A Calibrated Neutral Atom Spectrometer for Measuring Plasma Ion Temperatures in the 0.165- to 10-keV Energy Region	ORNL-TM-3440
J. Rand McNally, Jr.	Speculations on the Configurational Properties of a Fusing Plasma	ORNL-TM-3471
R. C. Davis, O. B. Morgan, L. D. Stewart, W. L. Stirling, and H. K. Forsen ⁷	A Multi-Ampere DuoPIGatron Ion Source for Plasma Research	ORNL-TM-3472
G. E. Guest, C. L. Hedrick, and J. T. Hogan	Hot-Electron Equilibrium in the Canted Mirror	ORNL-TM-3473
C. F. Barnett and J. A. Ray	Energy-Dispersed Neutral Beams	ORNL-TM-3475
G. R. Haste and N. H. Lazar	Electron Heating Effect on Power Balance in Mirror Reactors	ORNL-TM-3479
Melvin M. Widner ⁸ and Robert A. Dory	An Implicit Numerical Method for Simulating Tokamak Plasma Discharges	ORNL-TM-3498
A. Hirose ⁹ and I. Alexeff	Electrostatic Instabilities Driven by Currents Perpendicular to an External Magnetic Field	ORNL-TM-3532
H. K. Forsen ⁷ and J. C. Sprott	The Use of Synchrotron Radiation to Provide Ionization of Wall Originated Impurities in a Thermonuclear Reactor	ORNL-TM-3539

-
1. Reactor Division.
 2. Florida Atlantic University.
 3. Consultant, Clemson University.
 4. Consultant, Massachusetts Institute of Technology.
 5. University of Iowa.
 6. Consultant, University of Tennessee.
 7. Consultant, University of Wisconsin.
 8. Sandia Laboratories.
 9. University of Saskatchewan, Saskatoon, Canada.

Author(s)	Title	Number
A. Sen ¹⁰ and John F. Clarke	Regularization Method of Unfolding X-ray Spectrum	ORNL-TM-3582
N. Betz, ¹¹ R. A. Dory, J. E. Francis, and O. C. Yonts	Proposal for Computer Assisted Data Acquisition for ORNL Fusion Experiments	ORNL-TM-3593
G. G. Kelley, O. B. Morgan, L. D. Stewart, W. L. Stirling, and H. K. Forsen ⁷	Neutral Beam Injection Heating of Toroidal Plasmas for Fusion Research	ORNL-TM-3594
E. A. Ferguson	Evaluation of the Plasma Dispersion Function	ORNL-TM-3610
R. A. Dory, G. E. Guest, J. T. Hogan, M. M. Widner, ⁸ and E. G. Harris ⁶	Containment in Tokamak and Bumpy Torus	ORNL-TM-3637
Thermonuclear Division Staff	Thermonuclear Division Annual Progress Report for Period Ending December 31, 1970	ORNL-TM-4688
J. E. Francis and O. C. Yonts	New Data System for INTEREM	ORNL-TM-3401
R. A. Dandl, H. O. Eason, A. C. England, G. E. Guest, C. L. Hedrick, and J. C. Sprott	The ELMO Bumpy Torus Experiment	ORNL-TM-3694

10. University of Tennessee.

11. Mathematics Division.